NASA CR 135290
R77–912184–21

DEVELOPMENT OF SiAlON MATERIALS

G.K. Layden

UNITED TECHNOLOGIES RESEARCH CENTER

prepared for

NATIONAL AERONAUTICS AND SPACE ADMINISTRATION

NASA LEWIS RESEARCH CENTER

Contract NAS 3–19712

December, 1977

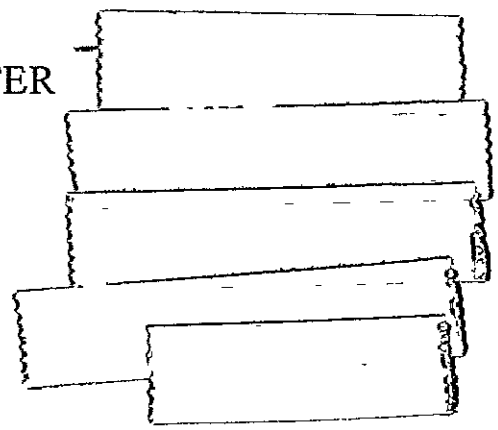

1 Report No	2 Government Accession No	3 Recipient's Catalog No
CR-135290		

4 Title and Subtitle	5 Report Date
Development of SiAlON Materials	November 1977
	6 Performing Organization Code

7 Author(s)	8 Performing Organization Report No
G. K. Layden	R77-912184-21
	10 Work Unit No

9 Performing Organization Name and Address	11 Contract or Grant No
United Technologies Research Center East Hartford, CT 06108	NAS 3-19712
	13 Type of Report and Period Covered Contractor Report June 1975 to Sept. 1977

12 Sponsoring Agency Name and Address	14 Sponsoring Agency Code
National Aeronautics and Space Administration Lewis Research Center Cleveland, Ohio 99135	

15 Supplementary Notes

Interim Report
Project Manager, T P. Herbell, Materials and Structures Division, NASA Lewis Research Center, Cleveland, Ohio

16 Abstract

Cold pressing and sintering techniques were used to produce ceramic bodies in which the major phase was B' $Si_{3-x}Al_xO_xN_{4-x}$ solid solution. A variety of foreign oxides were used to promote liquid phase sintering, and this resulted in the incorporation of additional solid phases in the ceramic bodies which controlled elevated temperature properties. None of the bodies studied to date exhibited both adequate high temperature mechanical properties and oxidation resistance. Criteria are suggested to guide the formulation of bodies with improved high temperature properties.

17 Key Words (Suggested by Author(s))	18 Distribution Statement
SiAlON, Silicon Nitride, Nitrogen Ceramics, Oxynitride ceramics, Gas Turbine materials, Sintering, Ceramic Processing	Unclassified-unlimited

19 Security Classif (of this report)	20 Security Classif (of this page)	21 No of Pages	22 Price*
Unclassified	Unclassified		

* For sale by the National Technical Information Service, Springfield, Virginia 22151

Development of SiAlON Materials

TABLE OF CONTENTS

LIST OF TABLES

LIST OF FIGURES

LIST OF FIGURES (Cont'd)

LIST OF FIGURES (Cont'd)

SECTION I

SUMMARY

The objective of this program is to develop formulations for ceramic bodies which can be fabricated to complex shapes by conventional sintering techniques and which exhibit properties suitable for highly stressed applications in a gas turbine. The class of materials being investigated is β' SiAlON, which is understood to denote materials in which the major phase is a solid solution based on the β Si_3N_4 structure having a range of compositions $Si_{3-x}Al_xO_xN_{4-x}$. As a pure phase β' SiAlON cannot be sintered to full density, but bodies formulated such that some liquid forms at the sintering temperature can be prepared which are fully dense. This can be accomplished with formulations within the system Si_3N_4 - SiO_2 - Al_2O_3 - AlN, or by the addition of foreign oxides to β' formulations which react with β' constituents to produce liquid. In either case, a grain boundary phase or phases is retained in the sintered body, and the nature of the grain boundary assemblage has a controlling influence on the properties of the body.

Over the course of this program to date a variety of sintering aids were investigated including $AlPO_4$, $GaPO_4$, ZrO_2, ZrC, Cr_2O_3, TiO_2, HfO_2, Y_2O_3, La_2O_3, Er_2O_3, Nd_2O_3 and $GdSmO_3$. Uniformly dense bodies were obtained only with ZrO_2, Y_2O_3 (and mixtures of these), and rare earth oxide additions. Bodies prepared with Y_2O_3 additions exhibited room temperature flexural strengths on the order of 550 MPa (80,000 psi). In the absence of other more deleterious types of flaws, room temperature strength of these bodies was controlled by the presence of metallic inclusions. At 1370°C β' containing Y_2O_3 exhibited strengths up to 450 nPa (65,000 psi) and a creep rate of 6×10^{-5} hr^{-1} at a stress level of 69 nPa (10,000 psi). Samples containing ZrO_2 exhibited totally inadequate mechanical properties at 1370°C.

The oxidation behavior could be correlated with minimum liquidus temperatures in the systems containing the oxidation products. All systems containing Y_2O_3, La_2O_3, or rare earth oxides in time developed oxide films that were liquid at 1400°C and afforded little protection. For compositions where the minumum ternary eutectic temperature in the systems containing the oxidation products was above the test temperature, (i.e., in the SiO_2 - Al_2O_3, and SiO_2 - ZrO_2 - Al_2O_3 systems) thin protective crystalline scales developed and the static oxidation rates were low.

No compositions have been developed as yet which combine both good oxidation behavior and good high temperature mechanical properties, and this remains the primary goal of this program. Criteria are suggested that define in general ways the types of systems that must be explored, and approaches are outlined that may correct shortcomings in present formulations.

SECTION II

INTRODUCTION

The gas turbine is considered a serious candidate for an alternative engine for automotive and marine use as well as for power generation. Efficient use of fuel can be achieved by high turbine operating temperatures and light rotating parts. These considerations, plus the necessity of using nonstrategic and potentially inexpensive materials, have led to serious consideration of the use of ceramic components. Stringent property requirements have limited the ceramic candidates for rotating parts to Si_3N_4 and SiC based materials. While hot pressed Si_3N_4 would appear to offer the most attractive properties at the present time, the great expense of machining parts from this material is prohibitive, and alternative materials are sought that can be formed to near net shape by conventional sintering process.

The object of the current program is to develop a formulation or formulations for ceramic bodies which can be fabricated to complex shapes by conventional sintering techniques and which exhibit properties which make them suitable for highly stressed applications in a gas turbine.

One class of materials which offers the potential of meeting this objective is β′ SiAlON. The term SiAlON first referred to the product of high temperature reaction between Al_2O_3 and Si_3N_4, described independently by Jack and Wilson (Ref. 1) and by Oyama and Kamigaito (Ref. 2). A number of workers have subsequently investigated SiAlONs, and properties reported for the material have excited considerable interest. Desirable properties reported include low coefficient of thermal expansion (Refs. 3, 4, 5), good thermal shock resistance (Ref. 3), good high temperature modulus of rupture (Ref. 3), good high temperature creep resistance (Refs. 3, 5) and good oxidation resistance (Refs. 3, 5, 6). It has further been reported that, unlike Si_3N_4 which requires hot pressing in order to achieve high density, SiAlON can be fabricated in dense shapes by conventional sintering techniques (Refs. 1, 3). The major phase resulting from the reaction of Al_2O_3 and Si_3N_4 is a solid solution based on an expanded β Si_3N_4 structure and labeled β' (Refs. 1, 6). However, many workers who have reacted mixtures of Al_2O_3 and Si_3N_4 report the presence of other phases besides the β' phase (Refs. 1, 4, 6, 7, 8, 9, 10). Morgan (Ref. 11) predicted that in fact β' compositions had stoichiometries given by the formula $Si_{3-x}Al_xO_xN_{4-x}$, and that the equilibrium products of the reaction of Si_3N_4 and Al_2O_3 were multiphase. He further predicted that single phase β' SiAlONs having the above stoichiometry would not sinter. Recent reports of phase equilibrium studies in the system Si_3N_4 - SiO_2 - Al_2O_3 - AlN (Refs. 12, 13, 14, 15, 16) have confirmed that β' SiAlONs have the above stoichiometries and that these materials do not sinter (Ref. 15).

The above phase diagram studies showed that the reason Si_3N_4 - Al_2O_3 mixtures sinter to full density is the presence of a liquid phase existing in equilibrium with the β' phase at temperatures above about 1700°C. Layden (Ref. 17) attempted to use this liquid region to effect a transient liquid phase (TLP) sintering of single phase β' bodies. A second approach to sintering and hot pressing of Si_3N_4 and β' SiAlON bodies - and one most widely employed - is the use of foreign additions, generally refractory oxides, which react with other constituents to form a liquid phase at the firing temperature. (Refs. 18, 19, 20, 21, 22, 23, 24, 25). This is also the approach taken in the work reported here.

The use of additives to effect a liquid phase sintering almost invariably introduces phases other than the major β' phase, and these have an overriding effect on the properties of the ceramic bodies, particularly at elevated temperature and under oxidizing conditions.

Since the work on these nitrogen and oxynitride ceramics is all quite recent, limited phase equilibria data on important systems - and virtually no property data on new oxynitride phases other than β' - have yet been published. Therefore, the approach to developing sinterable nitrogen ceramics having properties adequate to stand up to severe conditions of a gas turbine must be an emperical one. Many systems must be screened in terms of sinterability, microstructures, and properties. This is an interim report of work in progress. The goal has not yet been achieved, but criteria are suggested that define in general ways the types of systems that must be explored, and approaches are outlined that may correct shortcomings in present formulations.

SECTION III

EXPERIMENTAL PROCEDURES

A. Sample Preparation

1. Compositions Studied

Nominal β' $Si_{3-x}Al_xO_xN_{4-x}$ compositions studied over the courses of this investigation are listed in Table 1 and are plotted on the phase diagram, Fig. 1. Actual compositions will vary somewhat from the nominal compositions because of different formulation and processing techniques to be described, and codes will be introduced at the appropriate places in this report to identify the particular processing treatments that samples received. Deviations from nominal stoichiometry will be discussed in Section IV. Where sintering aids were added to basic β' compositions, the overall composition will generally be described in terms of the β' composition plus the weight percent of added sintering aid.

TABLE 1

COMPOSITIONS OF β' $Si_{3-x}Al_xO_xN_{4-x}$
SOLID SOLUTIONS INVESTIGATED

		Atom Percent			
β'	x	Si	Al	O	N
0	0	42.86	0	0	57.14
1	0.30	38.58	4.28	4.28	52.86
2	0.55	35.00	7.86	7.86	49.28
3	0.90	30.00	12.86	12.86	44.29
4	1.07	27.50	15.36	15.36	41.78
5	1.25	25.00	17.86	17.86	39.29
6	1.60	20.00	22.86	22.86	34.28
7	1.78	17.50	25.43	25.43	31.71

SYSTEM Si_3N_4–AlN–Al_2O_3–SiO_2 1650°C ISOTHERMAL SECTION (PARTIAL) SHOWING β' COMPOSITIONS INVESTIGATED

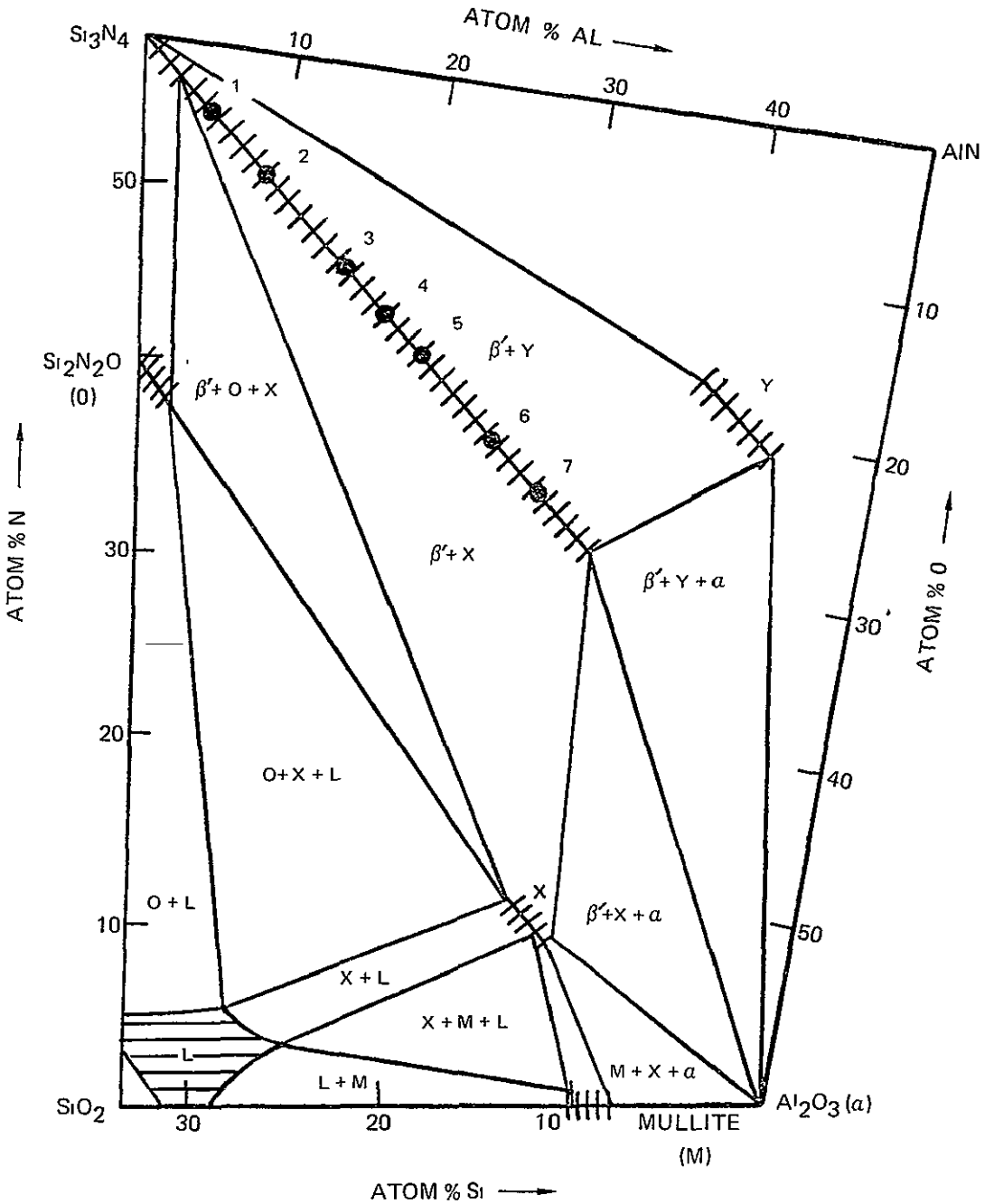

ORIGINAL PAGE IS
OF POOR QUALITY

77–09–36–1

2. Raw Materials

Materials used for compounding the basic β' compositions for samples with numbers below 750 are AME high purity Si_3N_4 90% α phase -300 mesh powder, Atlantic Equipment 99.9% -325 mesh AlN and Al_2O_3. Samples numbered 750 through 918 were Kawecki Berylco high purity 85% α phase -325 mesh Si_3N_4 powder, shipment 1, and samples with numbers above 918 used Kawecki Berylco Si_3N_4 shipment 2. Spectro-chemical analyses for impurities in these various starting powders are given in Table 2, as are neutron activation analyses for oxygen in the Si_3N_4 powders. Compounds added to basic β' compositions to promote sintering are listed in Table 3. Chemical analyses were not performed on these compounds.

3. Usual Powder Preparation Techniques

Over the course of the program various powder processing techniques were employed. These arose mainly from the necessity to improve sample homogeneity and were derived from studies of milling and drying of prefired and unfired powders. Some of these studies were carried out under another program and are described elsewhere (Ref. 17). The powder processing techniques are best described in terms of unit operations listed below.

a. Formulation of Batch Compositions

i. Stage 1 formulation

In initial sintering studies, the primary constituents were assumed to have compositions indicated by their conventional chemical formulae, and material introduced into the batches as a result of wear of grinding media and mill jars was ignored.

ii. Stage 2 formulation

As work progressed, extended ball milling was used to reduce particle size and promote homogeneity. Ball milling experiments indicated that substantial amounts of material worn from mill jars and media were introduced into the batches and it was necessary to take this into account in formulating compositions. Logs were kept of the media weight so that material introduced from this source could be predicted. The oxygen content of the "Si_3N_4" powder determined by neutron activation analysis, was taken into account in formulating the batches. A work sheet exemplifying stage 2 formulation is shown in Appendix 1.

b. Ball Milling

In the first stage of the program batch constituents and comminuted prefired materials were milled in Roalox jars with methanol and Burundum grinding media. Later, either high alumina or reaction sintered Si_3N_4 grinding media were used with

TABLE 2

IMPURITY, WEIGHT PERCENT

Reagent		Al	Si	Ca	Cl	Co	Cr	Fe	Mg	Mo	Ni	Zn	O*
Si_3N_4	AME	.15	> 10	< .02	< .02	< .05	< .01	.10	< .01	< .01	.02	.02	1.9
	KBI shpt 1	.05	> 10	< .02	< .02	< .05	.01	.40	< .01	< .01	.01	< .02	1.2
	KBI shpt 2	.05	> 10	< .02	< .02	< .05	< .01	.30	< .01	< .01	< .01	< .02	0.8
AlN		> 10	.20	< .02	.05	.10	< .01	.07	.40	.02	.05	< .02	
Al_2O_3		> 10	< .01	< .01	< .02	<.01	< .01	< .01	< .01	< .01	< .01	< .01	

*Determined by fast neutron activation analyses.

TABLE 3

COMPOUNDS ADDED TO BASIC β' SOLID SOLUTIONS

$AlPO_4$	Rocky Mountain Research 99.99% Purity
$GaPO_4$	
Y_2O_3	Gallard Schlesinger 99.9% purity
Zr_2O_2	
ZrC	
CeO_2	Molycorp oxalates (calcined)
$GdSmO_3$	
Er_2O_3	Apache Chemicals Inc. 99.9% purity
La_2O_3	
Nd_2O_3	
Sm_2O_3	American Potash oxalate (calcined)
Cr_2O_3	Fisher Certified reagent
TiO_2	
HfO_2	Wah Chang Spectrographic grade

methanol in 16 oz. wide mouthed polyethylene bottles. Standardized charges of batch materials, media, and methanol were used. Rolling speed was set for the different media by adjusting by ear for maximum uniform grinding action. The motor control setting so established was used in all subsequent runs using the given media.

c. Drying of Ball Mill Charges

Mill charges were originally dried by pouring into shallow aluminum foil trays and placing these above a laboratory furnace to evaporate the methanol. This procedure was found to lead to segregation of the sample constituents and was discontinued. A spray drying procedure was adopted in hope of preventing segregation. Mill jar contents were emptied into wash bottles. A large tray of aluminum foil was constructed, placed on a hot plate, and a smaller (8 in. square) plate of 1/4 in. aluminum placed in the center of the tray and heated to about 100°C. The wash bottles were kept continuously agitated while the contents were sprayed onto the hot aluminum plate. Evaporation of the methanol was rapid, and the dry powder was periodically scraped from the plate into the surrounding tray.

d. Deagglomerating

Tray dried material was caked and layered. This was broken up and dry ground using a large porcelain mortar and pestal. The spray dried material tended to be flakey. This material was forced through a 100 mesh screen using a bristle brush.

e. Prefiring

i. 600°C air firing

Materials that had been milled in polyethylene jars, spray dried, and screened were placed in alumina crucibles and heated in air to 600°C for 1 hour. The purpose of this firing was to burn off organic contamination from the jars and brush. Weight measurements before and after various heat treatments in air (to be described later) showed that no weight gain of ball milled powders occurred during this air prefiring.

ii. 1650°C firings

Samples of β' compositions that were to be prereacted and comminuted prior to the addition of sintering aids were cold pressed at about 15,000 psi into cyclindrical pellets about 1.25 in. in diameter and 1.25 in. high. These were placed in boron nitride crucibles and heated to 1650-1700°C in nitrogen in a graphite susceptor induction furnace for 2 hours. The furnace details will be described more fully in Section III.A.6.a.

f. Comminution of Prefired Pellets

Initially, the fired pellets were crushed to -10 mesh in a steel mortar and ground to powder in a rotary hammer pulverizing mill. A magnet was used in an attempt to remove iron particles introduced by the mill. Later in the program a Trost air mill was used to reduce -10 mesh material to the -25μ size range.

g. Flow Sheets for Different Powder Preparations

The powder preparation techniques most often used over the course of the program were various combinations of the above unit operations. These are codified for easy reference in Table 4. In special cases powders were prepared by other techniques, and these cases will be described individually.

4. Special Powder Preparation Techniques

In many instances, special powder preparation techniques were used to study specific effects, particularly effects of the particle size of the prereacted β' compositions and CeO_2 sintering aid. These are best described briefly along with the results in Section IV of this report. Several experiments involved the use of materials derived from the acid milling process described below.

a. Acid Milling and Particle Size Separations

A sample of prereacted powder was milled for different lengths of time in a 50 percent solution of HCl and H_2O in Roalox jars using burundum media with the primary purpose of dissolving metallic iron particles. After milling, the material was allowed to settle, the liquid decanted, fresh water added, sample agitated with a magnetic stirrer, and the washing procedure repeated until a litmus test indicated that the acid was substantially removed. After these washing operations the heavier particles settle quite rapidly but even after standing overnight some solid material still remained in suspension. The liquid decanted after standing overnight was retained in one container. During the work day, washings were repeated at about 3 hour intervals. Liquid decanted after standing for 3 hours was stored in a second container. The decanted fractions were then centrifuged down, washed, recentrifuged, and finally ground under acetone in a mortar and pestle to redistribute and dry the fine powder.

5. Cold Pressing Test Samples

Samples were uniaxially pressed from the prepared powders without the use of auxiliary binders either in the form of right circular cylinders about 0.375 in. x 0.375 in., or rectangular bars about 0.188 in. x 0.375 in. x 6 in. The 6 in. long bars were cut into three or four shorter bars. The uniaxially pressed samples were placed individually into latex bags which were evacuated and sealed. These were then placed in an isostatic press and loaded to 40,000 psi.

TABLE 4

FLOW CHARTS FOR DIFFERENT POWDER PREPARATIONS

Process		1	2	3	4	5
Formulation (Stage)		β' only 1	β' only 2	β' only 2	β' + sintering aid 2	β' + sintering aid 2
Ball Milling	Jars	Roalox	Polyethylene	Polyethylene	Polyethylene	Polyethylene
	Media	Burundum	High alumina	Si_3N_4	High Alumina	High Alumina
	Time (hrs)	18	1	1	96	18
Drying		Tray	Spray	Spray	Spray	Spray
Deagglomerating		Mortar	--	--	Screen	Screen
Prefiring	Temp. (°C)	1650	1650	1650	600	600
	Atmosphere	Nitrogen	Nitrogen	Nitrogen	Air	Air
	Time (hrs)	2	2	2	1	1
Comminution		Hammer mill	Air mill	Air mill		
Reformulation		Sintering aid added	Sintering aid added	Sintering aid added		
Ball Milling	Jars	Roalox	Polyethylene	Polyethylene		
	Media	Burundum	High alumina	Si_3N_4		
	Time (hrs)	18	96	96		
Drying		Tray	Spray	Spray		
Deagglomerating		Mortar	Screen	Screen		
Prefiring	Temp (°C)		600	600		
	Atmosphere		Air	Air		
	Time (hrs)		1	1		

6. Firing of Test Samples

a. Vacuum Induction Furnace

Most of the sample firings were carried out in a graphite susceptor vacuum induction furnace. The susceptor and crucible arrangements are shown in Fig. 2. Cold pressed samples (cylinders or bars) were placed in 3/4 in. ID boron nitride crucibles. In some instances the samples were packed in powder of the same composition which was intended to serve as a buffer, hopefully to establish the equilibrium partial pressure of gas phase constituents above the samples. The boron nitride crucibles were fitted with tapered lids and placed inside graphite susceptor inserts fitted with screw tops that served to exert pressure on the crucible lids. The furnace chamber was evacuated and back-filled with nitrogen to one atmosphere and a low flow of nitrogen maintained through the chamber during firing. Bars without a powder pack were generally fired three or four per crucible. Samples were heated to a maximum temperature over a period of about 30 minutes and held at temperature for the desired length of time. The power was then shut off and the furnace allowed to cool at maximum rate. Most of the firings in this furnace relied on manual control of temperature. The precision of reported temperature will be discussed in Section III.A.6.c.i.

b. Graphite Resistance Furnace

Late in the reporting period a graphite resistance furnace was employed for firing of test samples. In this furnace temperature was sensed and controlled by an infrared pyrometer sighting on the outside of a hollow cylindrical graphite heating element near the point of maximum temperature. An alumina muffle extended through the heating element. Suitable end fittings for the alumina muffle permitted a boron nitride crucible containing a single sample to be inserted and positioned in the hot zone of the furnace. A piece of graphite was placed under the crucible in order to establish an atmosphere similar to that which existed in the vacuum induction furnace. The muffle was flushed with nitrogen for about 20 minutes prior to heat up, and a static nitrogen atmosphere was maintained in the furnace during the run. Because of the problem of thermal stress on the alumina muffle, slower heat-up rates were used for this furnace than those used previously. An arbitrarily established procedure allowed two hours for heating or cooling between room temperature and about 1700°C.

c. Furnace Calibrations and Temperature Measurement

i. Vacuum induction furnace

Holes were drilled through the crucible and susceptor insert tops shown in Fig. 2. so the junction of W/5 percent Re vs W/26 percent Re thermocouple could be positioned at the center of the crucible. Alumina powder was packed into the crucible to serve as a dummy sample. The furnace was allowed to reach steady state at a given control setting, and a calibration curve of temperature vs control setting was

INDUCTION FURNACE DETAILS

ATMOSPHERE· NITROGEN BACKFILL AFTER EVACUATION

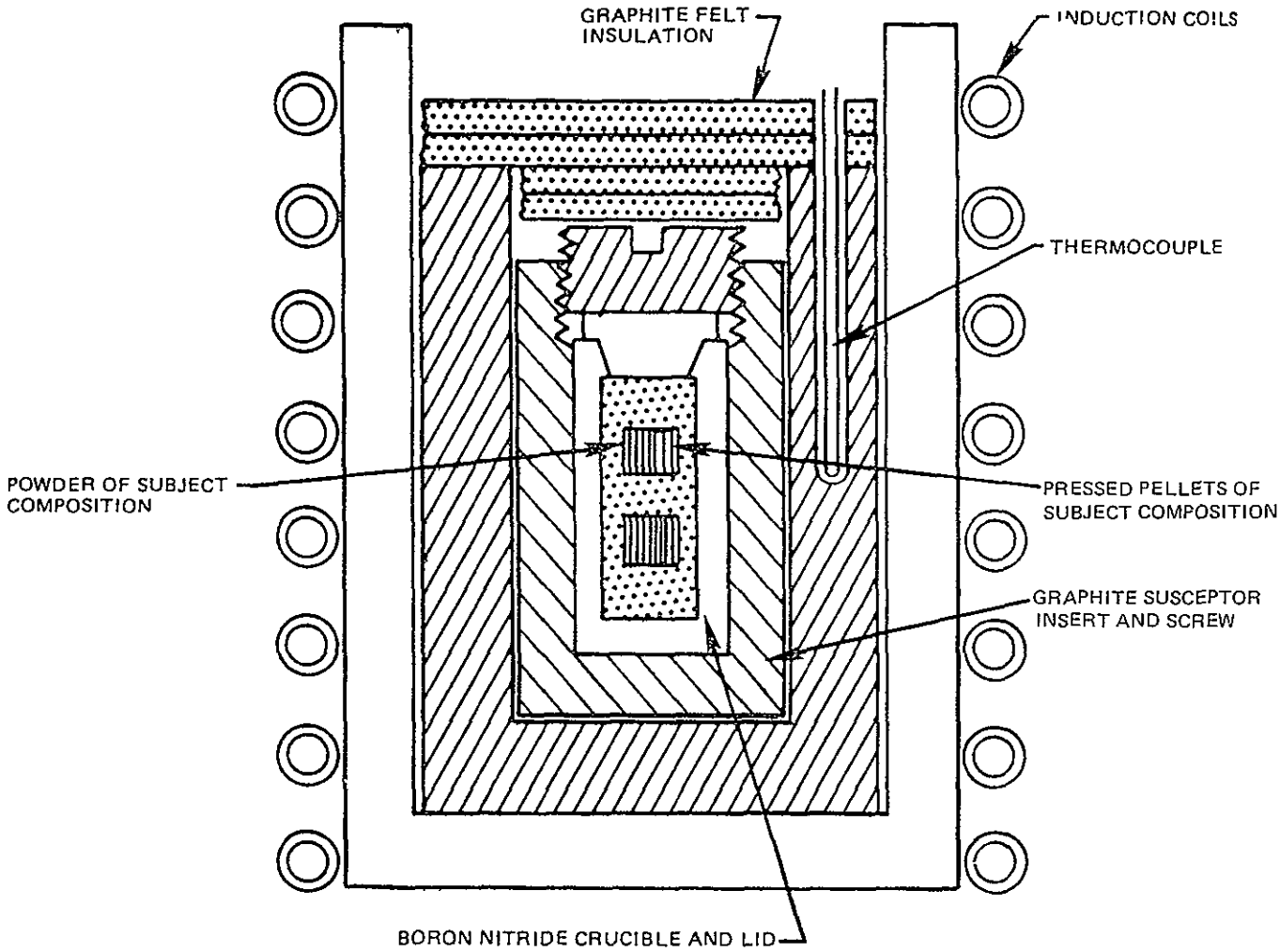

77–09–36–2

drawn. Early in the program, no thermocouples were in place during actual sample firings, and reliance was placed in the calibration curve to report the temperature. This proved unsatisfactory as will be seen shortly because of poor temperature reproducibility at a given control setting. Temperature reported on the basis of control setting are thought to be accurate to ±50°C.

In a second series of measurements, thermocouples were placed on axis in the center, or at the bottom, of a 1/2 in. ID crucible packed with alumina and the reproducibility of temperatures was checked at different variac settings. In several instances, two thermocouples were used, one at the bottom, and one in the center of the crucible. In some runs Pt-Pt/Rh thermocouples were substituted for the W-W/Re thermocouples. The third series of measurements used the same procedure as the second series, except that a 3/4 in. ID (thin walled) crucible was used. These results are listed in Table 5. It can be seen by examining these data the reproducibility of temperature for a given configuration and variac setting is about ±40°C for a given crucible configuration.

TABLE 5

VACUUM INDUCTION FURNACE
TEMPERATURE VS VARIAC SETTING FOR ORIGINAL CONFIGURATION

Variac Setting (%)	Crucible Size (ID, ")	Type of T.C. W/Re	Type of T.C. Pt/Rh	Temperature °C Center	Temperature °C Bottom
35	1/2		x	1615	
36	1/2		x	1700	
36.5	1/2		x	1675 1700 1720	
36.5	1/2	x		1640 1650	1640
37.0	1/2		x	1680 1715	
37.5	1/2		x		1730 1715
38.5	3/4	x			1850
40	1/2	x		1790	1820
40	3/4	x		1885	1915
40.5	1/2	x			1820

Runs with two thermocouples in place disclosed a temperature gradient of about 30°C across the 2 in. depth of the crucibles indicating greater heat loss from the top of the crucible. Additional insulation in the form of a circular lid 2 in. thick cast from alumina cement, with suitable holes for inserting thermocouples was fitted to the system and recalibration runs were made. Two thermocouples were used, one at either top or center, and at the bottom of a 1/2 in. ID crucible. Initial calibration runs used Pt/Rh couples, later runs, the W/Re couples. A W/Re thermocouple was then placed in a recess between the graphite susceptor and the susceptor insert (see Fig. 2), for comparison with the thermocouple in the crucible. The data obtained using the 1/2 in. ID crucible in the new furnace configuration are presented in Table 6. Because of line voltage fluctuations, it was difficult to maintain constant temperature using manual control. Examination of logs of a number of firings in which susceptor temperature was monitored indicates that a reasonble estimate of temperature control by this method was ±20°C.

An attempt was made to adopt the vacuum induction furnace to automatic control, but the circuitry proved to be unreliable and after a short time manual control was restored.

TABLE 6

VACUUM INDUCTION FURNACE
TEMPERATURE VS VARIAC SETTING FOR MODIFIED CONFIGURATION

Variac Setting (%)	Crucible Size	Type of T.C.		Temperature °C			
				Crucible			Susceptor
		W/Re	Pt/Rh	Top	Center	Bottom	
34	1/2		x		1545		1538
34	1/2		x		1569	1574	
34	1/2		x		1616	1622	
34	1/2		x	1588	1593		
36	1/2	x			1726		
38	1/2	x		1760	1770		
40	1/2	x		1727	1838		
42	1/2	x			1913		
34	1/2	x				1588	1593
36	1/2	x				1688	1693
38	1/2	x				1752	1752
40	1/2	x				1809	1818
42	1/2	x				1863	1863
38	3/4	x				1788	1794

ii. Graphite resistance furnace

A 3 ft long W/6Re - W/25 Re thermocouple, passing through a busing at the top of the alumina muffle was used to probe the temperature profile at steady state for various set points of the controller. The temperature profiles are sketched in Fig. 3. The temperature difference across the sample with the crucible positioned as shown was about 30°C at 1700°C. When available, a monitor thermocuple was placed just above the crucible. The reported temperature in this case is 40°C above the temperature indicated by the thermocouple. Once steady state was attained, temperature variations with time were undetectable with the monitor thermocouple. However because of the steepness of the gradient in the vicinity of the monitor thermocouple small variations in positioning either the thermocouple or the sample could lead to errors in the reported temperature estimated to be about ±10°C.

The initial runs using this furnace were made prior to the temperature profile measurements because a sufficiently long thermocouple was not available. It was anticipated that the temperature could be assigned with reasonable accuracy after furnace calibration was completed. However, some controller settings were altered inadvertently in the mean time so that runs made without the monitor thermocouples are thought to be accurate only at about ±50°C.

d. Sample Firing Codes

Codes describing methods used to fire specific samples and the estimated accuracy of the reported temperature are given in Table 7.

7. Grinding and Polishing of Test Bars

Fired bars were waxed to a metal plate and surface ground to a uniform thickness. The ground surfaces are then polished in lots of three or four on successively finer grit SiC papers finishing with 600 grit. They were then transferred to a nylon lap and final polished with Linde A micropolish. They were remounted with the polished faces down, and the back faces ground to final thickness (generally 0.125 in.). For flexural test specimens, bars were removed from the metal plate and edges of the polished surface polished down at a 45° angle for about 0.010 in. For oxidation test specimens, all faces were polished using Linde A.

B. Sample Characterization

1. Characterization of Prereacted and Ball Milled Powders

Phase identification of prereacted powders was made using x-ray diffractometer techniques. Particle sizes of ball milled powders were assessed by examining samples of ultrasonically dispersed powders in the scanning electron microscope (SEM).

TEMPERATURE DISTRIBUTION IN GRAPHITE RESISTANCE ELEMENT FURNACE

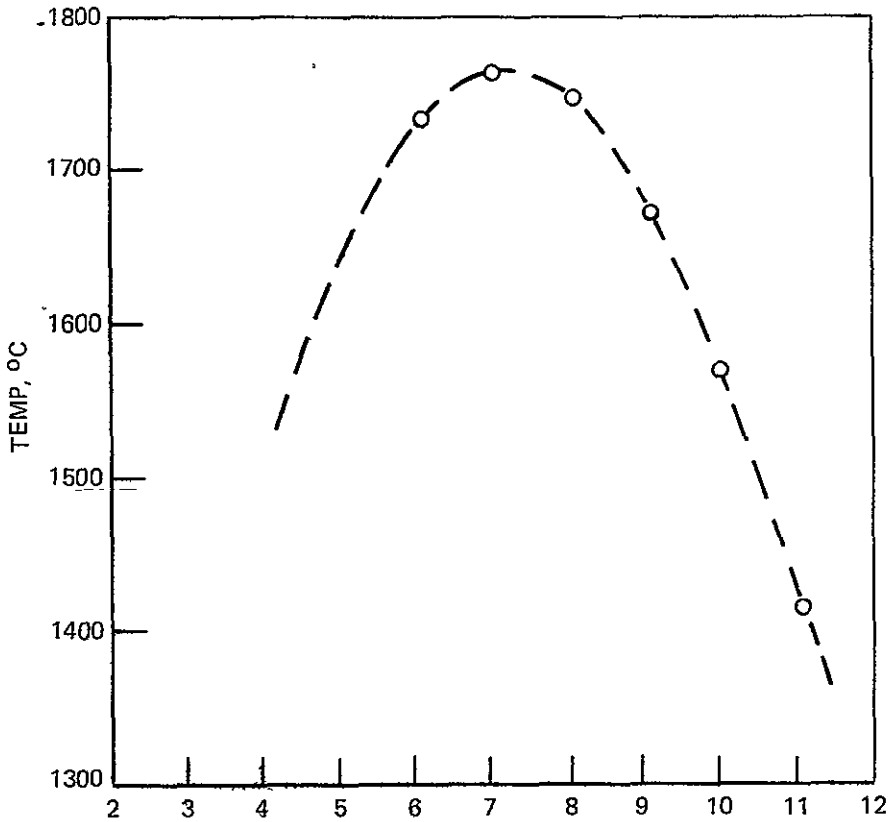

77–05–275–1

TABLE 7

SAMPLE FIRING CODES

Code	Furnace	Powder Pack	Thermocouple Monitor	Other Information	Estimated Accuracy of Reported Temperature (°C)
I a	induction	no	no	initial configuration	±50
I b	induction	yes	no		
I c	induction	no	yes	modified configuration	±20
I d	induction	yes	yes		
II a	resistance	no	no		±50
II b	resistance	no	yes		±10

a. Evaluation of Weight Changes During Powder Prefiring

Weight change experiments were run on dried and prefired batch materials in order to determine whether the low temperature air firings resulted in measurable oxidation of the prepared powders. Platinum crucibles were heated in air to 600°C, cooled to room temperature in a desicator, then weighed. About 2 to 4 grams of material of a prepared batch of compositions β'1 + 2.5 percent w/o (.75 ZrO_2, .25 Y_2O_3) were placed in the crucibles which were then heated to 125°C for 1 hour, cooled to room temperature in a desicator and weighed again. Crucibles were then heated in air to temperatures of 500, 550, 600, and 650° for periods of 1 hour, cooled in the desicator and reweighed.

2. Characterization of Sintered Samples

Bulk density, specific gravity, and apparent porosity of sintered specimens were determined by ASTM test C373-5. Microstructures were examined on polished and etched sections of test samples. Thermal stability was assessed qualitatively on the basis of the amount of decomposition observed at different firing temperatures. In selected instances, x-ray diffraction patterns were obtained either from the surfaces of test bars or from crushed and ground samples.

a. Mechanical Testing

Room temperature testing was performed in four point flexure using inner and outer spans of 0.375 in. and 0.75 in., respectively. Cross head speed was 0.02 in./min. Tests at 1370°C were performed in three point flexure using a span of 0.75 in. and a cross head speed of 0.02 in./min. Test atmosphere was argon, the lower sample supports were alumina, and the loading nose was a tungsten bar. Fracture surfaces of selected test specimens were examined in the scanning electron microscope. Flaws that initiated failure were examined in EDAX (energy dispersion analyses of x-rays) and the scanning electron microprobe. Creep testing was done in three point flexure at a stress level of 10,000 psi in argon atmosphere.

b. Oxidation Testing

Samples prepared as described earlier were placed on a platinum tray so fashioned that the samples were contacted along two lines only. The tray was introduced into a preheated oven and removed periodically, cooled to room temperature and weighed. Following the oxidation tests, x-ray diffraction patterns were obtained from oxidized surfaces, and the samples were photographed. In most instances the samples were then mounted in resin, polished to give a cross sectional view of the oxide scale, and examined metallographically. X-ray fluorescent scans were made to show the distribution of elements in the neighborhood of the oxide scales.

SECTION IV

RESULTS AND DISCUSSION

A. Preliminary Screening Experiments

1. General Observations

A number of the β' compositions listed in Table 1, both with and without various sintering aids listed in Table 3, were prepared using process 1 of Table 4. These were compacted into either cylinders or rectangular bars and fired for various lengths of time at a nominal temperature of 1725°C using either firing code Ia or Ib of Table 7. Cylindrical pellets were evaluated by ASTM C373-56 procedures, by metallographic examination, and by x-ray diffraction. In selected cases lattice parameters were determined by the Nelson-Riley extrapolation technique. In addition to the above evaluations, rectangular bars were tested in 4 point flexure as described in Section III.B.2.a.

Fabrication and property data pertaining to sintered pellets of basic β' solid solutions and β' compositions doped with selected sintering aids are recorded in Table 8. The lattice parameters and theoretical (x-ray) densities of β' compositions are recorded in Table 9. Fabrication and property data pertaining to samples prepared as modulus of rupture specimens are presented in Table 10.

Bulk densities measured by the ASTM water immersion test, divided by the x-ray density are used to calculate the percent theoretical density of sintered pellets. Porosities estimated by statistical metallographic techniques are in reasonable agreement with values measured by the ASTM test and with the calculated percent theoretical densities, although they tend to be somewhat high, perhaps indicating a tendency for pull-outs during metallographic preparation.

2. Unadmixed β' Compositions

Micrographs of β' composition 7 fired for 1/2 hour and 4.5 hours are shown in Fig. 4. A grain boundary phase can be distinguished in the polished sections after etching with HF. The x-ray results (Table 8) would seem to indicate that this composition lies just outside of the homogeneity range of β'. Comparison of the apparent (open) and total porosity data given in Table 8 show that the gradual elimination of open porosity as sintering proceeds. The micrographs show that this is accompanied by grain growth and the tendency toward consolidation and spheroidization of pores. The trend would indicate that little further densification would occur with longer heat treatment at 1725°C. All of the other unadmixed β' compositions listed in Table 8 appeared to be single phase metallographically and x-raywise. The porosity and pore distribution of these samples were typified by the lower micrograph of Fig. 4.

TABLE 8

FABRICATION AND PROPERTY DATA FOR SINTERED PELLETS
(Early Screening Experiments)

Composition	Firing Time[1] (hrs)	Weight Loss (%)	Phases Determined by X-Ray Diffraction	ASTM C373-56 Apparent Porosity (%)	ASTM C373-56 Specific Gravity (g/cc)	ASTM C373-56 Bulk Density (g/cc)	Metallographically Determined Porosity	Calculated Percent Theoretical Density
β'5	3	< 2.5	strong β' only					
β'7	0.5	1.0		2.2	3.11	3.41	36	78
β'7	2	1.5		10	2.99	2.69	23	87
β'7	4.5	< 2.5	β' + trace Al_2O_3 and Y	1	2.65	2.62	17	85
β'5	3		β' (Table 9)					
β'6	3		β' (Table 9)					
β'3	3		β' (Table 9)					
β'2	3		β' (Table 9)					
β'5 + 5 $GaPO_4$	3		β' + trace cubic[2]				< 5	
β'7 + 5 $GaPO_4$	3		β' + trace cubic[2]				< 5	
β'5 + 2.5 $AlPO_4$	3		β' + U_1[3]				< 5	
β'5 + 4 Y_2O_3	3		β' + U_2[4]				< 5	
β'5 + 4 ZrC	3		β' + ZrC				< 5	
β'5 + 4.5 ZrO_2	3		β' + ZrO_2				< 5	

(1) 1750°C, Firing code I, Table 7

(2) Faint cubic pattern could be due to Si or GaP

(3) Extraneous d spacings are listed in Table 11

(4) Extraneous d spacings are listed in Table 12

TABLE 9

X-RAY DATA FOR SOME BASIC β' SOLID SOLUTIONS

β' Composition Number	a (Å)	c (Å)	V (A°3)	Formula Weight	ρ (g/cc)
0	7.606	2.909	145.7	140.35	3.20
2	7.623	2.936	147.8	140.85	3.16
3	7.647	2.950	149.4	141.10	3.14
5	7.658	2.987	151.7	141.40	3.10
6	7.706	2.985	153.5	141.75	3.07

3. Effect of Additions

a. $GaPO_4$ and $AlPO_4$

Basic β' compositions containing 5 percent $GaPO_4$ plus a pellet of unadmixed β' were fired simultaneously in a three position graphite susceptor insert. All of the samples including the control were found to have densified to over 90 percent density as judged from the micrographs (Fig. 5). It may be assumed that vapor phase transport of constituents of the doped samples effected the undoped samples. An excess of metallic inclusions is observed in Fig. 5, and a faint cubic pattern that could be attributed to GaP (or Si) was observed on the diffractometer trace.

The micrographs of the $AlPO_4$ doped sample are shown in Fig. 6. The low magnification picture shows that the material has sintered to high density with extensive areas of zero porosity more or less evenly distributed over the entire area of the sample. The high magnification micrographs of an area of zero porosity shows this to be essentially devoid of contrast except for the occasional metallic inclusions. There is no readily discernable difference in appearance between etched and unetched samples.

Faint x-ray reflections due to the presence of another foreign phase or phases could be observed in the diffractometer trace of the $AlPO_4$ doped sample but these have not been identified. The d-spacings of the minor phase are given in Table 11.

TABLE 10

FABRICATION AND PROPERTY DATA FOR SINTERED BARS,
INITIAL SCREENING EXPERIMENTS

Composition	Firing Code (1)	Weight Loss (%)	ASTM C373-56			Metallographically Determined Porosity (%)	Calculated Percent Theoretical Density	Modulus of Rupture (psi)
			Apparent Porosity (%)	Specific Gravity (g/cc)	Bulk Density (g/cc)			
β'5+ 2.15 $AlPO_4$	Ib					5		31,000
β'5+ 4 Y_2O_3	Ib		0	3.07	3.07	1	99	
β'5+ 4 Y_2O_3	Ia	1.9	0	3.06	3.06	< 1	98	27,000
β'5+ 4 Y_2O_3	Ia	1.1	0	3.01	3.01	6	97	33.000
β'5+ 4 Y_2O_3	Ia	1.1	0			5		35,000
β'5+ 4 Y_2O_3	Ia	0.5	0	2.95	2.95	6	95	33,000
β'5+ 4 ZrC	Ib		0.67	3.02	3.02	6	97	22,000
β'5+ 5 CeO_2	Ib		0.4	3.13	3.13	< 1	100	41,000
β'5+ 3$GaPO_4$	Ib		0.5	3.07	3.08		99	30,000
β'6+ 3$GaPO_4$	Ib		0.4	3.06	3.07		100	21,000
β'3+ 3$GaPO_4$	Ib		0.4	3.06	3.07		97	29,000
β'2+ 3$GaPO_4$	Ib		5	2.87	3.02	15	90	23,000

(1) 1750°C for 3 hours.

FIG. 4

MICROGRAPHS OF β' COMPOSITION 7, FIRED FOR DIFFERENT LENGTHS OF TIME AT 1725C

1/2 HR

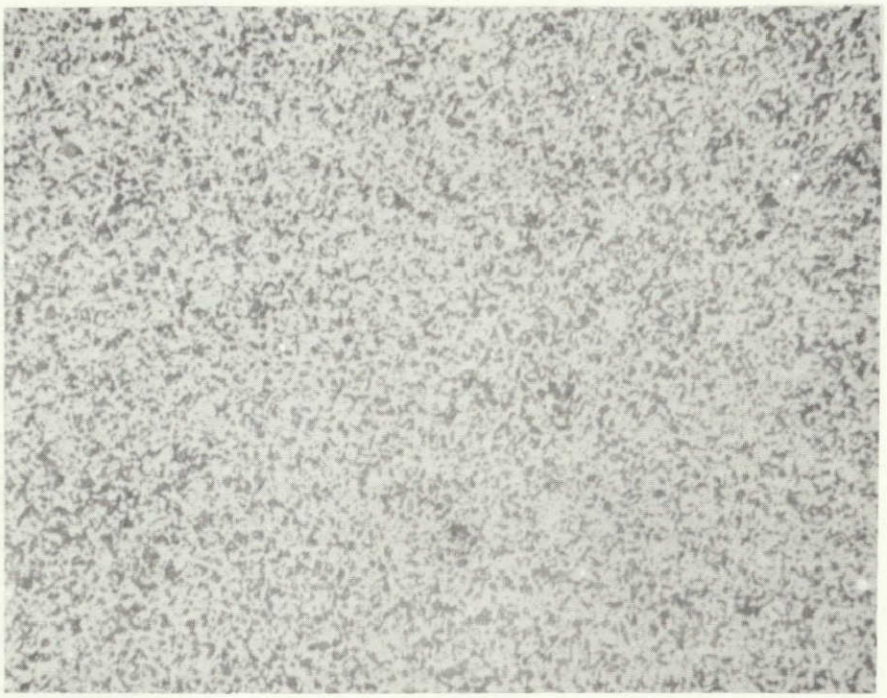

50 μ

4 1/2 HR

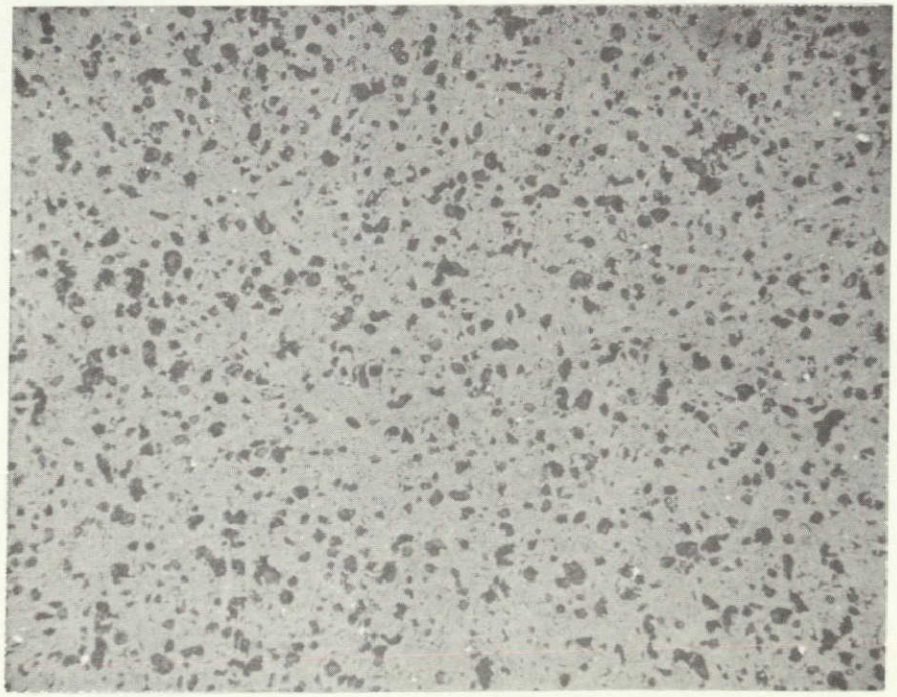

50μ

R 07–50–1

FIG. 5

MICROGRAPHS OF SINTERED PELLET OF COMPOSITION
$\beta'5 + 5\ GaPO_4$

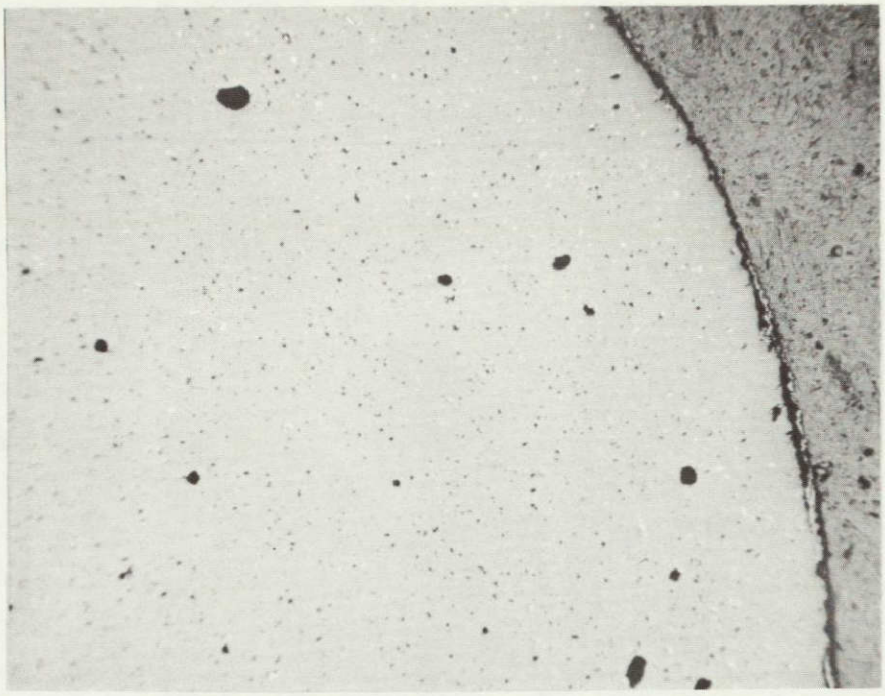

200 μ

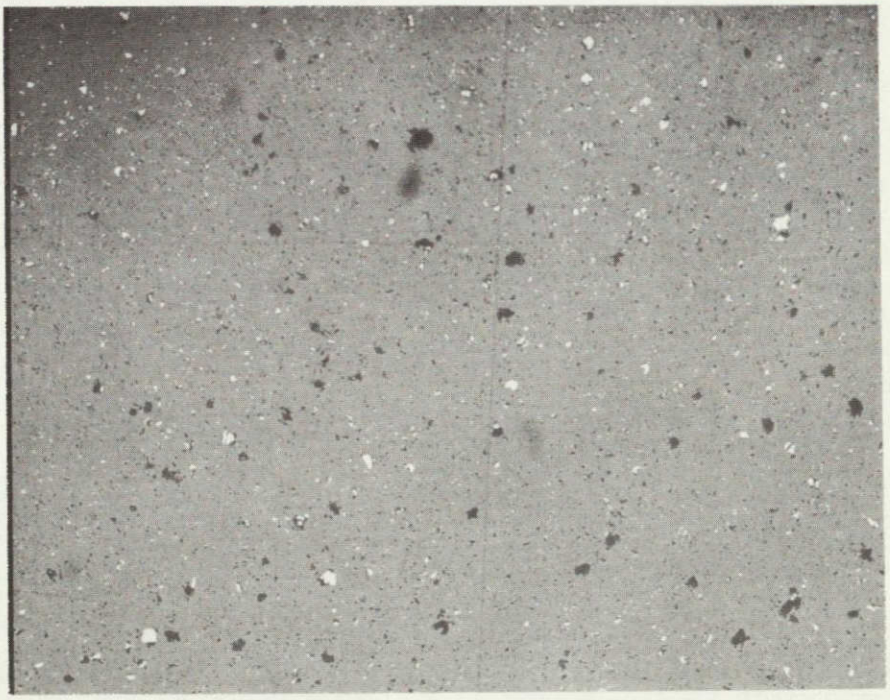

50 μ

FIG. 6

MICROGRAPHS OF SINTERED PELLET OF COMPOSITION
$\beta''5 + 2.5\ AlPO_4$

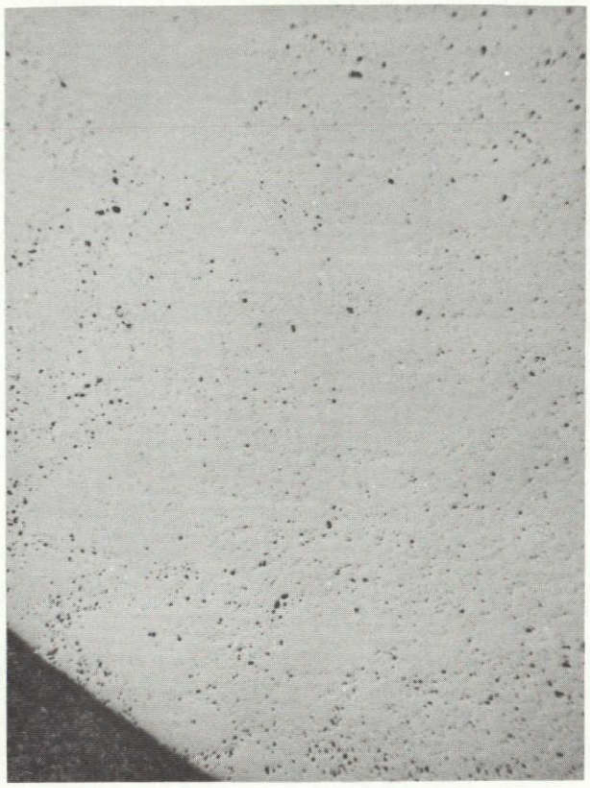

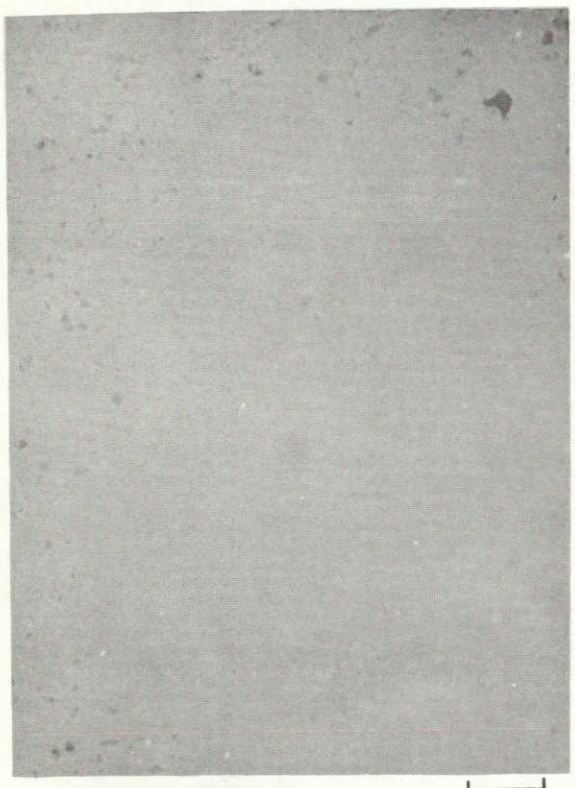

POLISHED

50 μ

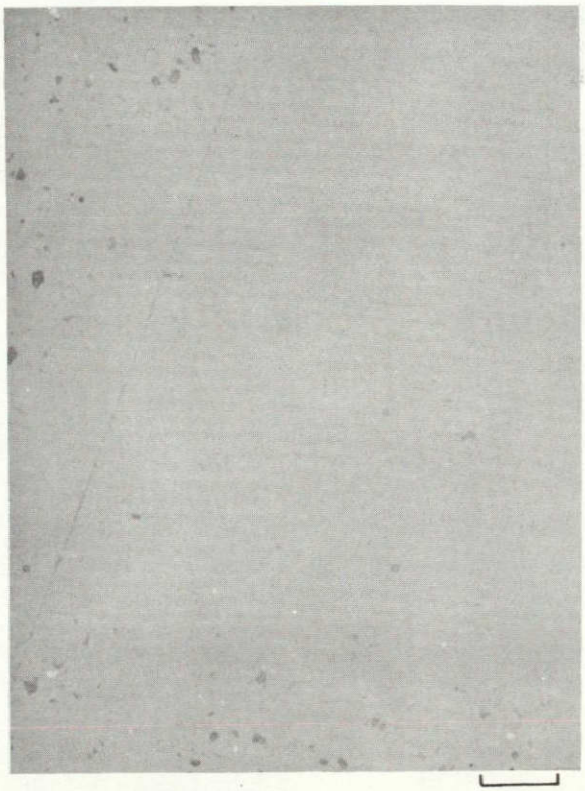

HF ETCHED

50 μ

R08–50–1

The reactions that lead to enhanced sintering have not been identified. Strength values for the samples containing both $AlPO_4$ and $GaPO_4$ (Table 10) were very low (21,000 to 31,000 psi), possibly as a result of the excessive amount of metallic inclusions in these samples.

TABLE 11

DIFFRACTION PATTERN d-SPACINGS FOR EXTRANEOUS PHASE U_1
IN $AlPO_4$ DOPED β'5

d(Å)
5.64
4.00
3.04
2.82
3.03

b. Y_2O_3 and CeO_2

Micrographs of a Y_2O_3 doped sample shown in Fig. 7 disclosed that, except for some very large isolated pores, the sample had sintered to a uniformly high density. The higher magnification micrographs appear to show a fine dispersion of second phase materials. X-ray diffraction patterns for the Y_2O_3 bearing sample show a faint pattern not belonging to the β' phase, but this was not identified. The extraneous d-spacings are given in Table 12. The average strength of the four Y_2O_3 bearing sample (33,000 psi), though somewhat above the average of all the samples screened (29,500 psi), still reflects the rather poor quality of these early samples. The CeO_2 bearing

TABLE 12

d-SPACINGS FOR EXTRANEOUS PHASE U_2
IN Y_2O_3 DOPED β'5

d(Å)
2.56
2.32
2.02

FIG. 7

MICROGRAPHS OF SINTERED PELLET OF COMPOSITION $\beta''5 + 4\ Y_2O_3$

200 μ

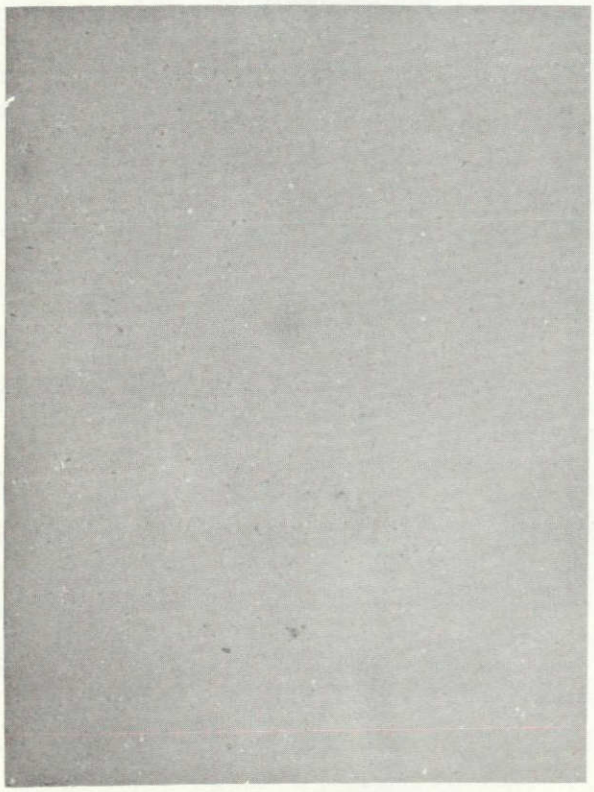

POLISHED

50 μ

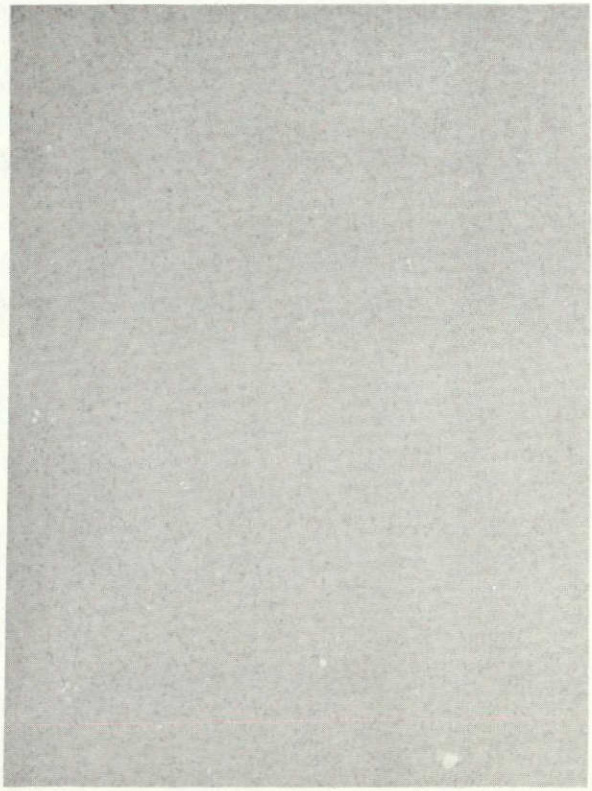

HF ETCHED

50 μ

R08–50–4

sample was similar to the Y_2O_3 bearing sample in polished section. No extraneous diffraction lines were observed in the x-ray pattern. The strength of this sample (41,000 psi) was the highest of early samples.

c. ZrC and ZrO_2

Micrographs of the ZrC bearing samples (Fig. 8) show that the material sintered to a reasonably high density and disclose a dispersed second phase which appeared to be preferentially etched by HF. A faint cubic pattern with lattice parameter slightly shifted from that of ZrC was identified in the x-ray pattern. Despite the good densification of the ZrC bearing sample, the strength value was very low (22,000 psi). The ZrO_2 bearing sample was similar in polished section to the ZrC bearing sample. The x-ray diffraction pattern exhibited weak reflections at 3.162 and 2.838Å that could possibly be the $(11\bar{1})$ and (111) reflections from monoclinic ZrO_2.

4. Summary of Screening Experiments

Prereacted β' SiAlON solid solution compositions sintered to about 85 percent of theoretical density when fired in nitrogen atmosphere in a pseudo-closed system to 1725°C for a period of 3 hours. The same compositions, to which various sintering aids were added, sintered to near theoretical density under similar conditions. Sintering aids investigated included $AlPO_4$, $GaPO_4$, ZrC, ZrO_2, Y_2O_3, and CeO_2. In all the samples containing additives studied, additional phases could be observed in optical micrographs, however, these could not always be observed (or identified) in the x-ray diffraction patterns. In the cases of $AlPO_4$ and $GaPO_4$, a high concentration of isolated metallic inclusions was present, and in the case of ZrC, isolated carbide inclusions were observed as well as unidentified grain boundary phases. It is probably not coincidential that the samples containing high concentrations of inclusions exhibited the lowest strengths (21,000 psi for one $GaPO_4$ doped sample, 22,000 psi for ZrC). Somewhat higher strengths were exhibited by $AlPO_4$ (31,000 psi) and Y_2O_3 (32,500 average of four tests). The highest strength was exhibited by the CeO_2 doped sample (41,000 psi).

B. Processing Refinements

The initial screening experiments indicated that densification of β' solid solutions was enhanced by a number of sintering aids. The most effective of those investigated as judged by microstructure and room temperature modulus of rupture was CeO_2. Studies were undertaken to improve the microstructure and mechanical properties of β' solid solution - CeO_2 samples.

FIG. 8

MICROGRAPHS OF SINTERED PELLET OF COMPOSITION
$\beta'5 + 4$ ZrC

200 μ

POLISHED

50 μ

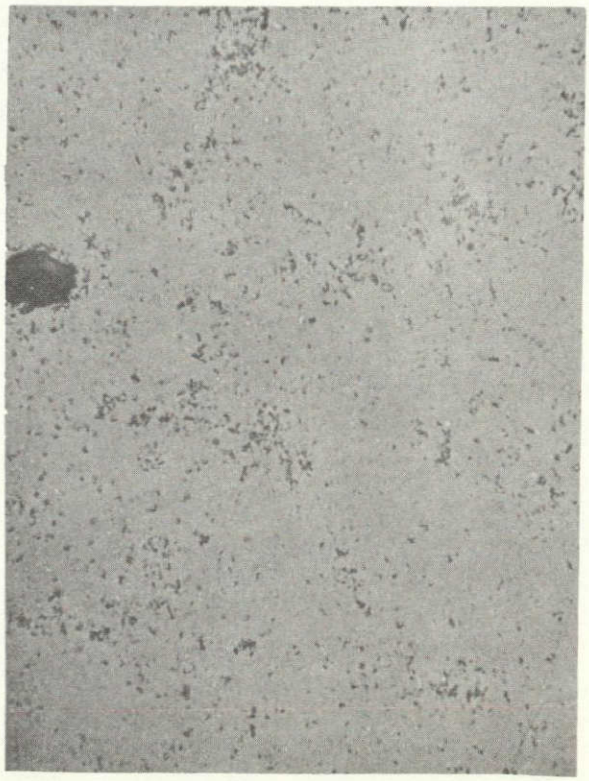

HF ETCHED

50 μ

R08–50–3

1. Ball Milling and Particle Size Effects

a. Stage 1 Formulations - Porcelain Mill Jars

β' compositions and CeO_2 were processed as shown in Table 13. Pulverization of the prereacted β' powders was done in the Cole Palmer mill, and an attempt was made magnetically to remove iron particles introduced by the mill. Ball milling of pulverized prereacted powders was done in size 000 Roalox porcelain jars filled with about 250 grams Burundum grinding media, 50 grams of sample, and sufficient methanol to cover the charge. Samples of several of the various powders listed in Table 13 were examined in the scanning electron microscope. SEM micrographs of a prereacted and ground β' composition, and of cerium oxide (calcined cerium oxalate) both before and after ball milling for 168 hours are shown in Figs. 9 and 10, respectively. The -200 mesh (75μ opening) prereacted β' materials appeared to consist of roughly isodimensional fragments ranging in size from about 25 to 0.25μ. The as-calcined CeO_2 appeared to range from plates roughly 10 x 10 x 1μ to small fragments on the order of 0.1μ. After milling for 168 hours, both the β' and the CeO_2 powders consisted mainly of submicron material, but some larger fragments up to about 5μ still remained.

TABLE 13

PROCESSING OF SOME β' AND CeO_2 BATCHES

Batch Number	Processing
β'5a	Mixture of Si_3N_4, Al_2O_3 and AlN milled in methanol, 18 hours
β'5b	β'5a reacted at 1650°C for 1 hour, pulverized and sieved to -200 mesh
β'5c	β'5b ball milled for 168 hours
β'6b	Prereacted at 1650°C for 1 hour from Si_3N_4, Al_2O_3 and AlN, pulverized, and sieved to -200 mesh
CeO_{2a}	Calcined cerium oxalate
CeO_{2b}	CeO_{2a} ball milled 72 hours
CeO_{2c}	CeO_{2a} ball milled 168 hours

MICROGRAPHS OF PRETREATED β' PARTICLES

a) PULVERIZED, 200 MESH

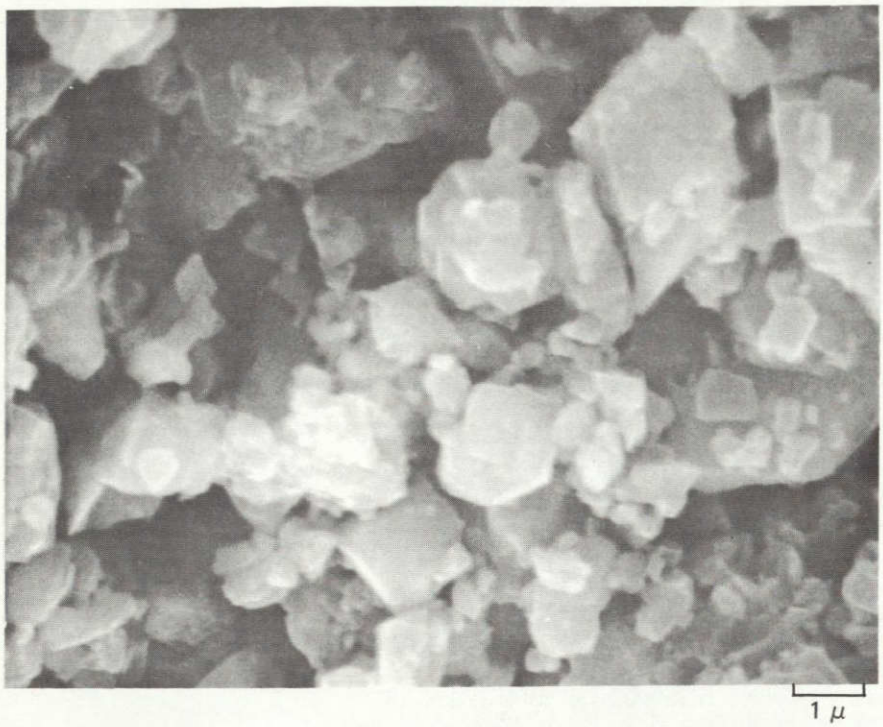

b) BALL MILLED FOR 168 HRS

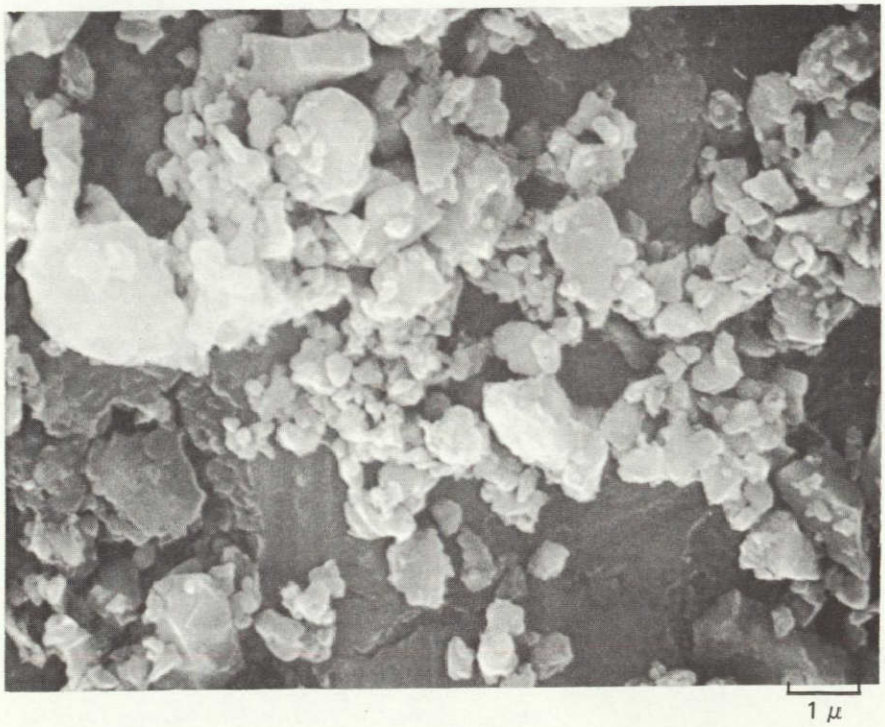

R12–124–4

FIG. 10

MICROGRAPHS OF CeO_2 PARTICLES

a) CALCINED CERIUM OXALATE

b) BALL MILLED FOR 168 HRS

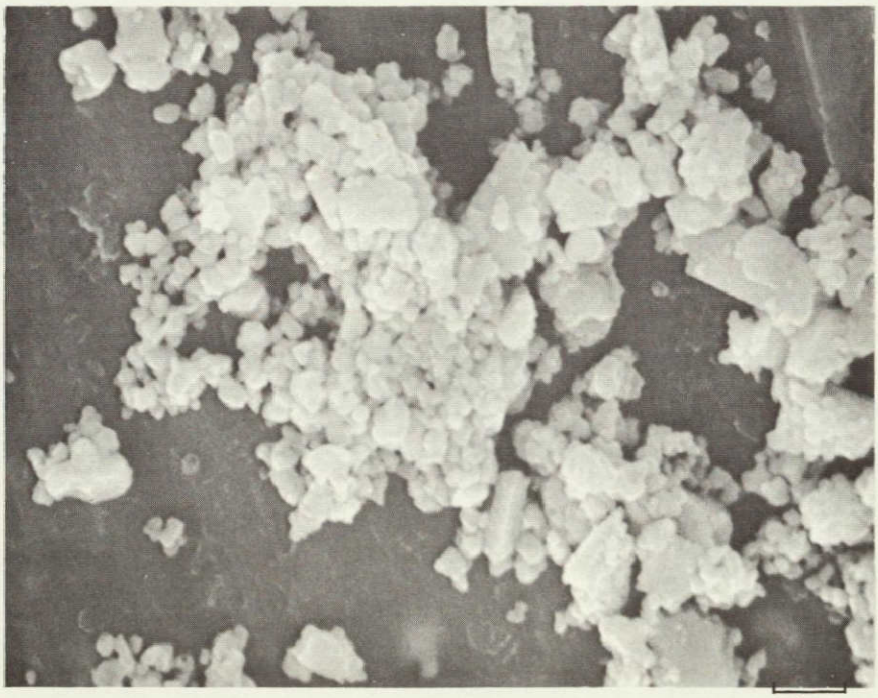

R12–124–3

Mixtures of the various β' and CeO_2 powders listed in Table 13 were blended, tray dried, compacted into bars and fired. The mixtures, mixing procedures, and firing conditions, as well as observations and test results are given in Table 14. Micrographs of polished surfaces of selected test bars are shown in Figs. 11 and 12. Examination of the test data and micrographs shows that samples were generally of poor quality. All of the samples that were prepared from the submicron prereacted β' and CeO_2 (168 hours milling times) were warped, bloated and worthless for mechanical testing even when fired in the modest temperature of 1600°C. The samples prepared from prereacted β' compositions which were pulverized to -200 mesh in the hammer mill but not ball milled, then mixed with CeO_2 that had been milled for long times showed a bimodal porosity distribution with reasonably uniform fine porosity distribution plus a small number of large voids (Fig. 12a). A small number of large voids in an otherwise dense matrix was also characteristic of samples blended from unreacted β' constituents which had been milled for 18 hours and CeO_2 which had been milled for long times (Fig. 11b). Samples prepared from the prereacted, pulverized, but unmilled powders had uniformly distributed porosity (essentially zero in the case of sample 127) as shown in Figs. 11a and 12b. (Also note in the above micrographs the variability in the size and amount of highly reflective metallic inclusions in the samples. These probably account for the very low strength of samples 125, 126 and 127 despite their high densities. The problem of metallic inclusions will be discussed latter.)

The fact that samples that had been ball milled for extended periods of time using Burundum media in Roalox jars warped and bloated when fired, whereas unmilled samples of identical composition did not, indicates that a large amount of contamination by low melting constituents was picked up from the mill. This observation led to the stage 2 formulations and modified milling procedures described in Section III. It was also observed during tray drying of ball mill charges that had been milled for extended periods of time that segregation took place on the basis of particle size that led to sample inhomogeneity. The large voids in samples 97 and 101, for instance, are thought to be the result of the presence of aggomerates of low melting constituents. This led to adoption of the spray drying techniques for mill charges described in Section III.A.3.c.

b. Particle Size Separations

Batches of β' compositions 2 and 6 were formulated, anticipating Burundum media contamination after periods of milling of 7 hours and 40 hours under standard conditions in methanol using polyethylene jars. The batches were prefired at 1650°C for 2 hours in nitrogen atmosphere. X-ray analysis of the prefired material showed that β'6 consisted largely of β' solid solution plus trace amounts of $SiAl_4O_2N_4$ and unreacted Al_2O_3. Composition β'2 on the other hand remained predominantly unreacted α Si_3N_4 with a small amount of β' solid solution. This composition was reground and fired to 1700°C for two hours, and was also found to be largely α phase after firing.

TABLE 14

FABRICATION AND TEST DATA FOR BARS PREPARTED FOR VARIOUS β' - CeO_2 BATCHES

Sample Number	Composition[1]	Mixing[2] Procedure	T (°C)	Time (hrs)	Code	Metallographic Observations — General	Concentration of Metallic Inclusions	Bulk Density	% Theoretical Density	Modulus Rupture ksi
93								2.96	92	33
94	β'5b + 5CeO_2a	A	1750	3	Ia	Uniformly distributed porosity (< 20μ)	Very low	2.93	91	25
95								2.87	89	23
97								3.17	98	33
98	β'5a + 6CeO_2b	A	1750	2	Ib	Few large pores (to 30μ)	low	3.14	97	28
99								3.10	76	35
101										
102	β'5b + 6CeO_2b	A	1750	1.5	Ib	Bimodal porosity (fine uniformly distributed, + large lenticular voids)	absent	N O T T E S T E D		
103										
105										
106	β'5C + 6CeO_2C	B	1750	2	Ib	Warped and bloated	high	N O T T E S T E D		
107										
109										
110	β'5C + 6CeO_2C	B	1600	2	Ib	Warped and bloated	absent	N O T T E S T E D		
111										
125								3.17	100	14
126	β'6b + 5CeO_2a	A	1750	3	Ib	Fully dense	high	3.29	(100)	20
127								3.10	98	28

(1) See Table 13.

(2) A. Ball Milled 18 hours, tray dried.
B. Ball Milled 2 hours, tray dried.

FIG. 11

MICROGRAPHS OF POLISHED SURFACES OF TEST BARS

(SEE TABLE 14,p35)

a) SAMPLE 95

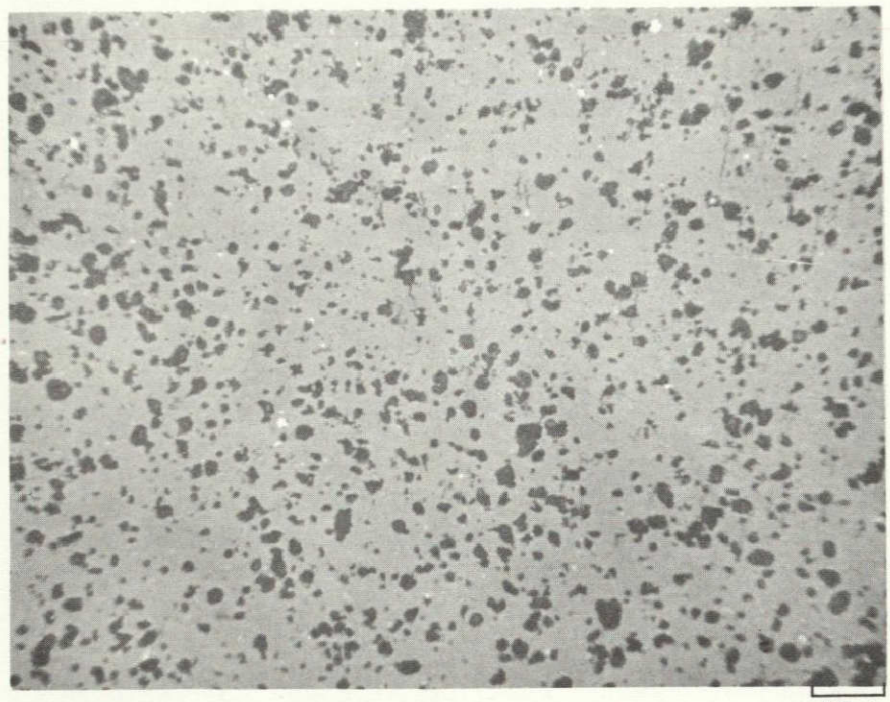

b) SAMPLE 97

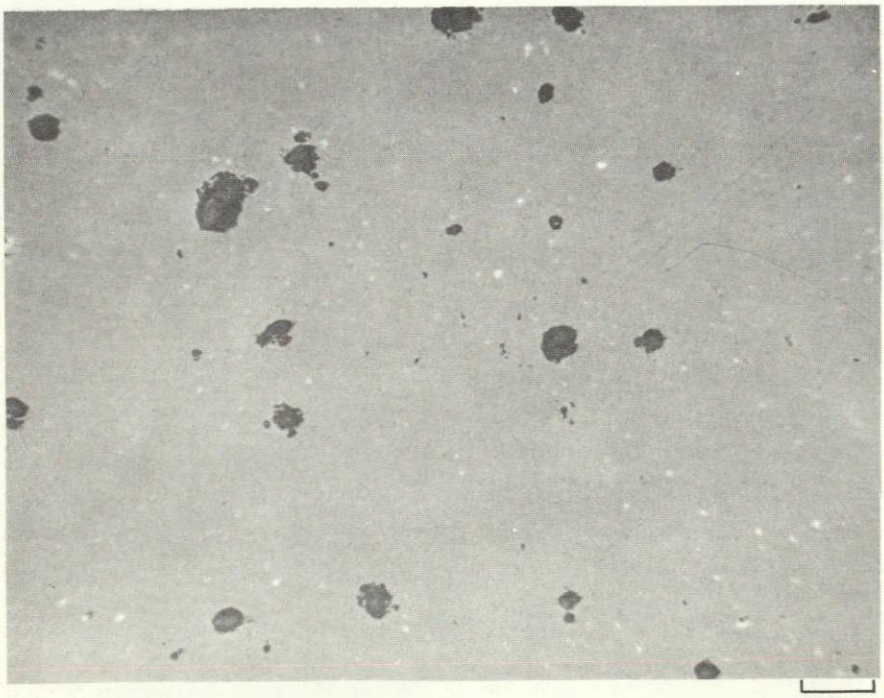

R12–124–1

FIG. 12

MICROGRAPHS OF POLISHED SURFACES OF TEST BARS

SEE TABLE 14,p35

a) SAMB 101

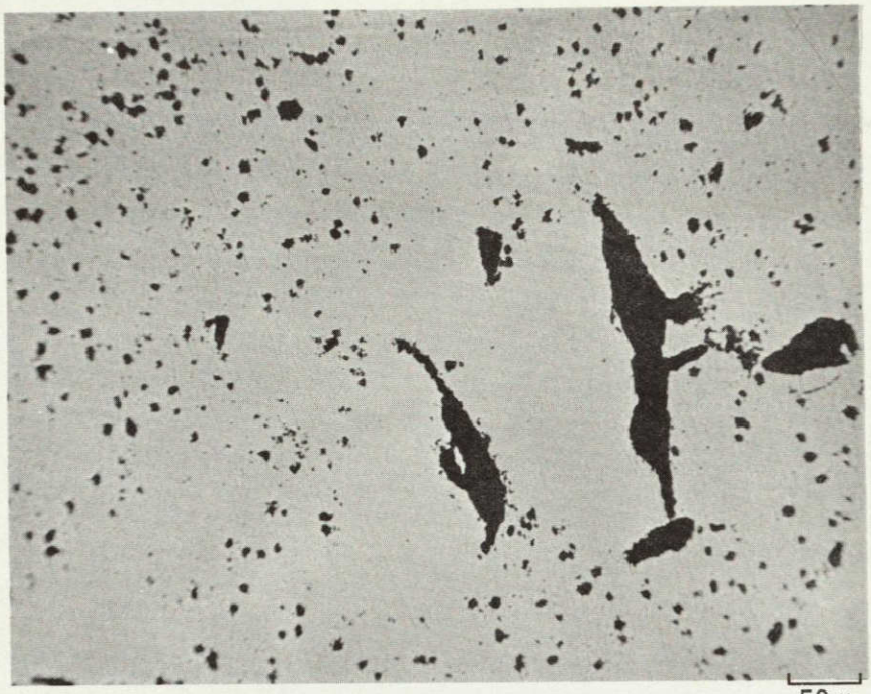

b) SAMB 127

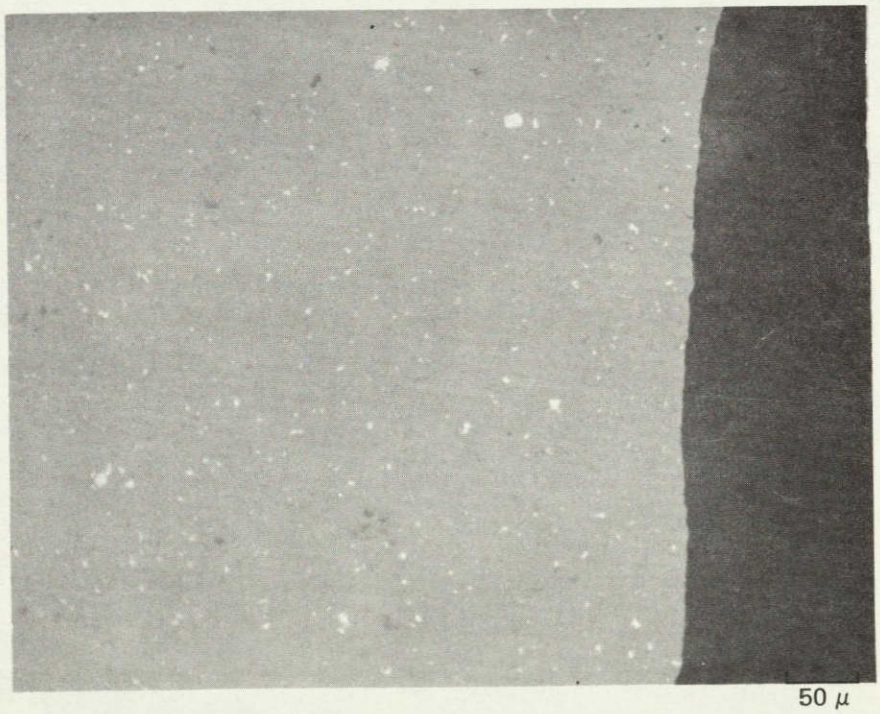

R12–124–2

These prereacted mixtures were passed through the pulverizing mill and through a 200 mesh screen, then ball milled for the predetermined length of time, and spray dried. Scanning electron micrographs of these prereacted and ball milled β' powders are shown in Fig. 13. Some of these materials were retained for sintering experiments to be described shortly, while some of the materials were given additional milling and various particle size fractions were separated by sedimentation as described in Section III.A.4.a. Scanning electron micrographs of composition β'2 particles decanted from suspension after standing for different lengths of time are shown in Fig. 14.

Ten weight percent additions of CeO_2 were made to approximately 12 gram portions of the various size fractions of β' compositions. There were ground under acetone in an agate mortar for about 10 minutes, then dried and hydrostatically pressed into 1/4 in. diameter pellets at 40,000 psi. Additional pellets of the various compositions without the CeO_2 addition were made to serve as controls. Samples were fired according to code Id of Table 7. Firing conditions and observational data for sintered pellets of the various prefired β' powders, with and without additions of CeO_2 are recorded in Table 15. Data for the extraneous phase observed in x-ray pattern of prereacted $\beta'2_{40}$ composition are listed in Table 16. Microstructures of various samples are shown in Figs. 15 through 20.

With the exceptions of the fine fractions of compositions $\beta'6_7$ and $\beta'6_{40}$, all of the pellets fired without the CeO_2 additions showed little densification. All of the pellets which contained the CeO_2 additions, including those made from the coarse β' fractions (Fig. 20), showed enhanced densification with large areas essentially pore free. A characteristic of all the dense microstructures was the occurrence of relatively large isolated pores which suggest that there were inhomogeneities in the powder mixtures. Other aspects of the microstructures, particularly those relating to differences between β'2 and β'6 will be discussed later. As regards the homogeneity of microstructures, it is postulated that material worn from the media and mill jars was ground to a finer average particle size than the very hard β' material. During the particle size separation the finely ground aluminosilicates became concentrated in the fine (decanted) particle size fractions thus throwing both the course and fine fractions off stoichiometry even though the total batch before separation may have been properly compensated for media wear. In the process of centrifuging down the fine fractions further segregation could occur leading to inhomogeneities that were not removed by the 10 minutes of hand grinding under acetone using the mortar and pestal.

c. Stage 2 Formulations, Polyethylene Mill Jars

The results described above indicated the effectiveness of CeO_2 in promoting sintering, and of the need for more careful preparative techniques to insure uniformity of the milled powder mixtures. The previous experiments indicated that sedimentation to separate out the fine particle fraction was undesirable since this concentrated the material worn from the grinding media in the fine fraction such

FIG. 13

PREREACTED β' 6 COMPOSITION MILLED FOR DIFFERENT LENGTHS OF TIME IN POLYETHYLENE JARS USING BURUNDUM MEDIA

A. 7 HRS

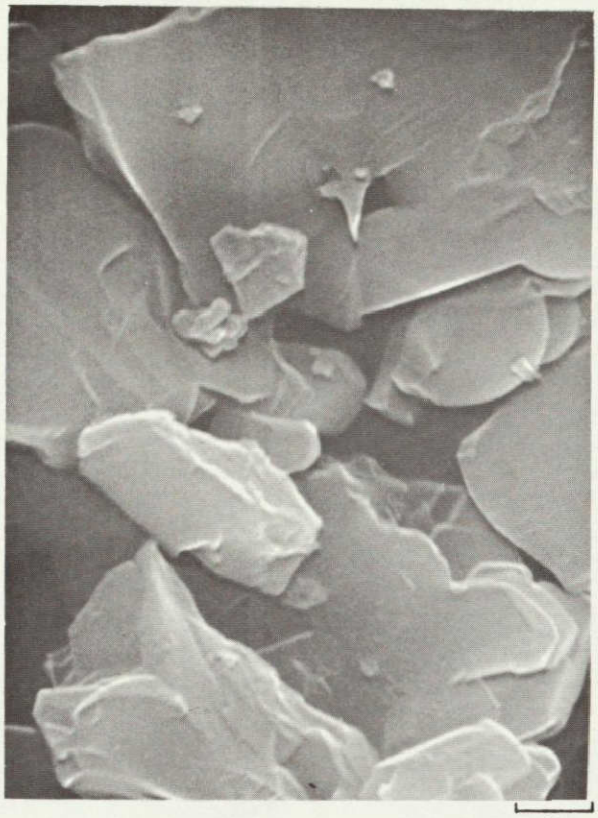

B. 40 HRS

FIG. 14

$\beta'2$ DECANTED FRACTIONS

A. DECANTED AFTER STANDING 16 HRS

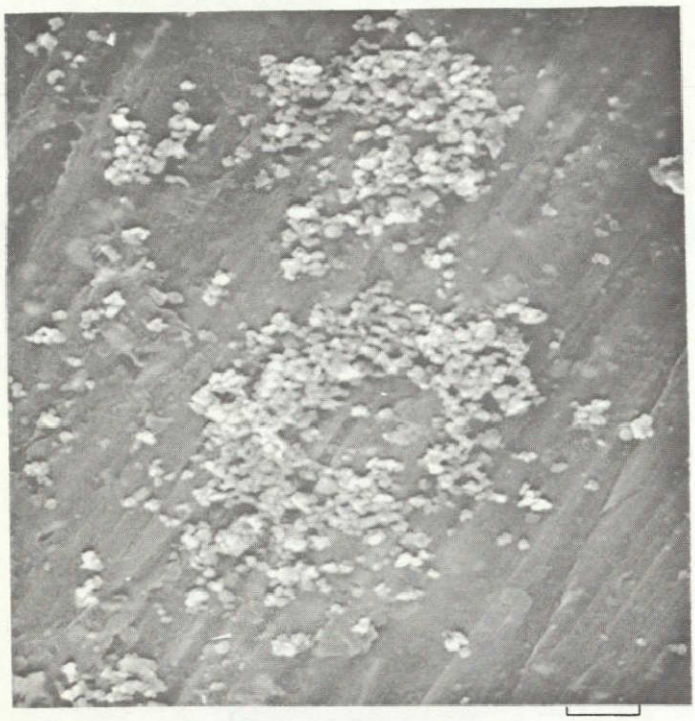

5μ

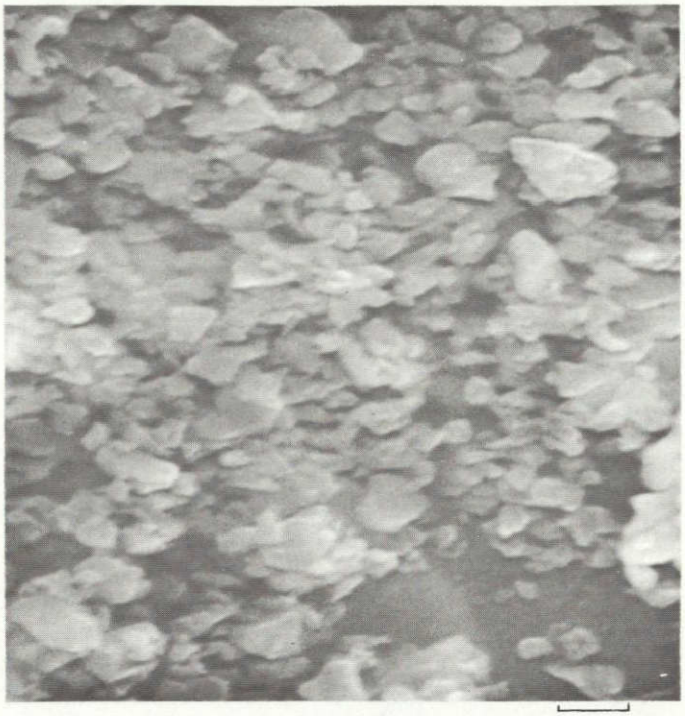

1μ

B. DECANTED AFTER STANDING 3 HRS

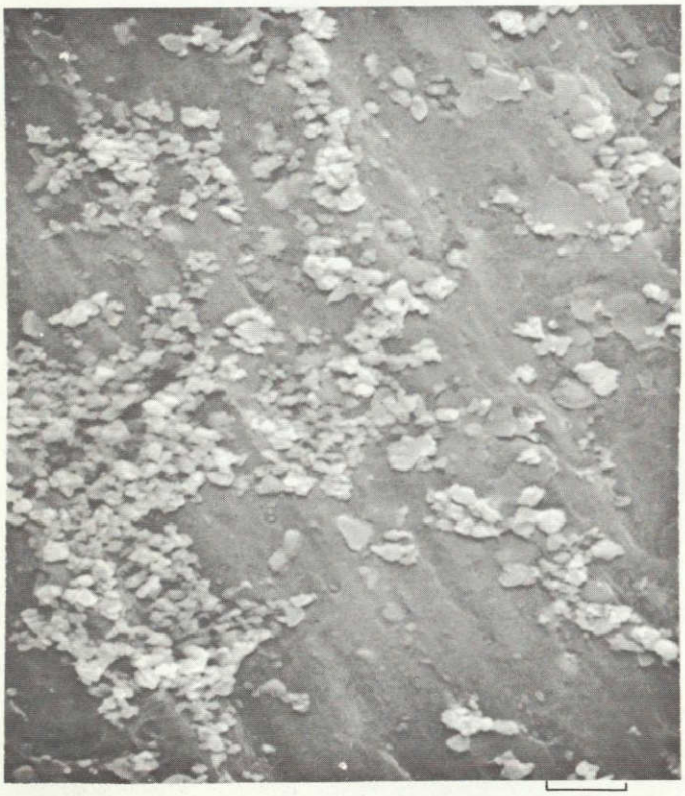

5μ

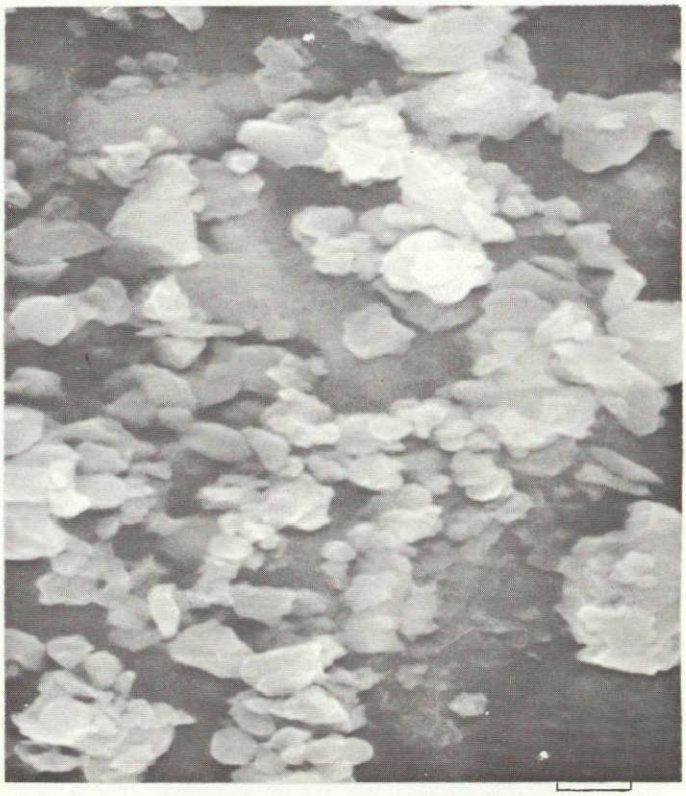

1μ

TABLE 15

DATA FOR FIRED PELLETS OF VARIOUS STARTING POWDERS

Sample Number	Starting[1] Powder	Firing Schedule Temp (°C)	Firing Schedule Time (hrs)	Observations and Metallography (Fig. No.)	X-ray Data
234	$\beta'6_7$	1785	1	15 A	Strong β'
237	$\beta'6_{40}$	1785	1	15 B	
238	$\beta'2_{40}$	1785	1	Surface Reduced	Core of pellet; strong β', medium α. Reduced portion; medium β', strong Si, strong U_3.[2]
243	$\beta'2_{40}$ + 10% CeO_2	1785	1	16	Strong β', weak Si, weak J .[3]
245	$\beta'2_{40}$ + 10% CeO_2	1785	1	17	Strong β', weak Y.[4]
262	$\beta'6_7$ fines	1790	1	Large spherical	
263	$\beta'6_{40}$ fines	1790	1	isolated voids similar to Fig. 19	
264	$\beta'6_7$ coarse	1790	1	Similar to Fig. 18	
265	$\beta'6_{40}$ coarse	1790	1	Similar to Fig. 18B	
266	$\beta'2_{40}$ fines	1715	1	18A	
267	$\beta'2_{40}$ coarse	1715	1	18B	
268	$\beta'2_7$ coarse	1715	1	Similar to Fig. 18B	
269	$\beta'2_7$ fines	1715	1	Similar to Fig. 18B	
281	$\beta'6_7$ fines + 10 CeO_2	1730	1	Large spherical voids	
282	$\beta'6_{40}$ fines + 10 CeO_2	1730	1	Similar to Fig. 19	
283	$\beta'6_7$ coarse + 10 CeO_2	1730	1	Similar to Fig. 20	
291	$\beta'2_{40}$ fines + 10 CeO_2	1730	1	19	
292	$\beta'2_{40}$ coarse + 10 CeO_2	1730	1	20	

(1) Subscript indicates period of ball milling ("fines" indicates material in suspension after at least 3 hrs; "course" indicates material that had settled from suspension in 3 hrs.)

(2) Unidentified phase(s). X-ray pattern given in Table 16.

(3) Apparently isomorphous with $Y_4Si_2O_7N_2$

(4) Apparently isomorphous with $SiO_2 \cdot 4AlN$

TABLE 16

UNIDENTIFIED X-RAY DIFFRACTION PATTERN U_3

d Å	I/I_o
3.04	50
3.00	40
2.74	100
2.63	100
2.55	10
2.45	25
2.37	50
2.35	20
2.05	5
1.894	10
1.819	30
1.515	60
1.150	20
1.390	15
1.326	30
1.298	15
1.277	10

that stoichiometry was no longer that which was calculated. It was concluded that milling time of the prereacted compositions should be extended so that fine particle size (-3μ) would be achieved without a seperation, and that the CeO_2 additions should be added to the basic β' composition prior to the extended ball milling in order to assure an intimate mixture. These conclusions led to the powder preparation techniques 2 and 3 of Table 4. Powder preparation technique 4 abandoned the use of prereacted β' powders in favor of blending the CeO_2 with the Si_3N_4, AlN and Al_2O_3 constituents.

Scanning electron micrographs of powder of composition β'2 + 10 CeO_2 prepared by process 2 are shown in Fig. 21. Bars were pressed from powders prepared by processes 2, 3 and 4. These were fired and evaluated in terms of microstructure, density, and room temperature modulus of rupture. Process, firing, and test data for the bars are presented in Table 17. Micrographs of polished surfaces of representative test bars are shown in Figs. 22 through 26.

It can be seen from examining the micrographs of the polished samples and the density data that all three powder preparations yielded dense structures with none of the gross inhomogeneities exhibited by all previous samples. There is little to distinguish between the polished sections of the different β' compositions or between

POLISHED SECTIONS OF SINTERED β' COMPOSITIONS

(SEE TABLE 15,p41)

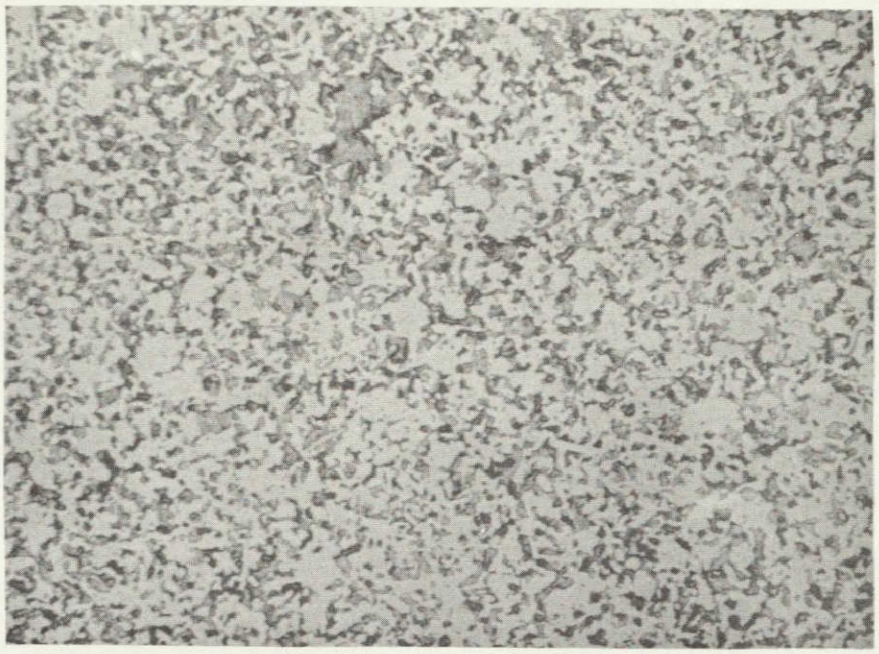

A. (SAMPLE 234)

50μ

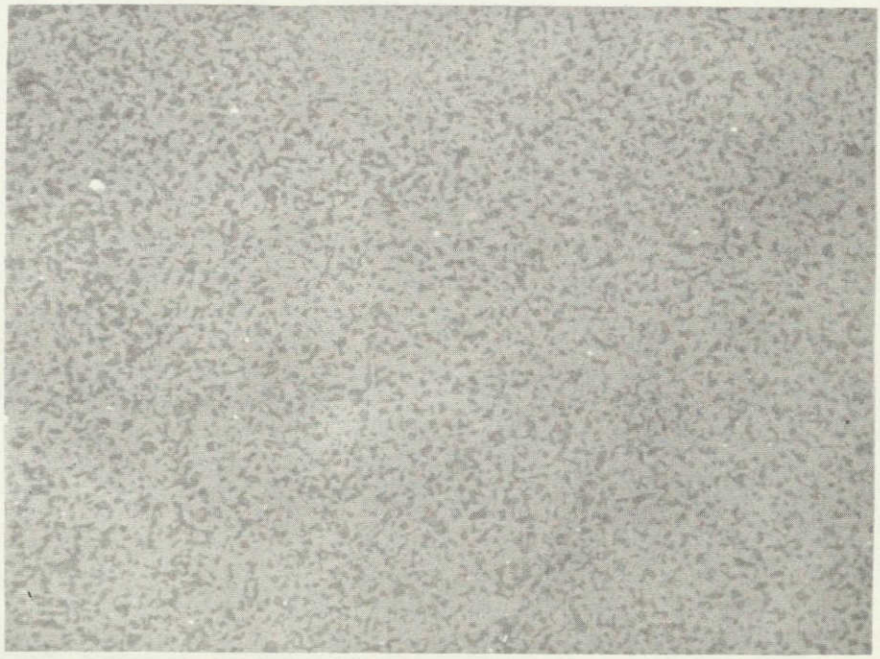

B. (SAMPLE 237)

50μ

POLISHED SECTIONS OF SAMPLE 243

FIG. 16

($\beta'2_{40}$ + 10 w/o CeO_2)

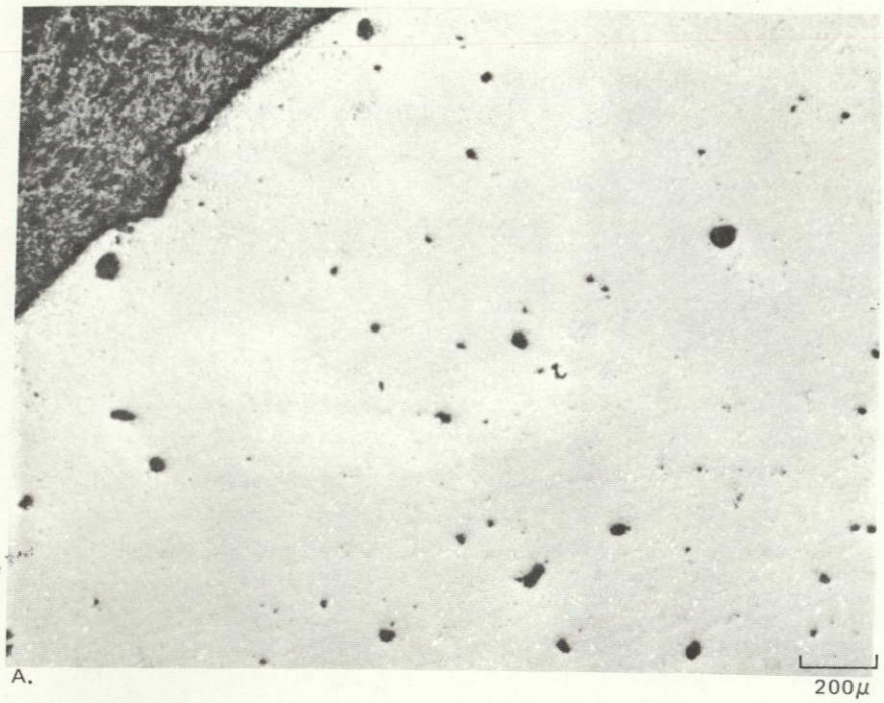

A.

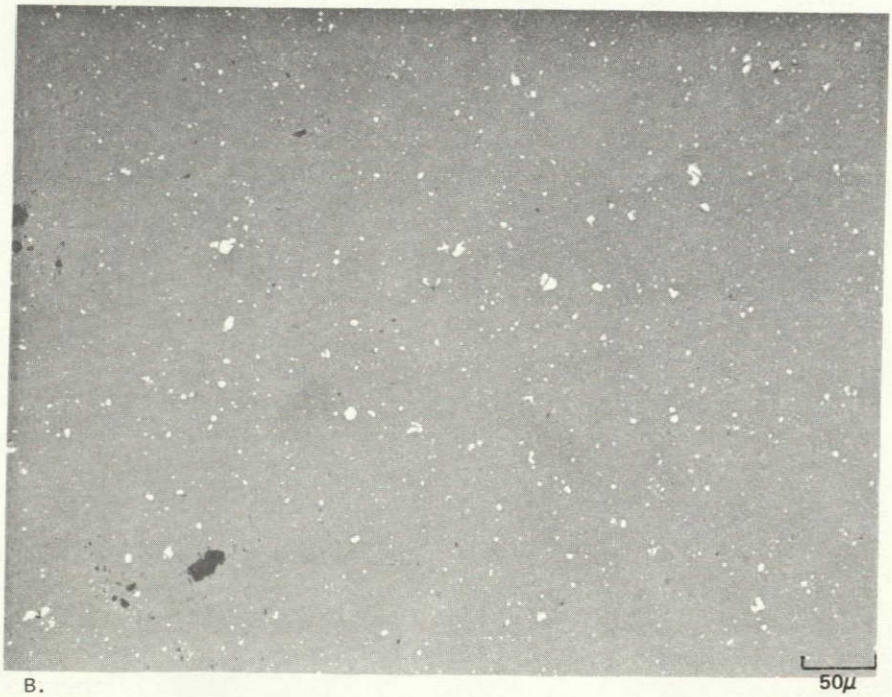

B.

FIG. 17

POLISHED SECTIONS OF SAMPLE 245

($\beta'6_{40}$ + 10 w/o CeO_2)

A.

200 μ

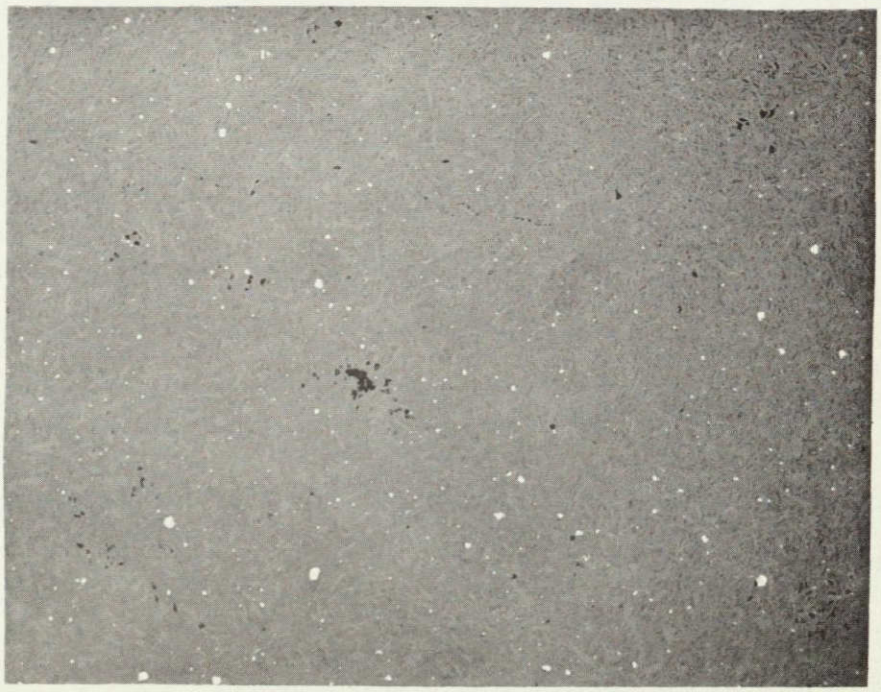

B.

50 μ

76–06–8–3

FIG. 18

SINTERED PELLETS OF COARSE AND FINE FRACTIONS OF $\beta'_{2_{40}}$

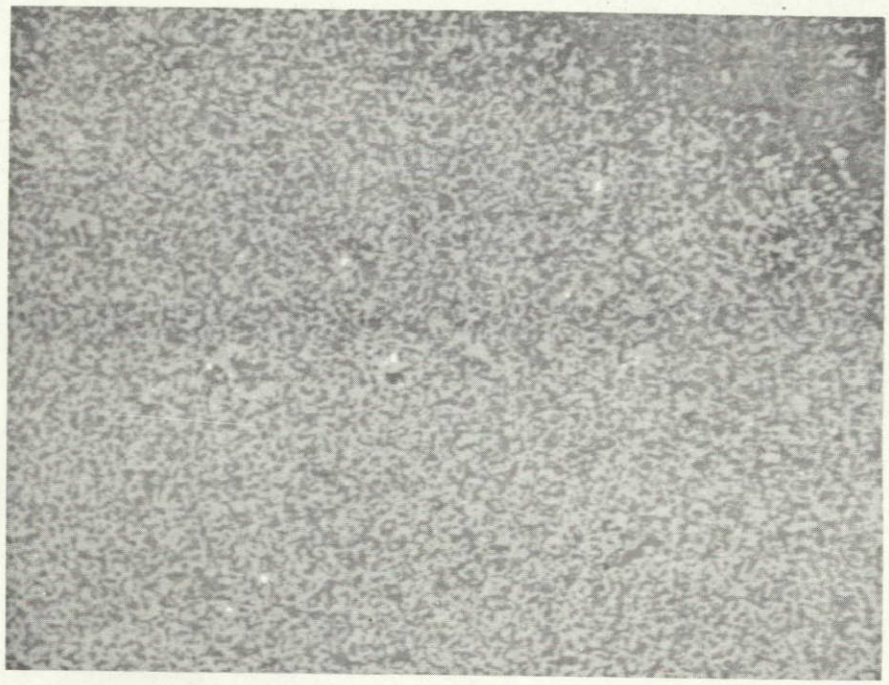

A. FINE (SAMPLE 266)

50μ

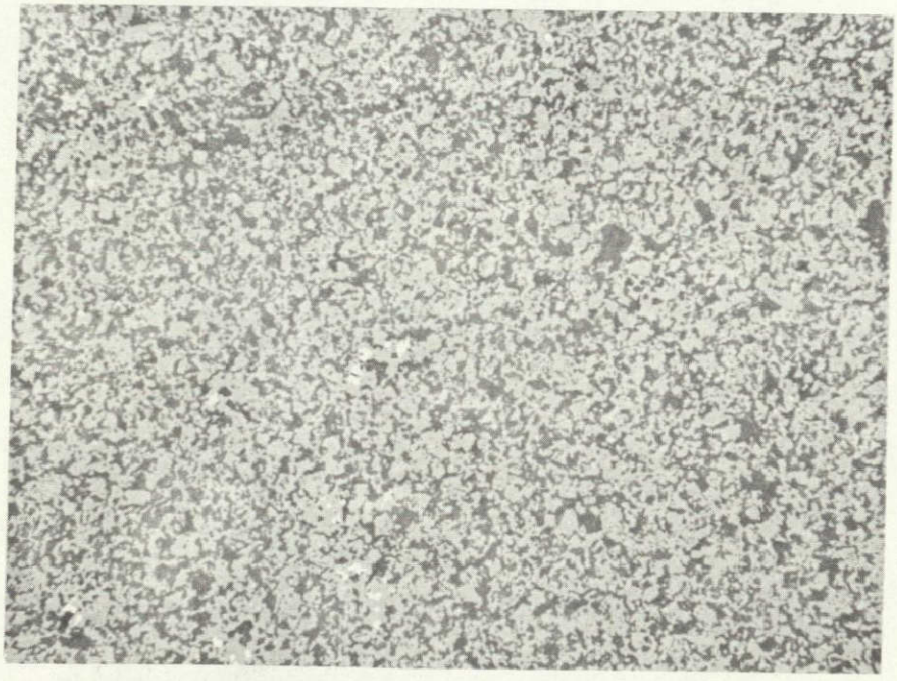

B. COARSE (SAMPLE 267)

50μ

76–06–8–2

POLISHED SECTION OF SAMPLE 291

(β' 2_{40} FINE FRACTION + 10 w/o CeO_2)

A.

200μ

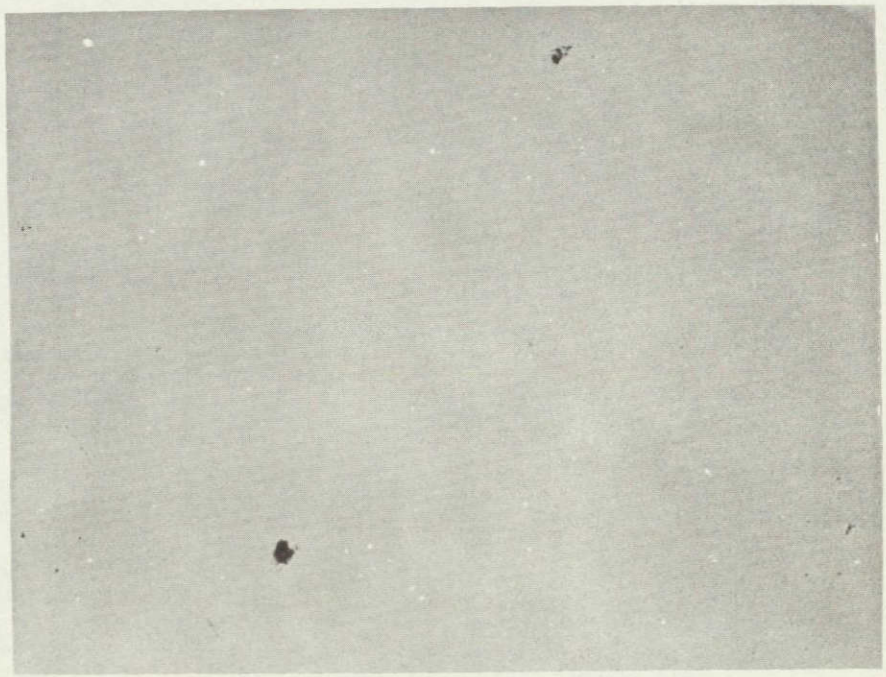

B.

50μ

76–06–8–4

POLISHED SECTION OF SAMPLE 292

(β' 2_{40} COARSE FRACTION + 10 w/o CeO_2)

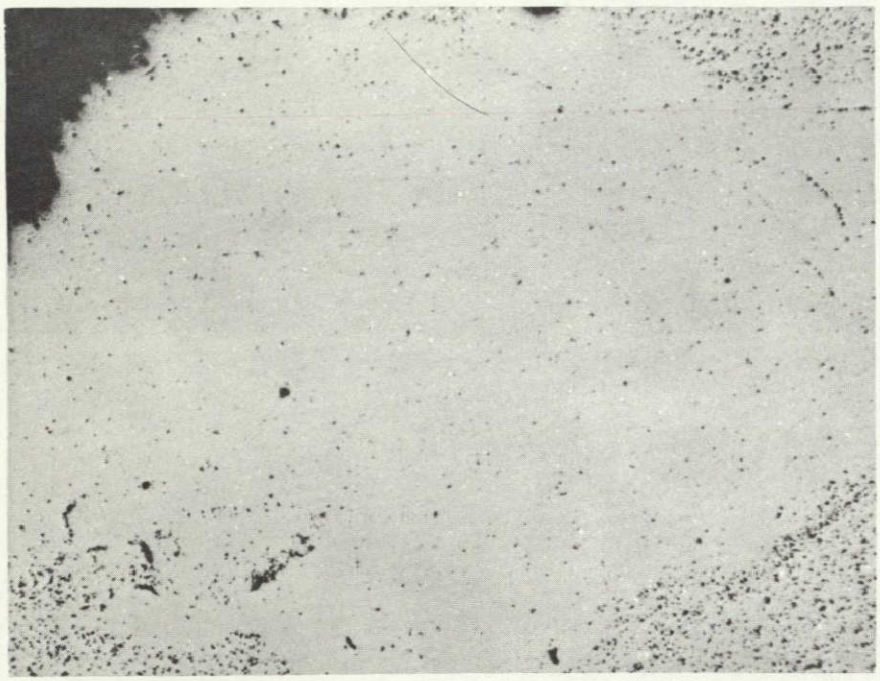

A.

200μ

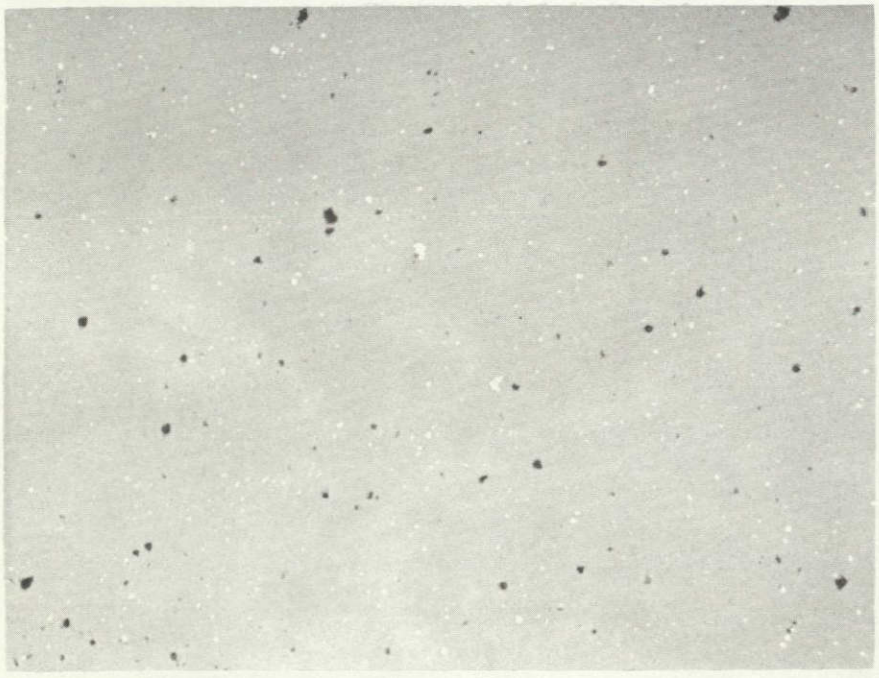

B.

50μ

76–06–8–6

$\beta'2$ + 10 w/o CeO_2 POWDER PREPARED
BY PROCESS 2, TABLE 4

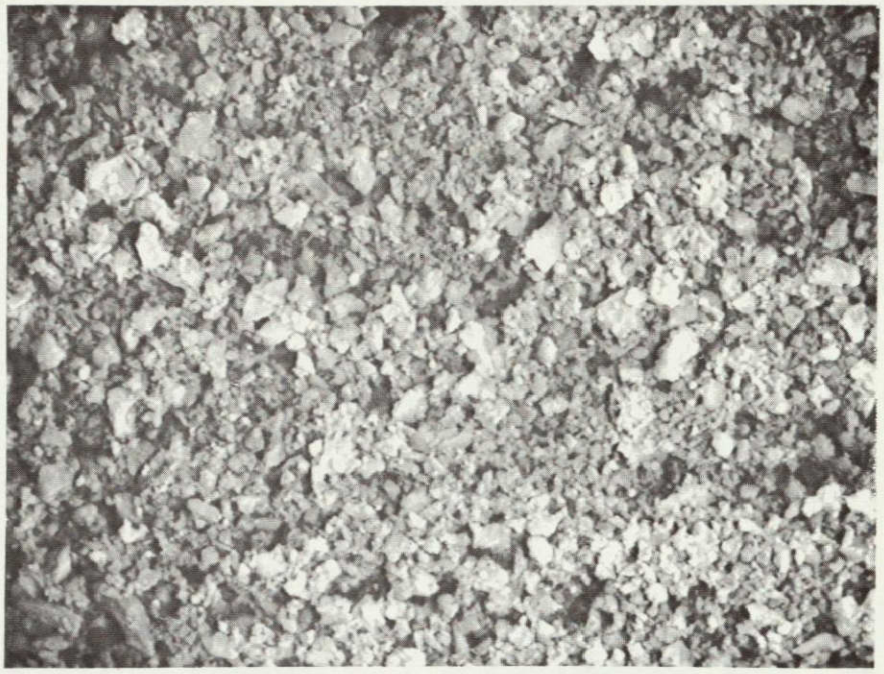

A.

5μ

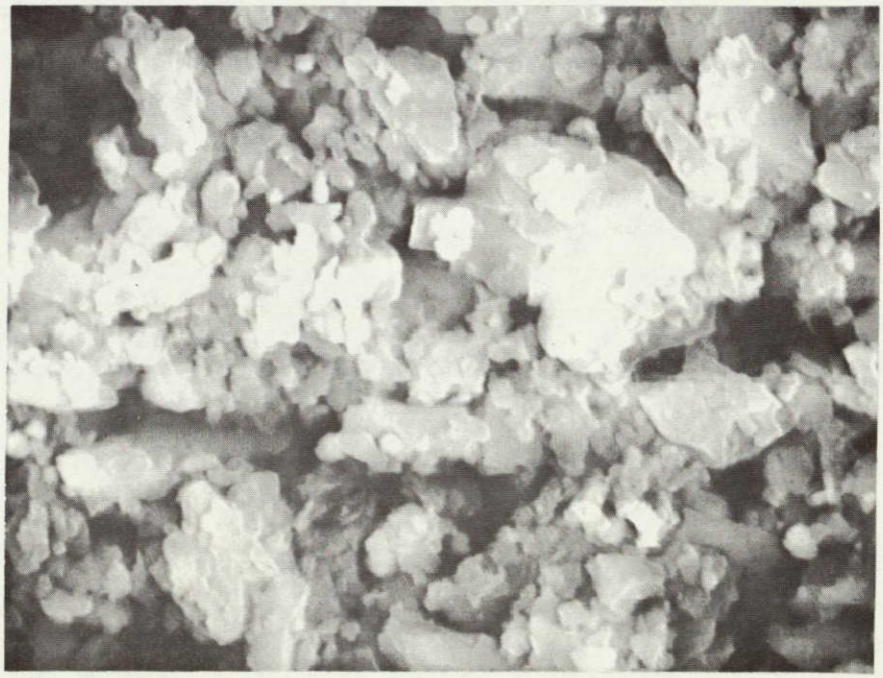

B.

1μ

TABLE 17

PROCESS AND TEST DATA FOR BARS OF VARIOUS β' + 10 w/o CeO_2 POWDERS

Sample Number	β' Composition	Powder Preparation Technique	Firing Condition (Code Ic) T(°C)	Firing Condition (Code Ic) t (hrs)	Bulk Density (g/cc)	Flexural Strength Kpsi	Mean Strength
325						56	
326	2	2	1735	2	3.33	57	59.3
327						59	
328						65	
329						61	
330	2	2	1735	3	3.34	56	58.5
331						53	
332						64	
333						57	
334	2	2	1785	2	3.34	62	56.0
335						54	
336						51	
362						40	
363	2	2	1700	3		44	43.5
364						44	
365						46	
381						34	
382	6	2	1700	1	3.25	45	37.3
383						33	
385						43	
386	6	2	1735	1	3.24	42	45.7
387						52	
402						38	
403	4	2	1700	1	3.28	59	51.7
404						58	
406						57	
407	4	2	1735	1		57	55.3
408						52	
428							
429						44	
430	2	3	1735	2	3.34	37	39.3
431						37	
						39	
436							
437	2	4	1735	2	3.32	78	76
438						74	
439							
440						63	
441	2	4	1750	2	3.33		69
442						71	
443						72	

MICROGRAPH OF SAMPLE 325

(β'' 2 + 10 W/O CeO_2 PROCESS 2)

A. POLISHED

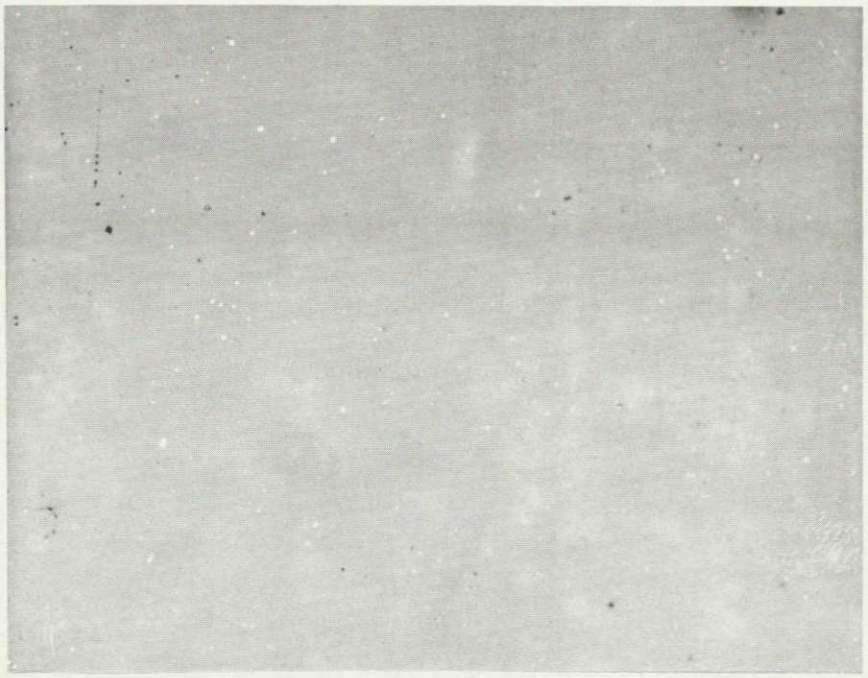

50μ

B. HF ETCHED

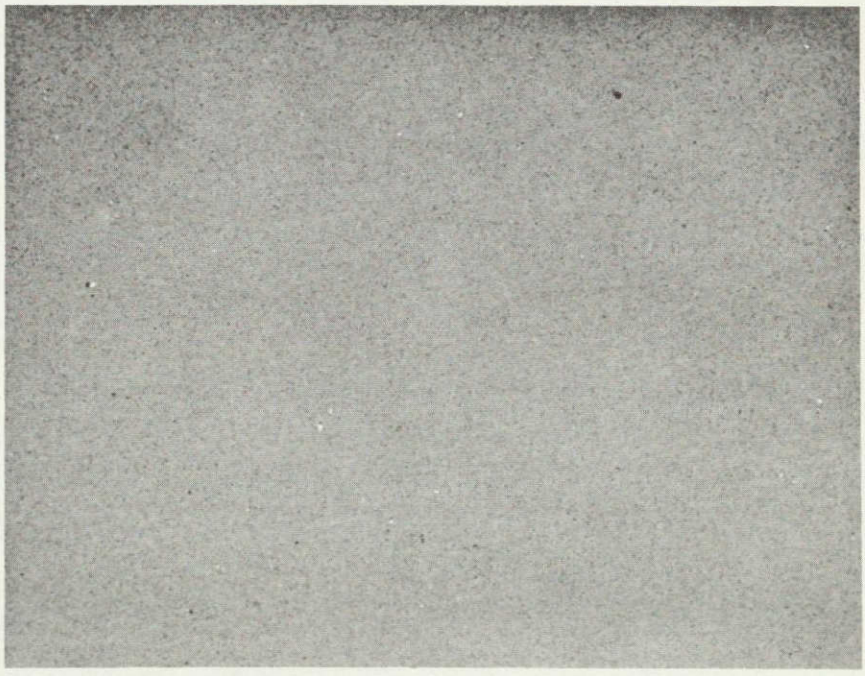

50μ

FIG. 23

MICROGRAPH OF SAMPLE 406

($\beta'4$ + 10 W/O CeO_2 PROCESS 2)

A. POLISHED

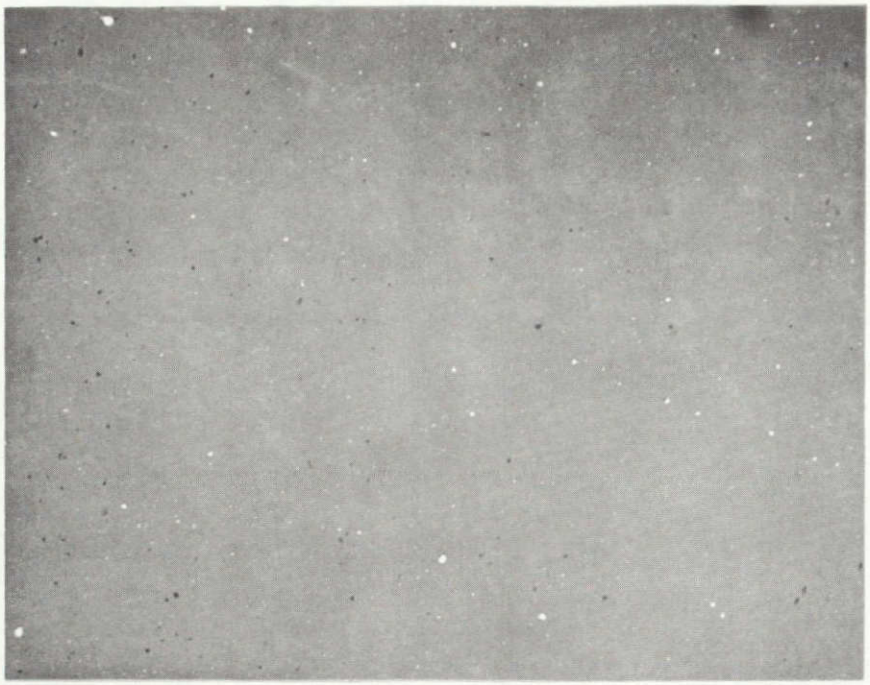

50μ

B. HF ETCHED

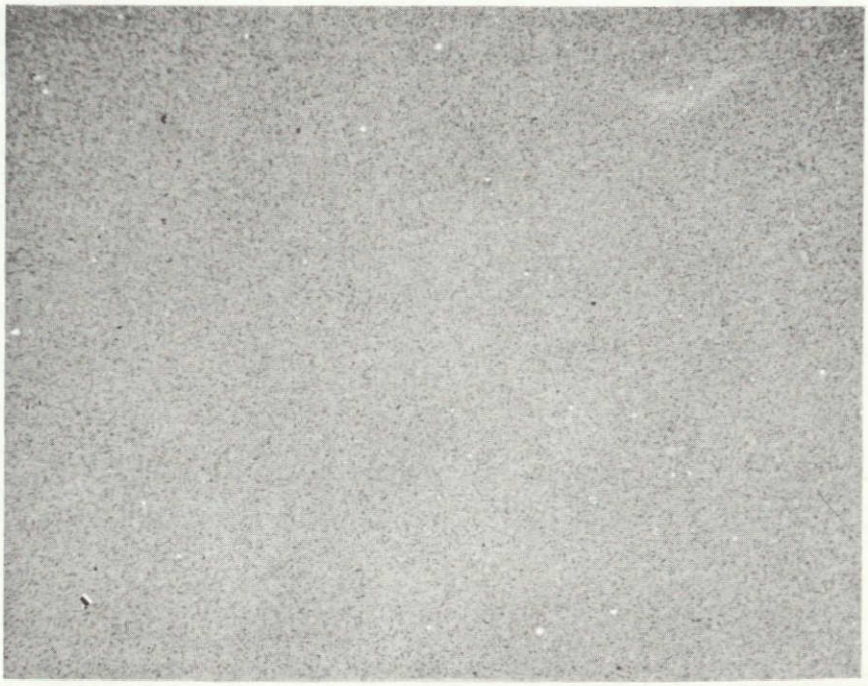

50μ

76–09–139–9

FIG. 24

MICROGRAPH OF SAMPLE 385

(β'' 6 + 10 W/O CeO_2 PROCESS 2)

A. POLISHED

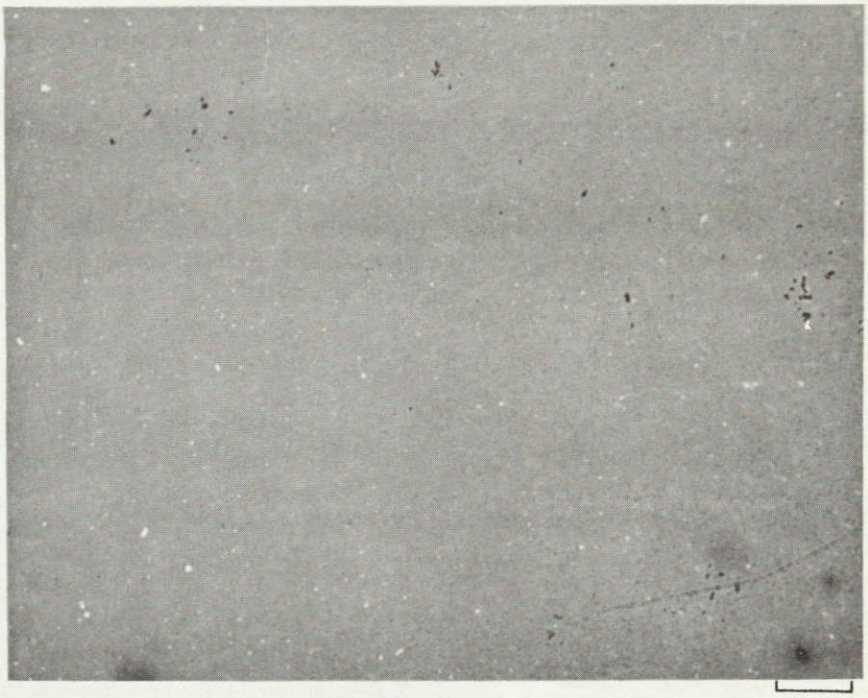

B. HF ETCHED

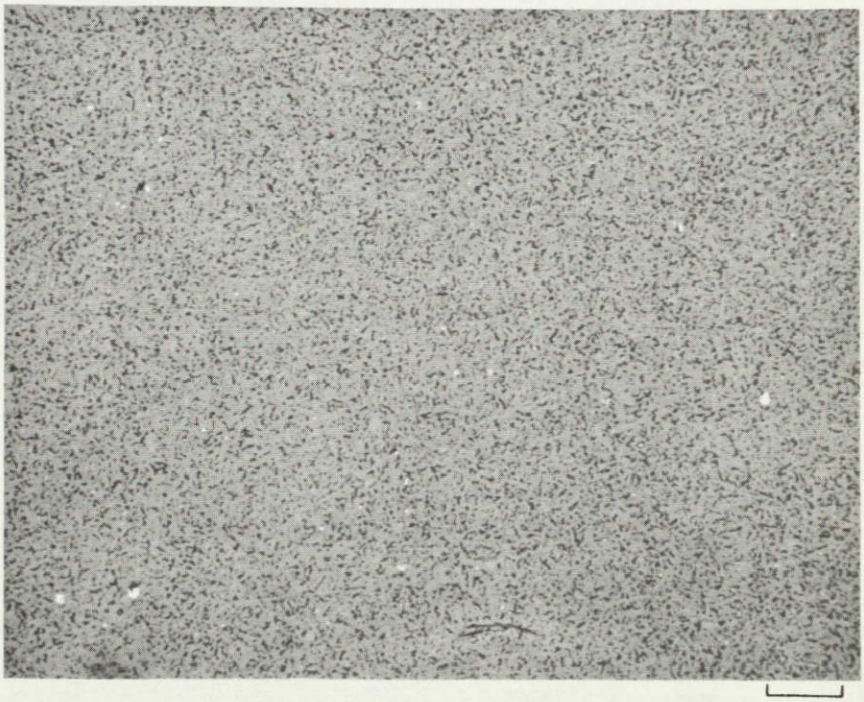

76–09–139–8

FIG. 25

MICROGRAPH OF SAMPLE 431

($\beta''2$ + 10 W/O CeO_2 PROCESS 3)

A. POLISHED

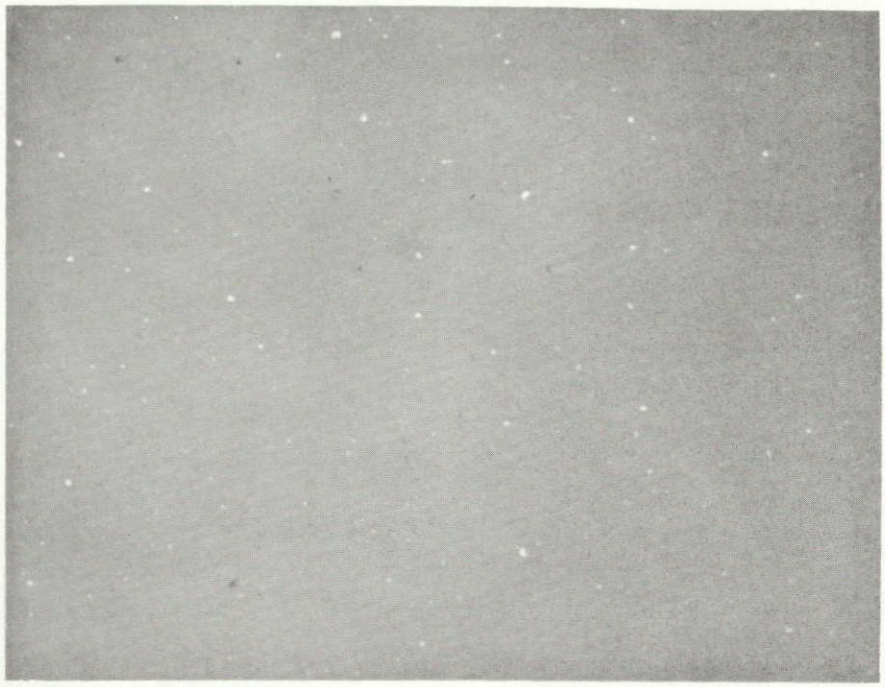

50μ

B. HF ETCHED

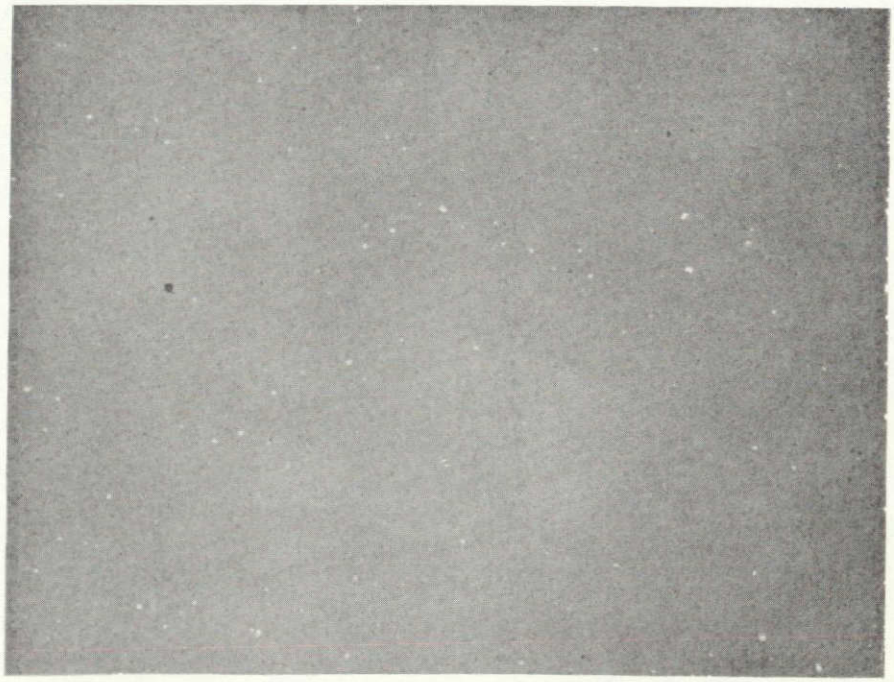

50μ

76–09–139–2

FIG. 26

MICROGRAPH OF SAMPLE 437

(β' 2 + 10 W/O CeO_2 PROCESS 4)

A. POLISHED

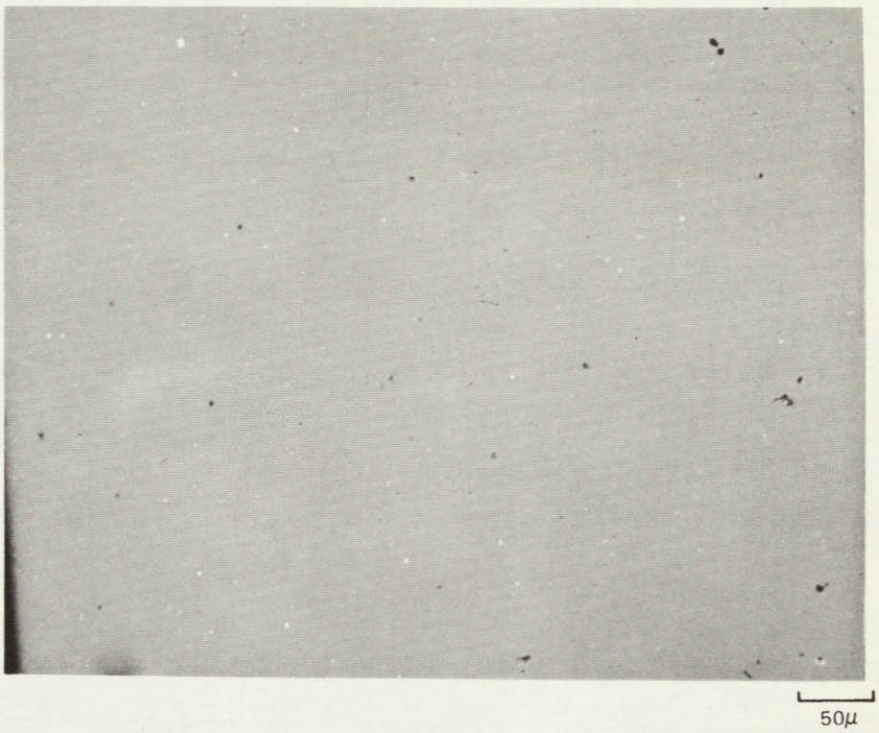

B. HF ETCHED

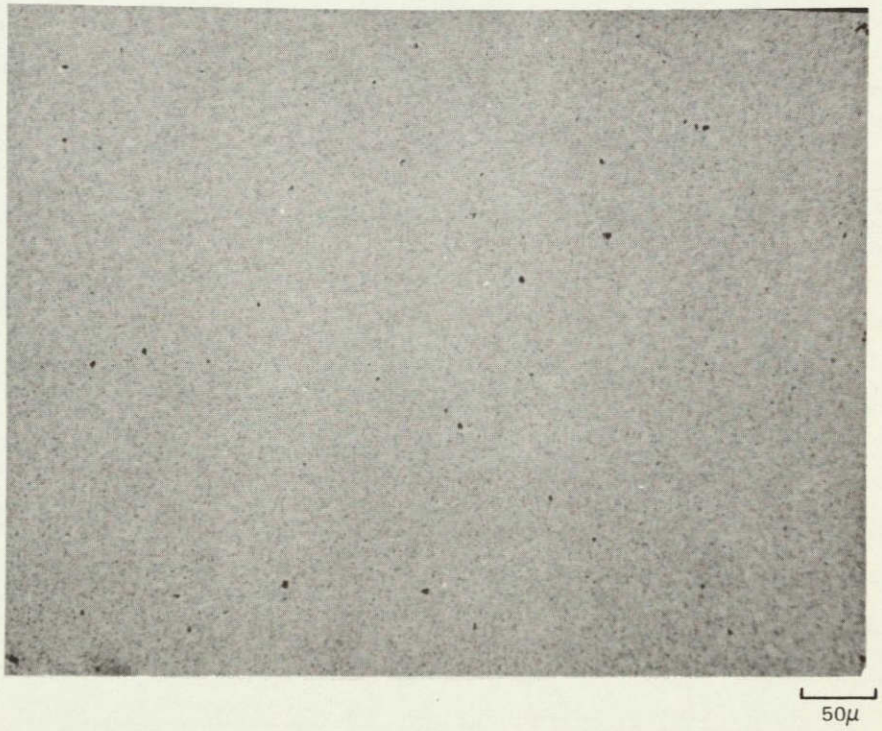

76–09–139–3

the β'2 prepared by the different processes. Differences between the basic β' compositions are apparent on surfaces etched with HF. The etched microstructures show that the samples consist of predominantly acicular β' grains embedded in a matrix phase or phases which, with the exception of sample 431, were deeply etched by the HF. There appear to be substantial differences in the average strengths of bars of the same nominal composition that were fabricated from powders prepared by the different processes. The strongest bars of composition β'2 + 10 w/o CeO_2 (mean strength 72,000 psi) were those fabricated from the unreacted constituents (process 4), the weakest (mean strength 39,000 psi) were those prepared from the process 3 powder. Factors effecting the strength of the bars will be discussed in detail in Section IV.C. There it will be shown that similar variations in strength can occur between batches of the same composition prepared by the same techniques, or even between different firings of powders from the same batch, so that with hindsight perhaps little significance should be placed on the higher strength of the process 4 samples recorded in Table 17. However, the greater simplicity of process 4 compared to 2 and 3 reduces the chances for introducing flaw-inducing impurities into the batch. This fact, coupled with the fact that the highest strength values that had been attained up to this point in the program were prepared by process 4 led to its adoption as the standard technique for most subsequent samples.

2. Summary of Process Refinements

Prereacted powders ball milled in Roalox jars using Burundum media picked up substantial contamination. Attempts to obtain fine particles by sedimentation concentrated the contaminants (aluminosilicates) in the fine fraction resulting in bloating of samples during firing. Milling of both prereacted or unreacted constituents together with CeO_2 in polyethylene jars using either Si_3N_4 or high alumina media and compensating batch compositions for media pick up resulted in powders that yielded dense microstructures when fired to around 1750°C. Highest room temperature strengths were obtained from unreacted constituents milled using high alumina media.

Because of the greater strength exhibited by process 4 samples, and because of the simplicity of this process, it was used for most of the samples discussed in the remainder of this report.

C. Properties of Sintered SiAlON Materials

1. Introductory Comments

Some of the test bars of β' + 10 CeO_2 compositions listed in Table 17 were subjected to static air oxidation of 1300°C and were found to have rather poor oxidation characteristics. Results of these tests will be presented later. Because of inadequate properties of these formulations, further process and formulation refinements guided solely by the results of room temperature property measurements

were suspended, and screening experiments of other formulations were pursued with emphasis on oxidation testing as well as microstructural evaluation, room temperature flexural testing, and later, elevated temperature flexural and creep testing. Compositions were prepared by process 4 (Table 4), compacted into rectangular bars, and fired. Fired bars were tested for apparent porosity, bulk density, and specific gravity. In general, no further testing was performed unless the apparent porosity was under 5 percent. Those samples which meet this criterion were prepared as required for mechanical and/or oxidation testing as described in Section III. In some instances, broken room temperature flexure test specimens were used for the oxidation test. All of the formulation, density, and flexural test data are presented in Appendix II. Data will be abstracted from Appendix II and presented in more convenient form as tables in the main text as required.

2. Second Screening Experiments

Dense samples were produced using additions of CeO_2, ZrO_2, Y_2O_3, Er_2O_3, Nd_2O_3, La_2O_3, Sm_2O_3 and $(Gd, Sm)O_3$, ZrO_2 and Y_2O_3. Additions of HfO_2, TiO_2, Cr_2O_3, $AlPO_4$ and $GaPO_4$ did not result in samples that met the density criterion, and no property data other than that in Appendix II will be presented for these materials.

3. Microstructural and Strength Data

a. β' + CeO_2 Compositions

The macrographs of different β' compositions containing 10 w/o CeO (Figs. 22, 23 and 24) show a coarsening of microstructure in going from $\beta'2$ to $\beta'6$, i.e., higher Al content. This coarsening of microstructure was also observed in earlier samples shown in Figs. 16 and 17. X-ray diffraction patterns obtained from the test specimens contained weak peaks as well as the strong β' pattern. Extraneous lines in the x-ray patterns obtained from several samples listed in Table 17 are presented in Table 18. A possible assignment of these lines to known phases was made on the basis of x-ray data presented by Lange (Ref. 26) for the system Si_3N_4-SiO_2-Y_2O_3 assuming that isomorphous phases exist in the Si_3N_4-SiO_2-Ce_2O_3 system.

The constitution of the grain boundary phase is seen to be different for each of the samples investigated, even for samples of presumably identical composition. One must conclude that either deviations from nominal compositions existed or that equilibrium was not necessarily achieved in the firings.

The mean strength and density also changed with composition is shown in Fig. 27. The decrease in strength with increasing aluminum substitution was accompanied by a decrease in the hardness of the samples as judged qualitatively by the ease with which samples could be cut and polished. The slope of the curve showing the decrease in density with composition is in agreement with the variation in x-ray density with β' composition given in Table 9. Thus the density variation shown in Fig. 27 most

TABLE 18

NON-β' LINES IN THE X-RAY DIFFRACTION PATTERNS OF SOME β' + 10 w/o CeO_2 SAMPLES

	PROCESS 2		PROCESS 3		PROCESS 4	
Composition	β'6 + 10 CeO_2		β'2 + 10 CeO_2		β'2 + 10 CeO_2	
Sample Number	386		428		442	
	d(Å)	Intensity	d(Å)	Intensity	d(Å)	Intensity
Spectra			3.50	s		
					3.42	m
					3.16	m
					3.06	m
			2.98	s		
			2.83	m		
	2.79	s	2.78	s	2.78	m
					2.68	m
	2.61	s	2.63	m		
			2.56	m		
	2.40	m	2.43	m		
	2.15	w	2.12	w		
			2.04	s	2.04	s
	1.95	w	1.95	m	1.96	m
	1.50	s	1.50	s		
Probable Identity	Y Phase		K Phase + Y Phase + unrecognized		H Phase	

FIG 27

STRENGTH AND DENSITY VARIATION OF β' + 10 w/o CeO_2 SAMPLES WITH COMPOSITION

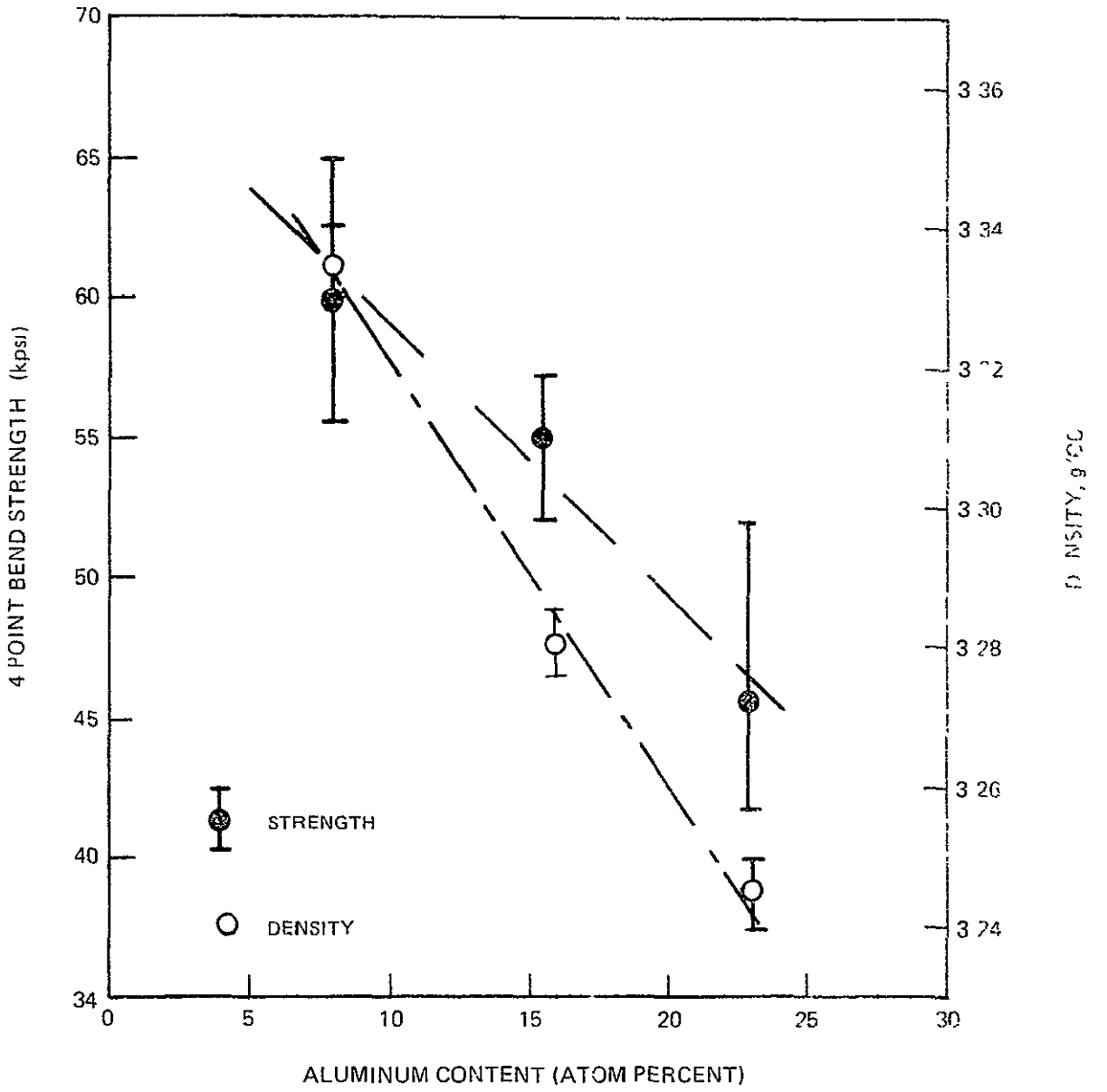

likely reflects primarily the change in the β' composition. The strength variation with composition on the other hand is most likely associated with the properties of the matrix or grain boundary phase, or the strength of the bond between the β' and the matrix phases. As well as the strength variation with β' composition, there appear to be substantial differences in the average strength of bars of the same nominal composition fabricated from powders that were processed differently. The strongest bars of composition β'2 + 10 w/o CeO_2 (mean strength 72,000 psi) were those fabricated from the unreacted constituents (process 4). The weakest (mean strength 39,000 psi) were those prepared from the process 3 powders. Clues to the strength differences can be found in examination of fracture surfaces, representative examples of which are shown in Figs. 28 through 33. Figures 28, 29 and 30 show fracture surfaces of bars prepared by process 2. In all examples of process 2 bars that were examined the fracture initiation site was found to be a surface or near subsurface flaw. The flaws shown are quite different in character. The flaw in sample 328 appears to result from a very large (about 200μ or 0.008 in.) inclusion. There is a zone of interaction with the sample which appears recrystallized and the material inside the zone appears very porous. The electron microprobe picked up no impurities in either the recrystallized or porous zones. No other example of this type of flaw was encountered. It is possibly the result of an agglomerate of lower melting constituents or a chip from the alumina grinding media that reacted with the sample.

The flaw shown in Fig. 29 was assumed to be roughly spherical before fracture. A fragment of an inclusion is adhering to the bottom of the void, and the electron microprobe showed this to be silicon with a high concentration of iron and lesser amounts of chromium and carbon impurities. (Carbon was detected in lower amounts over all the fracture surface and many have been deposited in the SEM from pyrolysis of pump oil. This is not an uncommon artifact.) This type of flaw (Si inclusion associated with Fe and other trace impurities) is a common type of flaw in these samples, and will be discussed again in Section IV.C.4. The flaw shown in Fig. 30 was not examined further but appears to be a large void below the fracture surface, possibly also associated with an inhomogeneity in the batch material.

Figures 31 and 32 are fracture surfaces of bars made from process 3. In these instances there are no gross flaws to be found at the initiation site, and it would appear the strength is limited either by the strength of the matrix phase, or the matrix -β' grain boundaries (or unresolved flaws associated with these). Figure 33 shows the β' fracture surface of a bar made by process 4. Again no gross flaws can be found at the initiation site, and strength again appears limited by the strength of the matrix phase or the grain boundaries. If this is so it would appear that the preferred grain boundary phase, at least in terms of strength, is the H phase ($Ce_5Si_7O_{23}N_4$).

FIG. 28

FRACTURE SURFACE OF SAMPLE 328

(σ_{max}=65,000 psi)

A. OVERALL

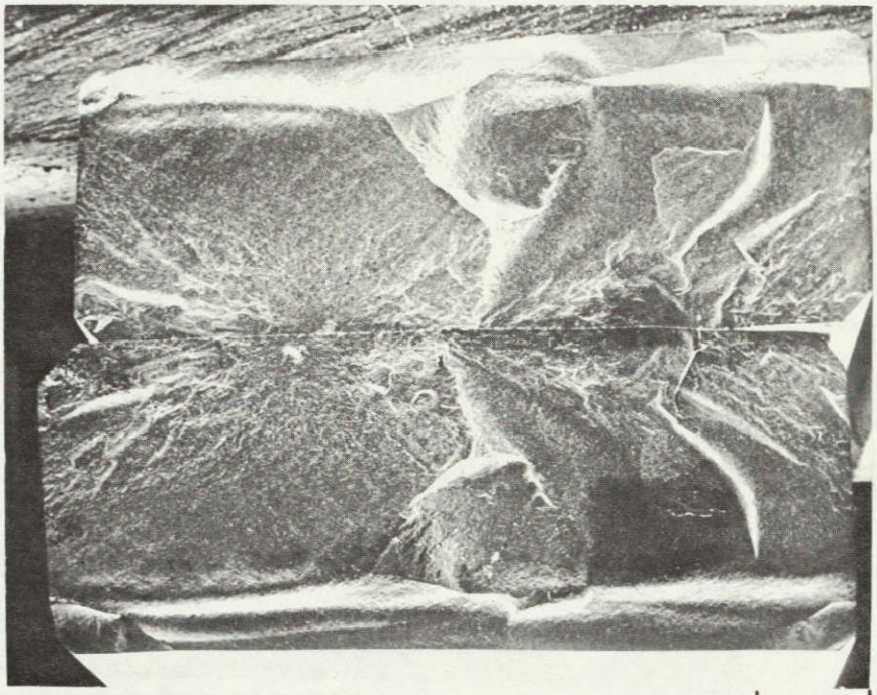

B. INITIATION SITE

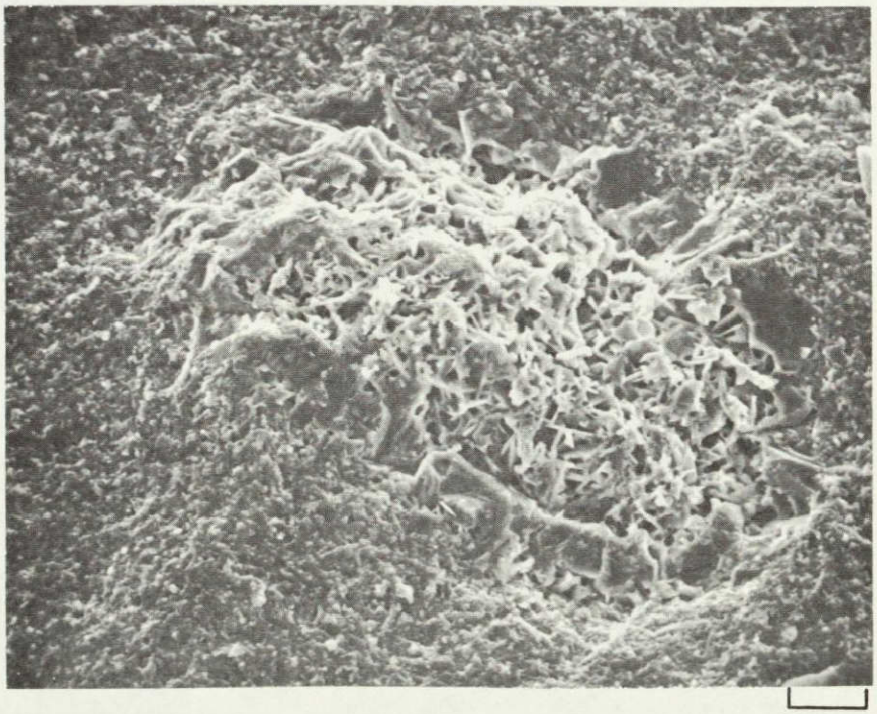

76–06–45–2

FRACTURE SURFACE OF SAMPLE 334

(σ_{max}=62,200 psi)

A. OVERALL

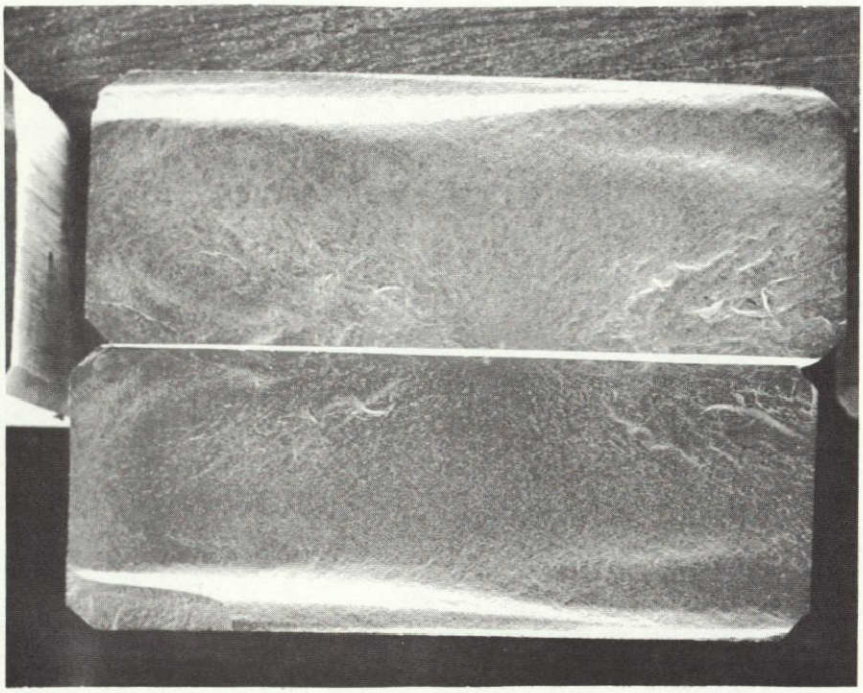

500μ

B. INITIATION SITE

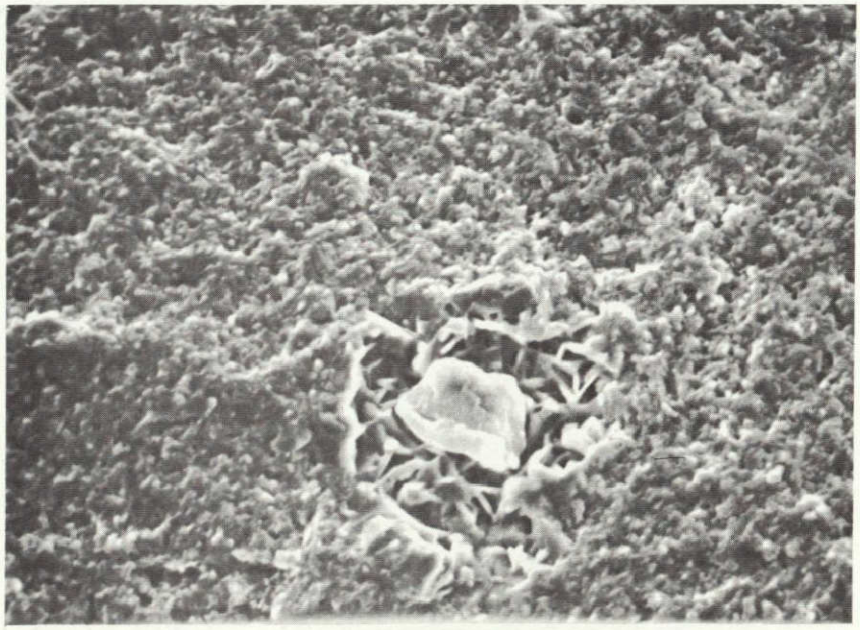

20μ

FIG. 30

FRACTURE SURFACE OF SAMPLE 336

(σ_{max}=50,500 psi)

A. OVERALL

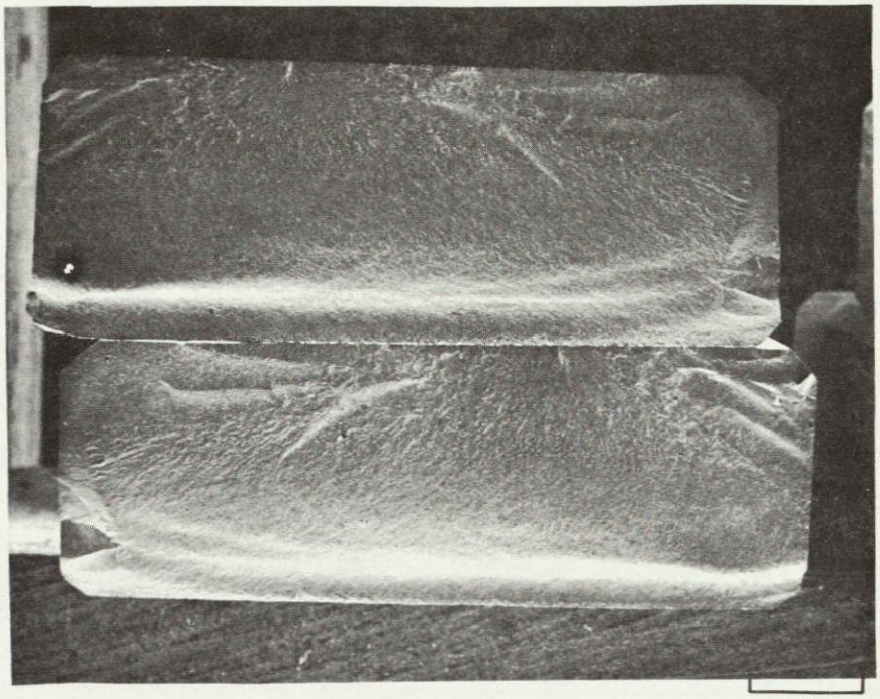

B. INITIATION SITE

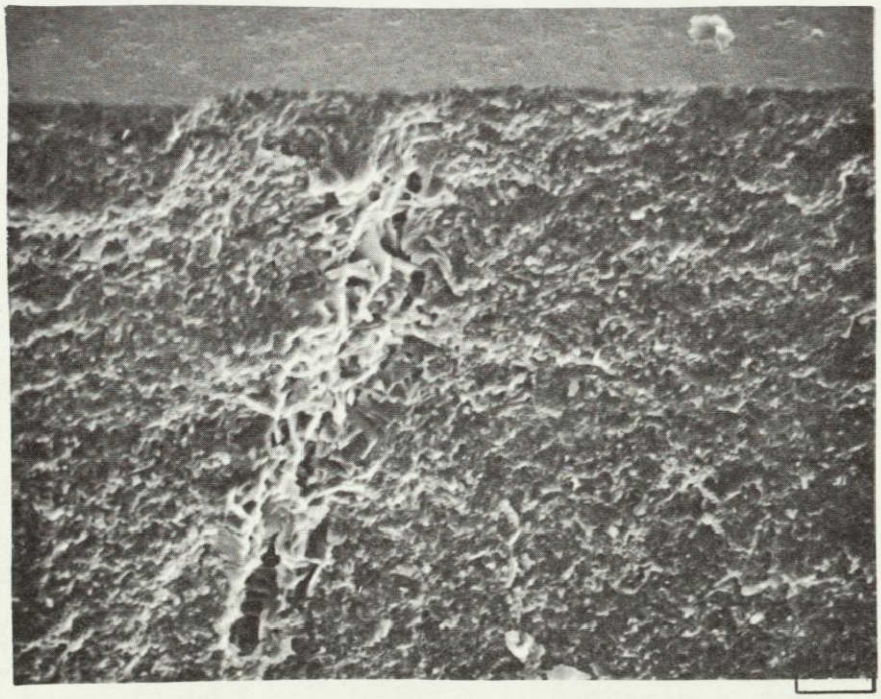

ORIGINAL PAGE IS
OF POOR QUALITY

76–06–45–1

FIG. 31

FRACTURE SURFACE OF SAMPLE 429

(σ_{MAX} = 37,000 psi)

A. OVERALL

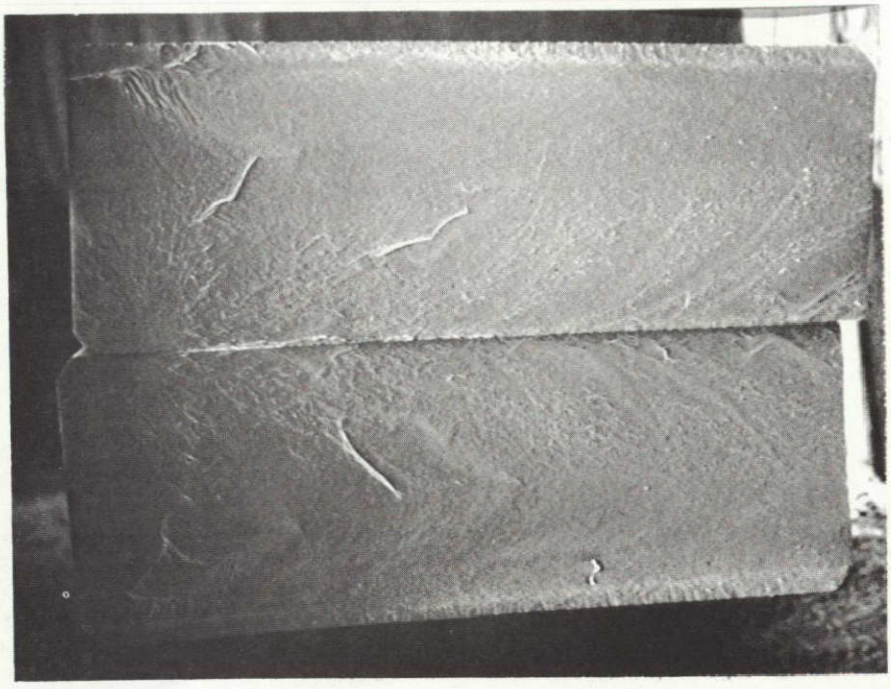

500μ

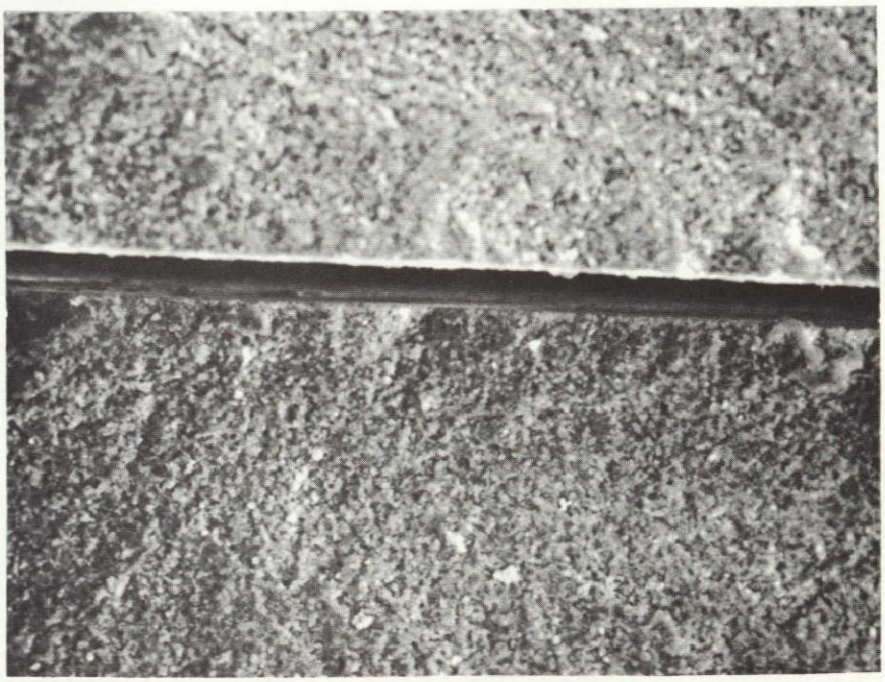

20μ

76–09–139–4

FIG. 32

FRACTURE SURFACE OF SAMPLE 430

(σ_{MAX} = 37,000 psi)

A. OVERALL

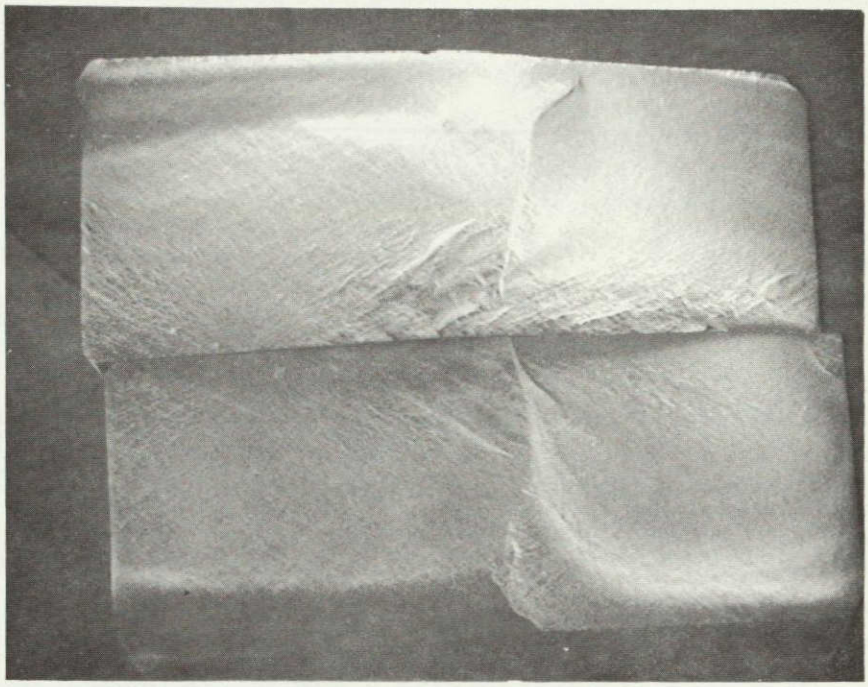

500μ

B. INITIATION SITE

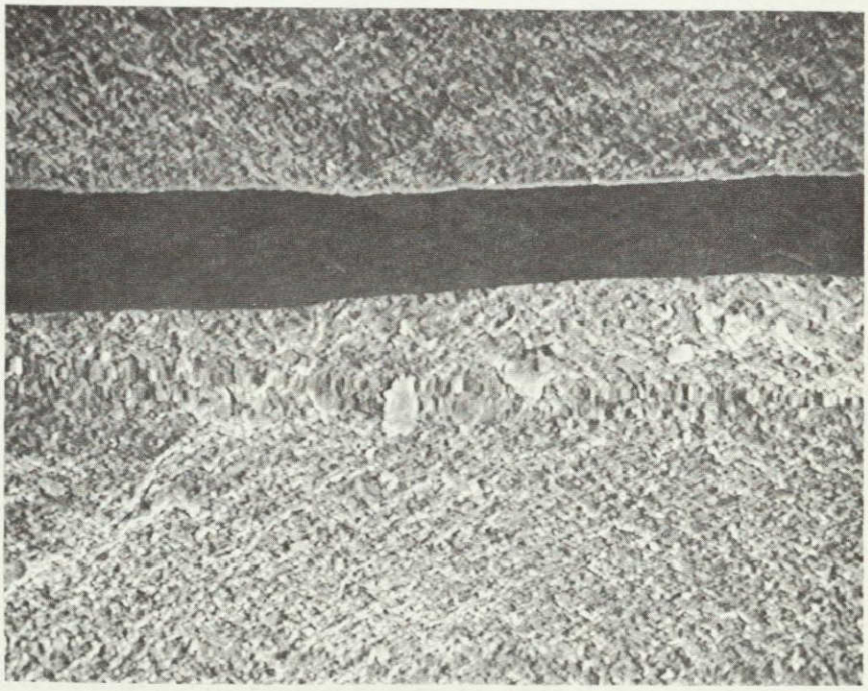

20μ

76–09–139–7

FIG. 33

FRACTURE SURFACE OF SAMPLE 439

(σ = 74,000 psi)

A. OVERALL

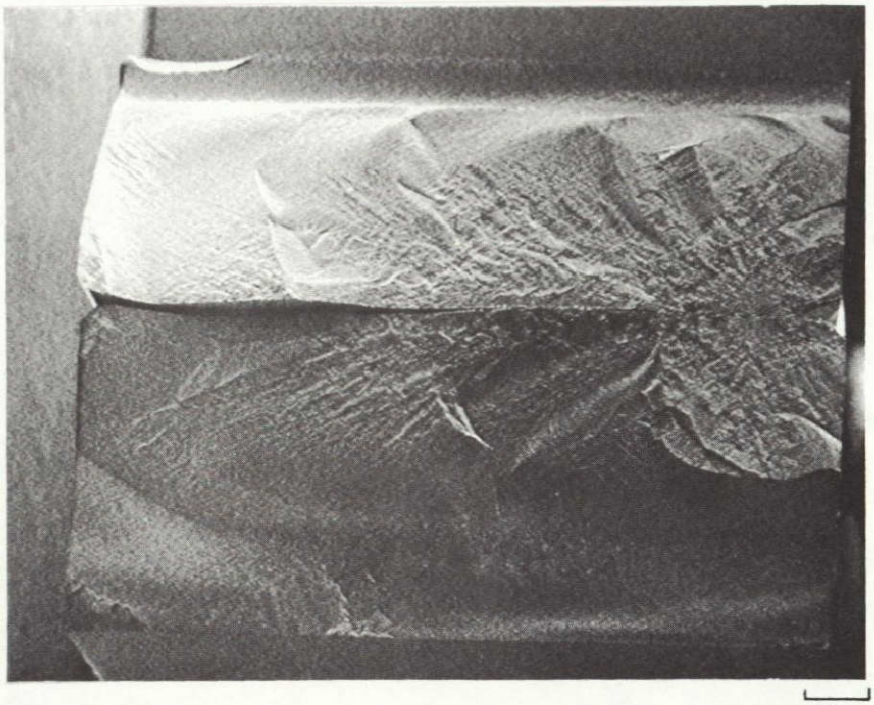

500μ

B. INITIATION SITE

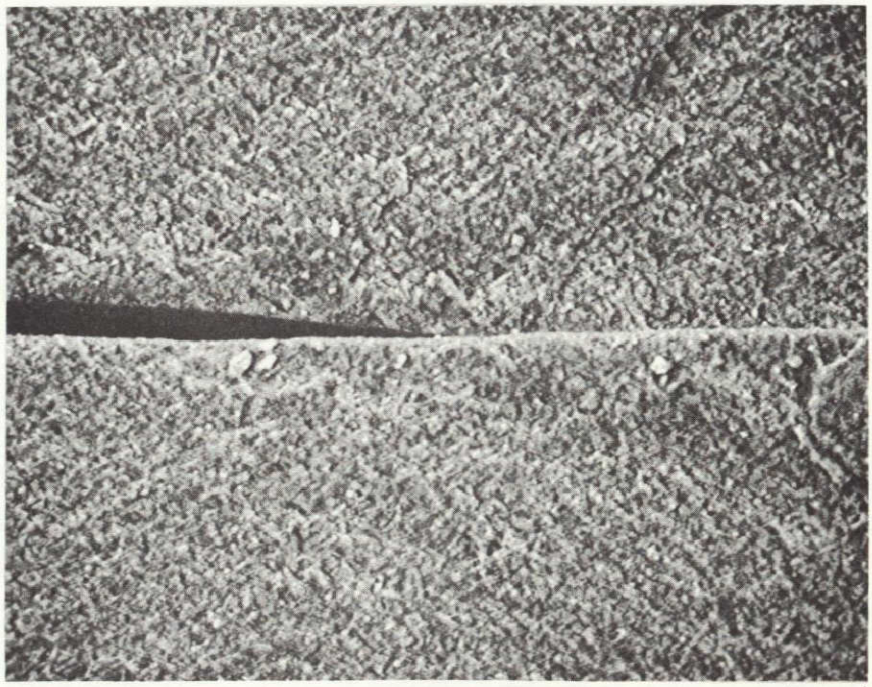

20μ

76–09–139–6

b. $\beta' + Y_2O_3$ Compositions

Strength data for $\beta' + Y_2O_3$ test bars gathered from Appendix II are presented in Table 19. Fracture surfaces were examined in the scanning electron microscope and EDAX. A number of different types of fracture initiation sites were observed. These are described and given a code designation below. In Table 19 the type of fracture site is identified by these code designations.

Tool Mark (tm)

Sample 521 was apparently mounted upside down in the test fixture so that the rough ground rather than the polished surface was in tension. Fracture initiated at a tool mark left by the grinding wheel.

Metallic inclusion (mi)

Five of the 14 room temperature fractures listed above initiated at flaws similar in appearance to that shown in Fig. 34. This shows an inclusion about 20 microns in diameter. EDAX of this inclusion showed a strong spectra for Si, and weaker spectra of Co, Cr, and Fe. These are presumed to be large inclusions of free metal (silicon-transition metal alloys) resulting from decomposition of the Si_3N_4 or β' phases during firing caused by the presence of the transition metal impurities. The reason that these impurities cause the decomposition will be discussed in Section IV.C.4.

Irregular voids (iv)

Three of the 14 fractures initiated at voids similar to that shown in Fig. 35. Microprobe analysis of the inside surface of the void again showed a high concentration of iron impurity. The similarity of this void to that shown in Fig. 29 which contains what appears to be a fragment of metallic inclusion, and the concentration of iron impurity at the void suggest that these voids are sites of inclusion that have been ejected when fracture occurred.

Cylindrical void (vc)

One fracture initiated at a cylindrical void about 50μ wide and of undetermined length since it intersected the surface of the bar. This is shown in Fig. 36. The source of this void is not known with certainty, but it is suspected that a residue of a fragment of a bristle from the brush used in screening the spray dried powder was included in the pressed bar and decomposed on firing to leave the void.

TABLE 19

SUMMARY OF TEST DATA FOR COMPOSITION
$[\beta' + Y_2O_3]$ SINTERED BARS

Batch Composition	Nominal Firing Temperature (°C)	Sample Number	Bulk Density (g/cc)	Flexural Strength (kpsi)	Test Temperature (°C)	Region of Initiation Site*	Type of Flaw**
$[\beta'1 + 2.5\ Y_2O_3]$ .1	1735	762	3.04	70	25	e	u
		763		80		e	mi
	1750	767	3.11	56	25	f	mi
		768		63		f	cv
		769		67		e	u
	1750	770		42	1370	e	u
		771		65		e	u
$[\beta'1 + 2.5\ Y_2O_3]$ .2	1750	833	2.93				
$[\beta'1 + 5\ Y_2O_3]$ .1	1750	814	2.78				
$[\beta'1 + 5\ Y_2O_3]$ .2	1750	836	3.20				
$[\beta'2 + 5$ w/o $Y_2O_3]$ .1	1735	513	3.25	49			
		514		60			
	1700	518	3.24	59	25		
		519		50			
	1750	521	3.24	71		f	tm
		522		53		f	mi
		523		67		f	mi
$[\beta'2 + 5$ w/o $Y_2O_3]$ .2	1735	587		74	25	f	iv
		588		69		e	cv
		589		85		e	iv
	1750	734	3.26	47	1370	e	u
		735		51		e	u
		736		50		e	u
	1750	737		57	RT	e	iv
		738		57		f	mi
		739		43		-	-
		740		37		e	u

* e = edge, f = face

** see text

FRACTURE SURFACE OF SAMPLE 767 INITIATED AT INCLUSION NEAR TENSILE FACE

X15

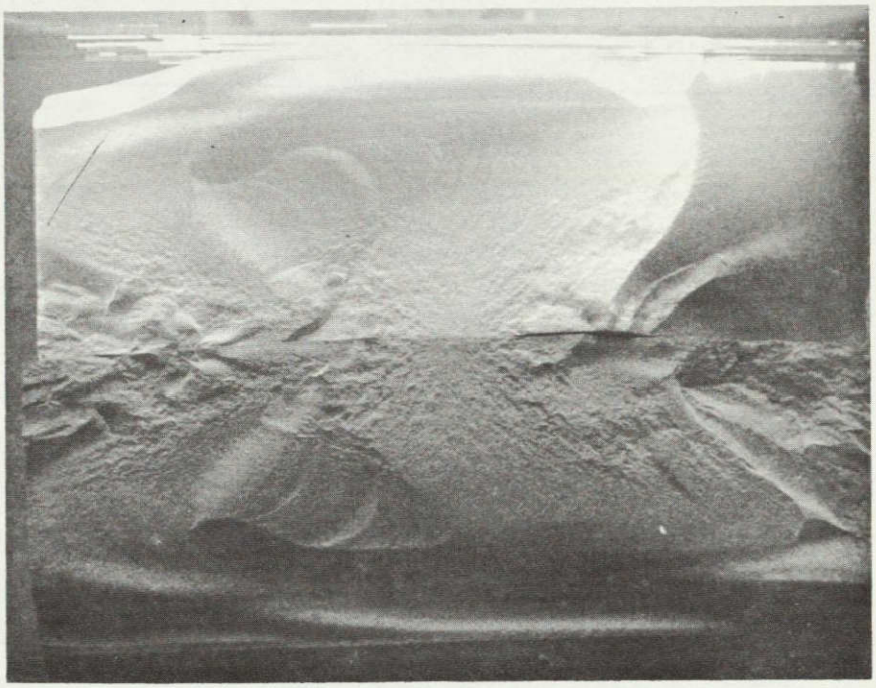

X1000

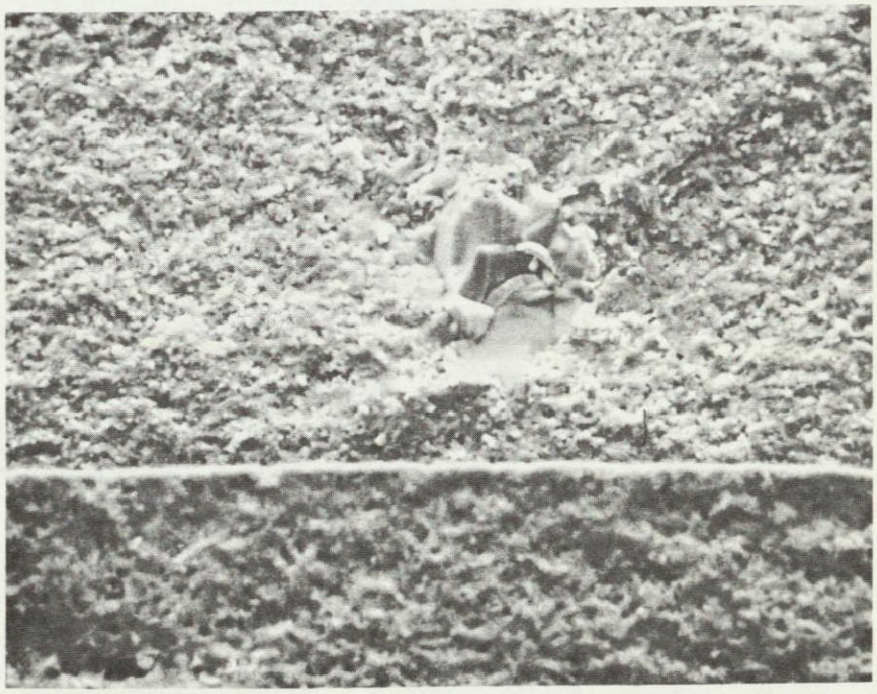

FIG. 35

FRACTURE SURFACE OF SAMPLE 587 INITIATED AT VOID NEAR TENSILE FACE

σ = 74,000 psi

X15

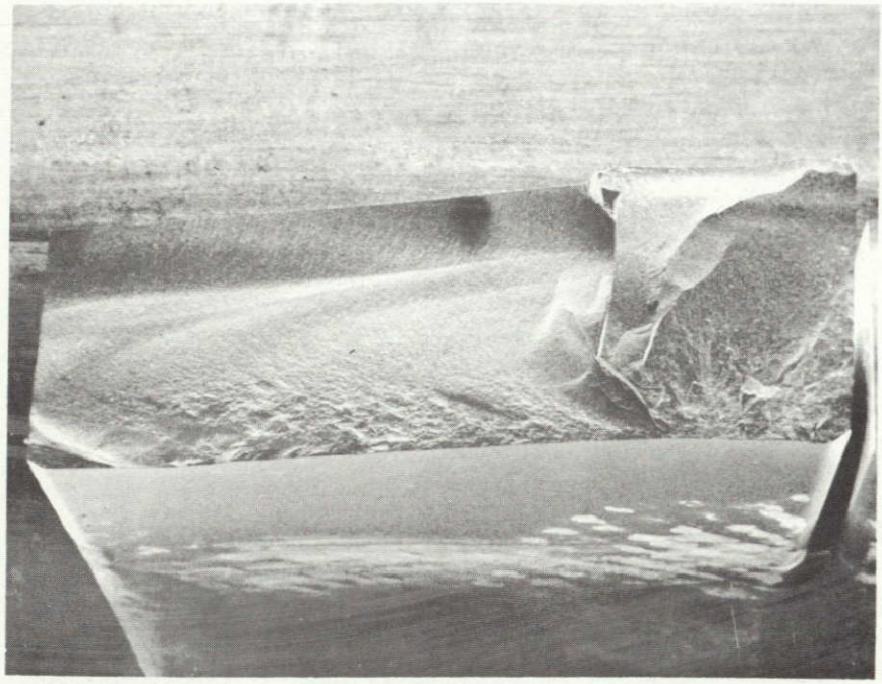

X25 00

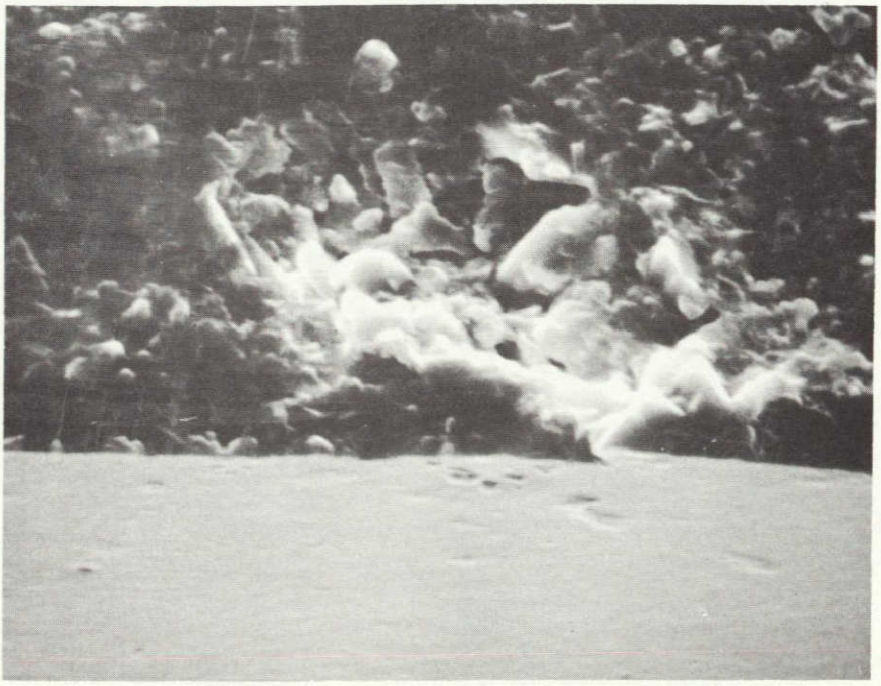

FRACTURE SURFACE OF SAMPLE 768 INITIATED AT CYLINDRICAL VOID ON TENSILE FACE

σ = 63,000 psi

X 15

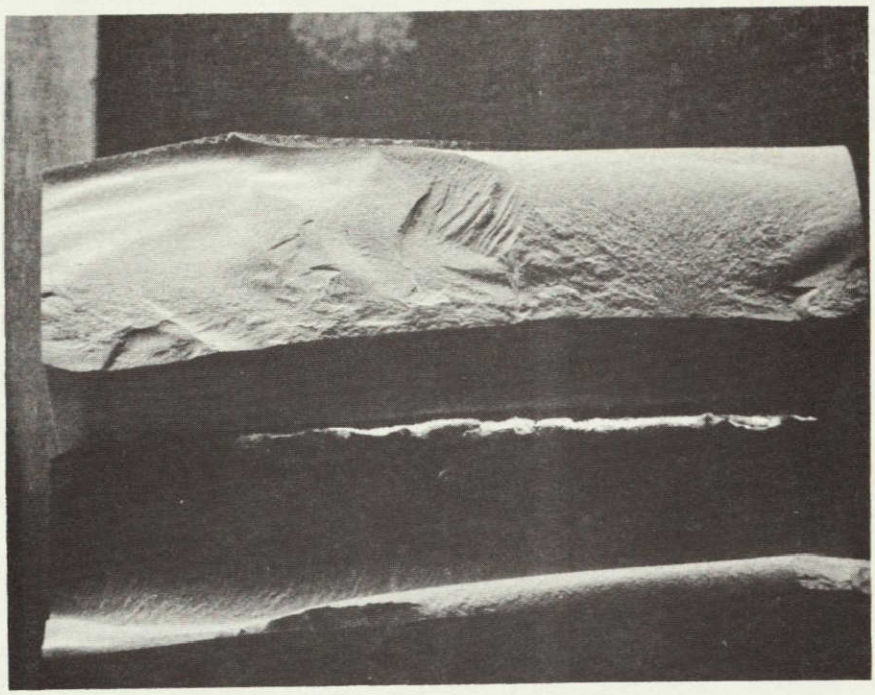

X 500

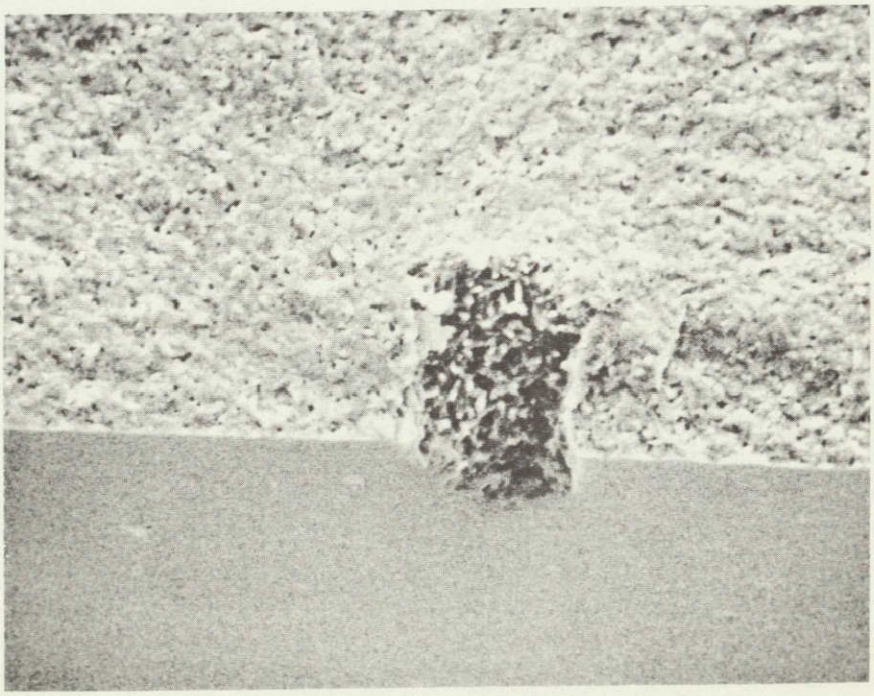

Flaw unresolved (u)

Three of the 14 room temperature fractures, and all of the 1370°C fractures initiated at the edges of the samples, and no flaw larger than the average grain size could be resolved. Similar initiation sites were discussed in connection with $\beta' + CeO_2$ samples.

All of the $\beta' + Y_2O_3$ samples listed in Table 19 were prepared from process 4 powders, and duplicate batches were used in each instance. For compositions of nominally identical composition there is seen to be a large variation in strength and, occasionally, density data. The variability in strength of the samples is about as great as was the variability in the $\beta' + CeO_2$ samples discussed previously. These variations are not entirely random. The spread in values within the groups of samples fired together is considerably smaller than the overall spread in values for all test bars of a given nominal composition. This would relate strength closely to firing step, although there does not seem to be a good correlation between nominal firing temperature and strength. However, because of the narrow range of nominal temperatures represented and the large uncertainty in the reported temperature (and also considering the possibility of unrecorded temperature overshoots during approach to nominal temperature) a correlation with true maximum temperature is not unlikely. Assuming that the nitrogen pressure over the samples was the same as the furnace ambient (1 atm) then a good index to the relative temperatures to which samples of the same batch had been exposed is the concentration of metallic inclusions observed in polished sections. It is possible however, because of the attempt to close the crucibles by means of the tapered lid that a variably higher N_2 pressure was seen by the samples. Whatever the factors that were responsible for the variation in the concentration of inclusions, the polished surfaces of the test bars were examined at high magnification in the light microscope to see if there was a qualitative correlation of strength with the concentration of inclusions. Micrographs shown in Figs. 37 and 38 tend to confirm that this is the case.

It is seen that the majority of room temperature fractures originated at various types of recognizable flaws - predominantly metallic inclusions - and only a few fractures originated at unresolved flaws presumed to be associated with the grain boundary phase. This latter type of fracture was the only one observed at 1370°C, indicating that the strength associated with the grain boundaries had fallen to the levels indicated by the test results (50,000 to 65,000 psi) so that the various other types of flaws were not strength controlling. One can conclude from this that the high temperature strength is determined by the nature of the grain boundary phase only, and processes refinements aimed at eliminating the flaws that control room temperature strength would not have any effect on high temperature strength. In general it was not possible to resolve the grain boundary phases in the x-ray patterns obtained from the test bars, so it was not possible to ascertain whether the few room temperature fractures having u-type initiation sites had grain boundary phases that differed from that of the high strength flaw initiated samples as was the case with $\beta' - CeO_2$ bars discussed earlier (Section IV C3a, p57).

MICROGRAPHS OF POLISHED SURFACES OF TEST BARS

A. SAMPLE 588, COMPOSITION $\left[\beta'2 + 5 \text{ w/o } Y_2O_3\right]$·2 σ = 69,000 psi

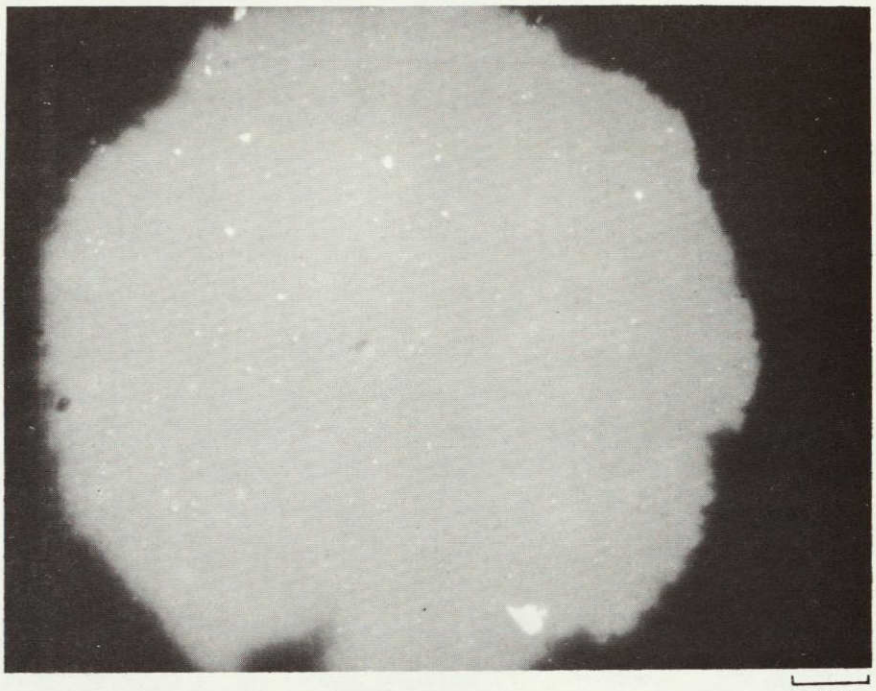

B. SAMPLE 762, COMPOSITION $\left[\beta'1 + 2.5\ Y_2O_3\right]$·1 σ = 70,000 psi

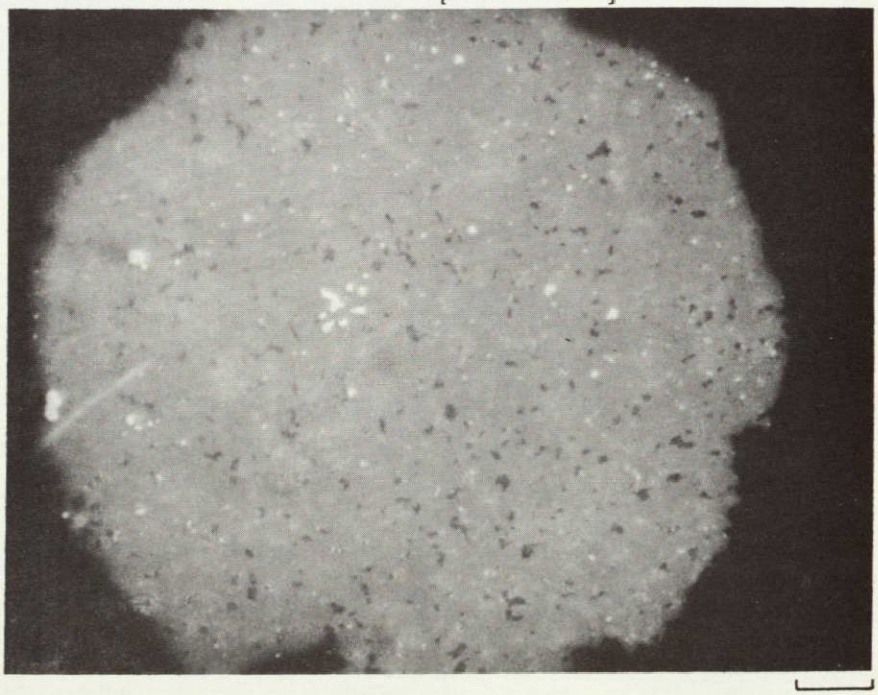

FIG. 38

MICROGRAPHS OF POLISHED SURFACES OF TEST BARS

A. SAMPLE 523, COMPOSITION $\left[\beta'2 + 5 \text{ w/o } Y_2O_3\right]$·1 σ = 53,000

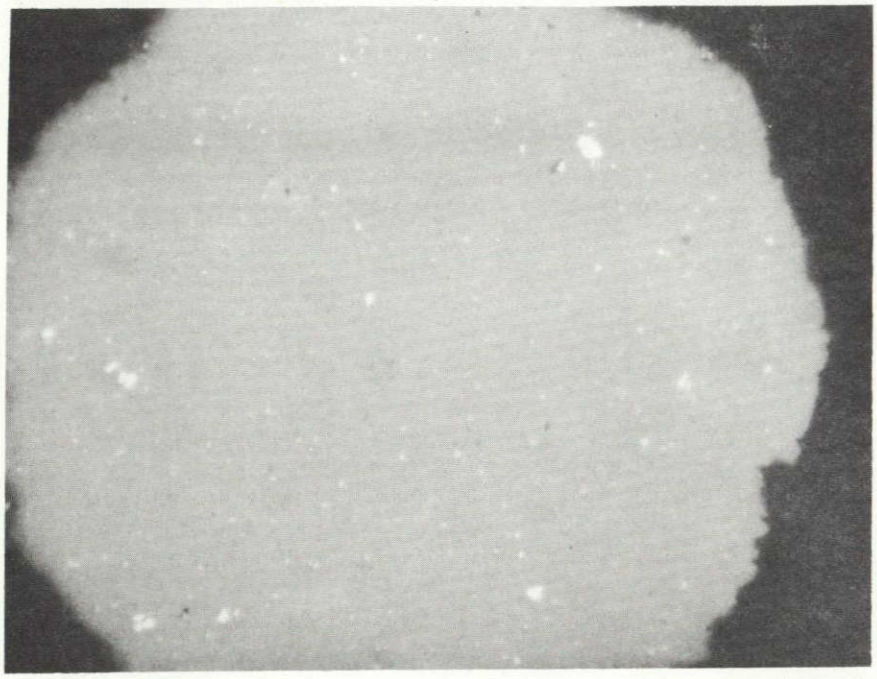

10μ

B. SAMPLE 740, COMPOSITION $\left[\beta'2 + 5 \text{ w/o } Y_2O_3\right]$·2 σ = 37,000

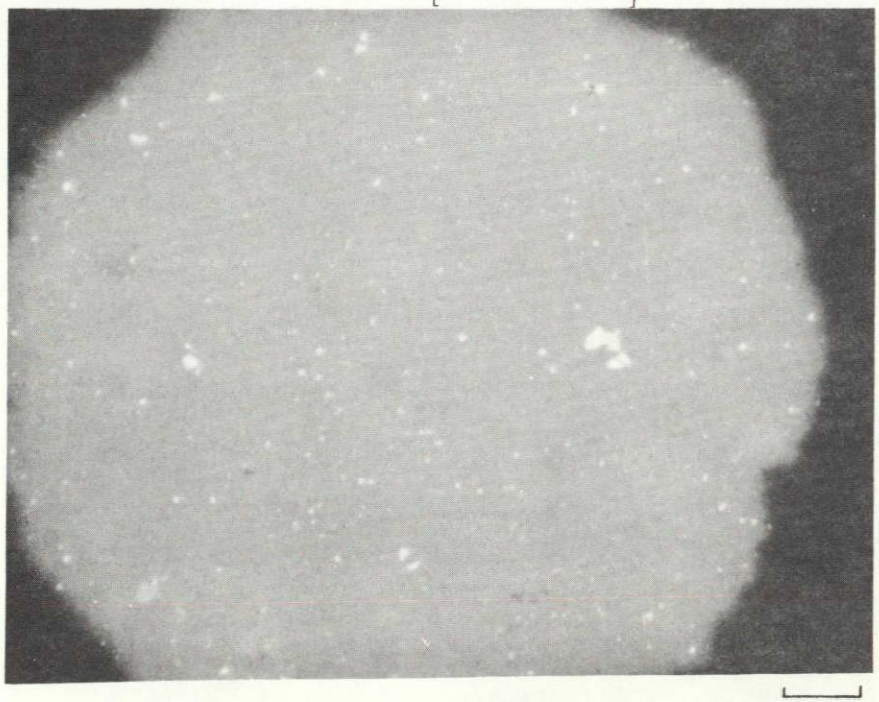

10μ

77–03–240–4

As well as the firing-to-firing strength variations exhibited by the samples that are thought to result because of varying concentrations of metallic inclusion, there appear to be batch-to-batch differences in the density of the β'1 + x Y_2O_3 samples fired to nominally identical temperatures. Some firings of batches were made with the intention of demonstrating whether this variability could be positively associated with the individual batches or the firing procedures. In these firings, one bar of each of 4 different batches was placed in the same boron nitride crucible and fired. The densities of individual bars from these firings are presented and compared with previous data for bars prepared from the various batches in Table 20. From these data it is clear that both firing-to-firing and batch-to-batch variations exist. Possible sources of batch variability will be discussed in Section IV.C.5.

c. β' + ZrO_2 and β' + (a ZrO_2 b Y_2O_3) Compositions

Strength data for these samples are presented in Table 21. Again room temperature strength values covered a wide range (25,000 to 80,000 psi) and appeared to be controlled by the presence of metallic inclusions. The concentration of these was high in all cases, as shown for two samples in Fig. 39. Not discernable in Fig. 39 because of insufficient contrast, is the fact that the inclusions appear to be of two types randomly intermixed. One type has a silver appearance under the optical microscope and the other type appears golden. The electron microprobe showed the first type to consist of major Si and Fe with minor Al, and trace Cr, V, Cu, and Zr. The second type consists of major Si and Zr and minor Al.

The strength of bars tested at 1370°C was uniformly low (33,000 psi). 1370°C fractures surface, (e.g., Fig. 40) exhibited a rough region of initial crack growth probably resulting from viscous flow in the grain boundary phase.

d. β' + Other Sesquioxides

Batches of β'2 compositions + 3.2 m/o additions of La_2O_3 and a number of rare earth oxides were prepared by process 5 of Table 4, pressed into bars and fired according to code 2a of Table 7. These were prepared for oxidation testing primarily and no mechanical tests were performed. Density measurements and metallographic observation showed that all these systems sintered to over 90 percent of theoretical density, but unlike earlier samples prepared from process 4 powders, exhibited substantial open porosity. Microstructures of these samples will be shown later in connection with the oxidation studies.

4. Origin of Metallic Inclusions

It has been shown that the strength of most of the samples tested at room temperature has been limited by the presence of metallic inclusions. Except for the second type of inclusion found in ZrO_2 bearing samples, the inclusions have been

TABLE 20

DENSITIES OF BARS FIRED FROM DIFFERENT BATCHES OF (β' + Y_2O_3) COMPOSITIONS

Sample Number	Batch Number*	Firing Temperature °C	Bulk Density (g/cc)
761	746.1	1735	3.04
765	746.1	1750	3.11
830	746.2	1735	2.87
833	746.2	1750	2.93
810	783.1	1735	2.72
814	783.1	1750	2.78
836	783.2	1750	3.20
846	746.2	1750	2.97
847	746.1		3.04
848	783.1		2.67
849	783.2		3.10
850	746.2	1750	2.93
851	746.1		3.01
852	783.1		2.66
853	783.2		3.11

* 746.1 = β'1 + 2.5 w/o Y_2O_3 batch 1

746.2 = β'1 + 2.5 w/o Y_2O_3 batch 2

783.1 = β'1 + 5 w/o Y_2O_3 batch 1

783.2 = β'1 + 5 w/o Y_2O_3 batch 2

TABLE 21

SUMMARY OF FLEXURAL STRENGTH DATA FOR SINTERED BARS
OF COMPOSITIONS β' + ZrO_2 and β' + 5 w/o (a ZrO_2 + b Y_2O_3)

Batch Composition		Sample Number	Bulk Density (g/cc)	Flexural Strength (kpsi)		Test Temperature (°C)
$\beta'2$ + 20 ZrO_2	1700	500 501 502	3.45	43 59 51	51	25
$\beta'2$ + 10 ZrO_2	1650	564 565 566 567	3.16	35 37 36 38	36.5	25
$\beta'2$ + 5 ZrO_2	1735	591 592 593 594	3.18	49 46 52 47	48.5	25
$\beta'2$ + 5(.8 ZrO_2 .2 Y_2O_3)	1735	673 674 675 676		80 74 60 69	70.8	25
$\beta'2$ + 5(.925 ZrO_2 .075 Y_2O_3)	1735	753 754 755	3.33	34 33 33	33.3	1370
$\beta'2$ + 5(.925 ZrO_2 .075 Y_2O_3	1735	757 758 759		67 47 42	52	25
$\beta'1$ + 5(.75 ZrO_2, .25 Y_2O_3)	1735	794 795 796	3.02	53 49 80	60.7	25

FIG. 39

MICROGRAPHS OF POLISHED SURFACES OF TEST BARS

A. SAMPLE 760, COMPOSITION $\beta'2$ + 5 w/o (0.925 ZrO_2 + 0.075 Y_2O_3) σ = 42,000

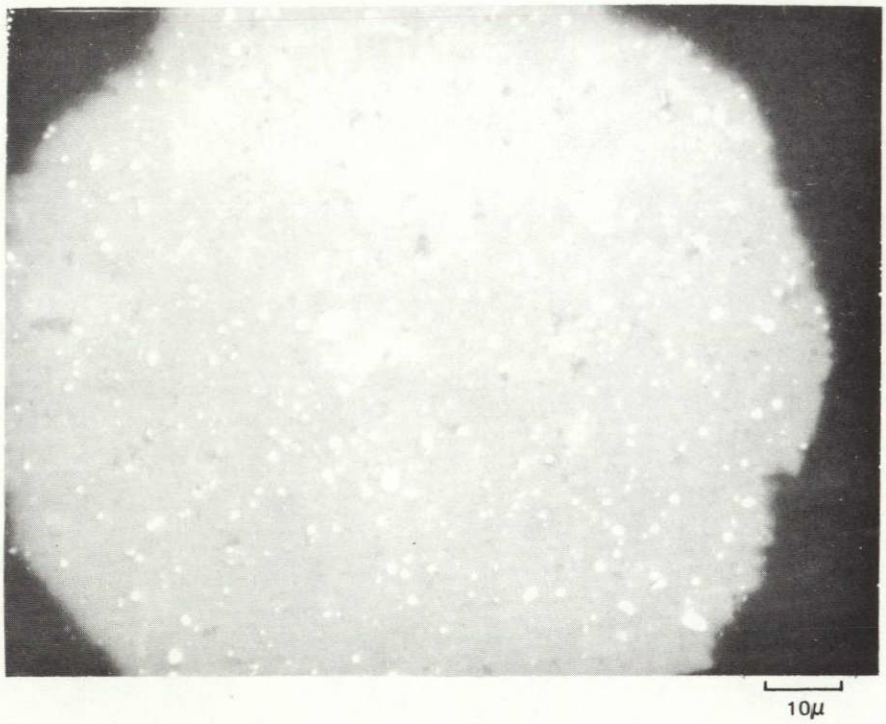

B. SAMPLE 793, COMPOSITION $\beta'1$ + 5 w/o (0.75 ZrO_2 + 0.25 Y_2O_3) σ = 53,000 psi

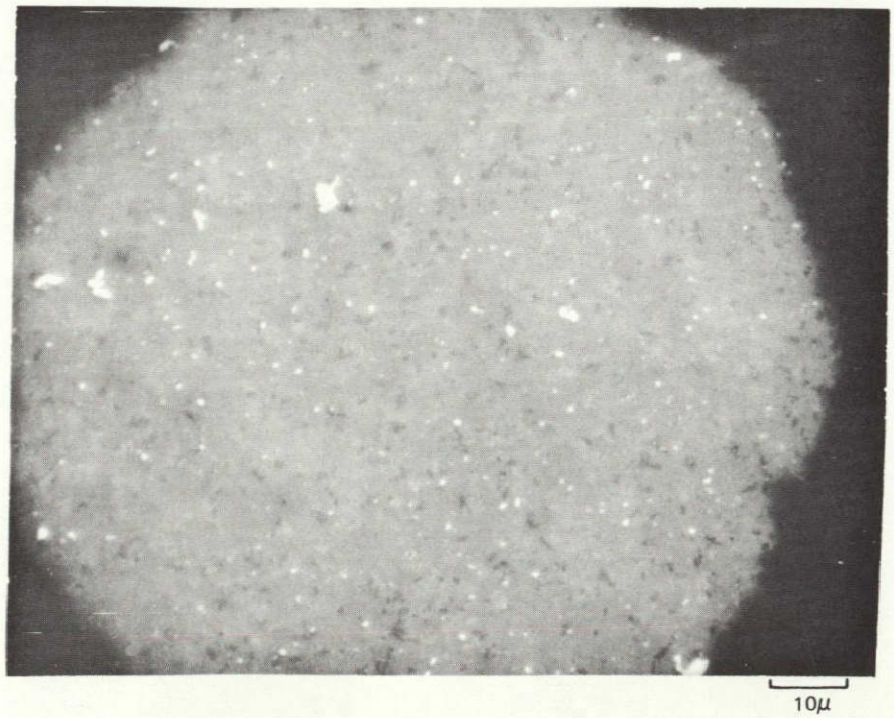

77–03–240–2

FIG. 40

1370°C FRACTURE SURFACES OF SAMPLE 753

(COMPOSITION $\beta''2+5W/O[\cdot925\ ZrO_2+0.075\ Y_2O_3]$, σ =34,000 PSI

A. OVERALL

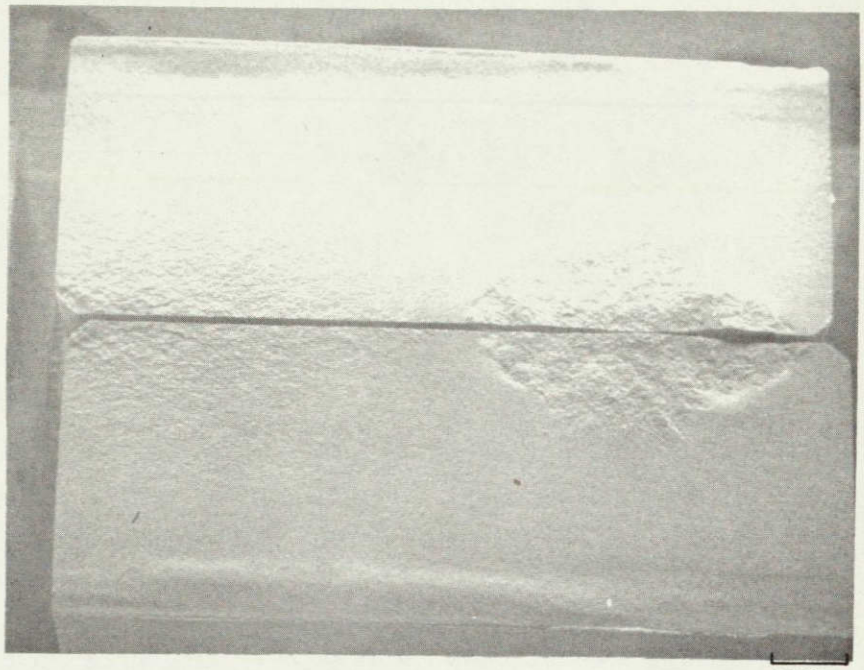

B. INITIATION SITE

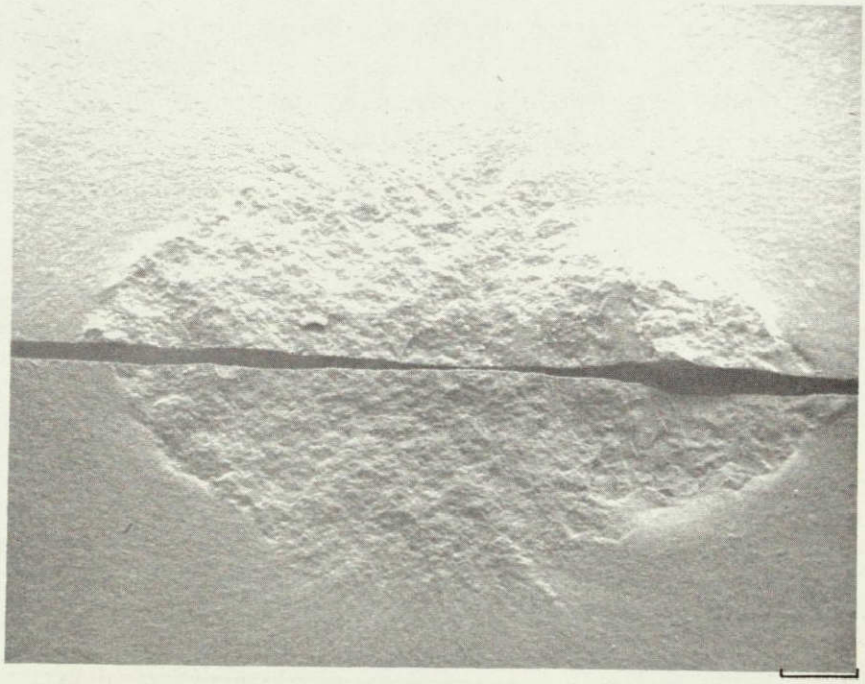

77–03–218–3

found to be a Si-Fe alloy with trace amounts of other impurities. It is known that alloying iron with silicon increases the oxygen and nitrogen partial pressures at which the metal and the various oxynitride phases are in equilibrium (Ref. 27). This is a consequence of the fact that the activity of silicon in the alloy is lower than that of pure silicon. As an example of how this effects the equilibrium nitrogen pressure, consider the following thermochemical equations:

$$3Si + 2N_2 = Si_3N_4 \tag{1}$$

$$K = \frac{a_{Si_3N_4}}{a_{Si}^3 a_{N_2}^2} \cong \frac{1}{a_{Si}^3 p_{N_2}^2} \tag{2}$$

$$p_{N_2} \cong K' a_{Si}^{-3/2} \quad . \tag{3}$$

Wild et al. (Ref. 27) and Colquhoun et al. (Ref. 28) used this fact to raise partial pressures of oxygen and nitrogen to practical and controllable levels in order to study equilibria between Si, α and β Si_3N_4, Si_2N_2O, and SiO_2. By the same token, one can take the quilibrium data of Refs. 27 and 28 to calculate the effect of iron impurities on the decomposition temperature of β Si_3N_4. Figure 41 shows thermochemical diagrams reproduced from Ref. 27 which indicate phase relationships in the Si-O-N system in equilibrium with pure silicon and with an Fe-14 percent Si alloy at 1294°C. These diagrams, and similar diagrams for the temperatures 1200, 1250, 1300 and 1350°C shown in Ref. 28 were used as source data for p_{N_2} at the above temperatures for reaction (1) above, and for the reaction

$$3(SiFe_x) + 2N_2 = Si_3N_4 + 3xFe \quad . \tag{4}$$

These data are plotted as log p_{N_2} vs $1/T^\circ K$ in Fig. 42 and extrapolated to log $p_{N_2} = 0$ to find the decomposition temperature at one atmosphere nitrogen pressure for pure βSi_3N_4 and for material containing iron impurity.

The curve for pure silicon gives a decomposition temperature around 1740°C. Colquhoun et al. calculated free energies of formation from the thermochemical data, and used a least square fit to express these as a function of temperature. From this they also find that β becomes unstable with respect to one atmosphere of nitrogen at 1740°C and comment on the fact that this is considerably below the often quoted decomposition temperature of 1900°C. They state that these data are not

FIG. 41

PHASE RELATIONS IN Si–O–N SYSTEM AT 1294°C

WILD, GRIEVESON, AND JACK

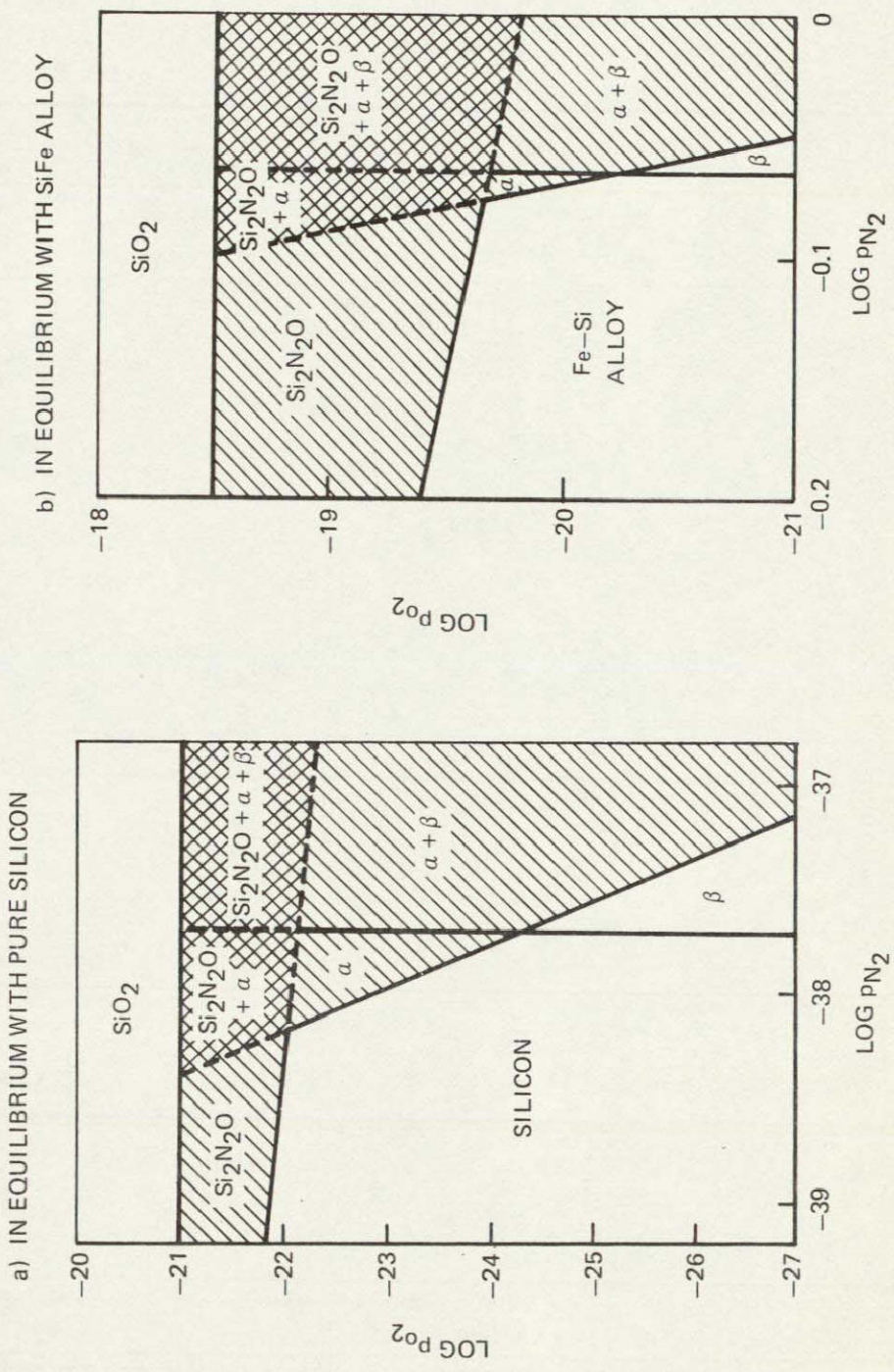

ORIGINAL PAGE IS
OF POOR QUALITY

77–08–81–1

FIG. 42

PRESSURE–TEMPERATURE CURVES

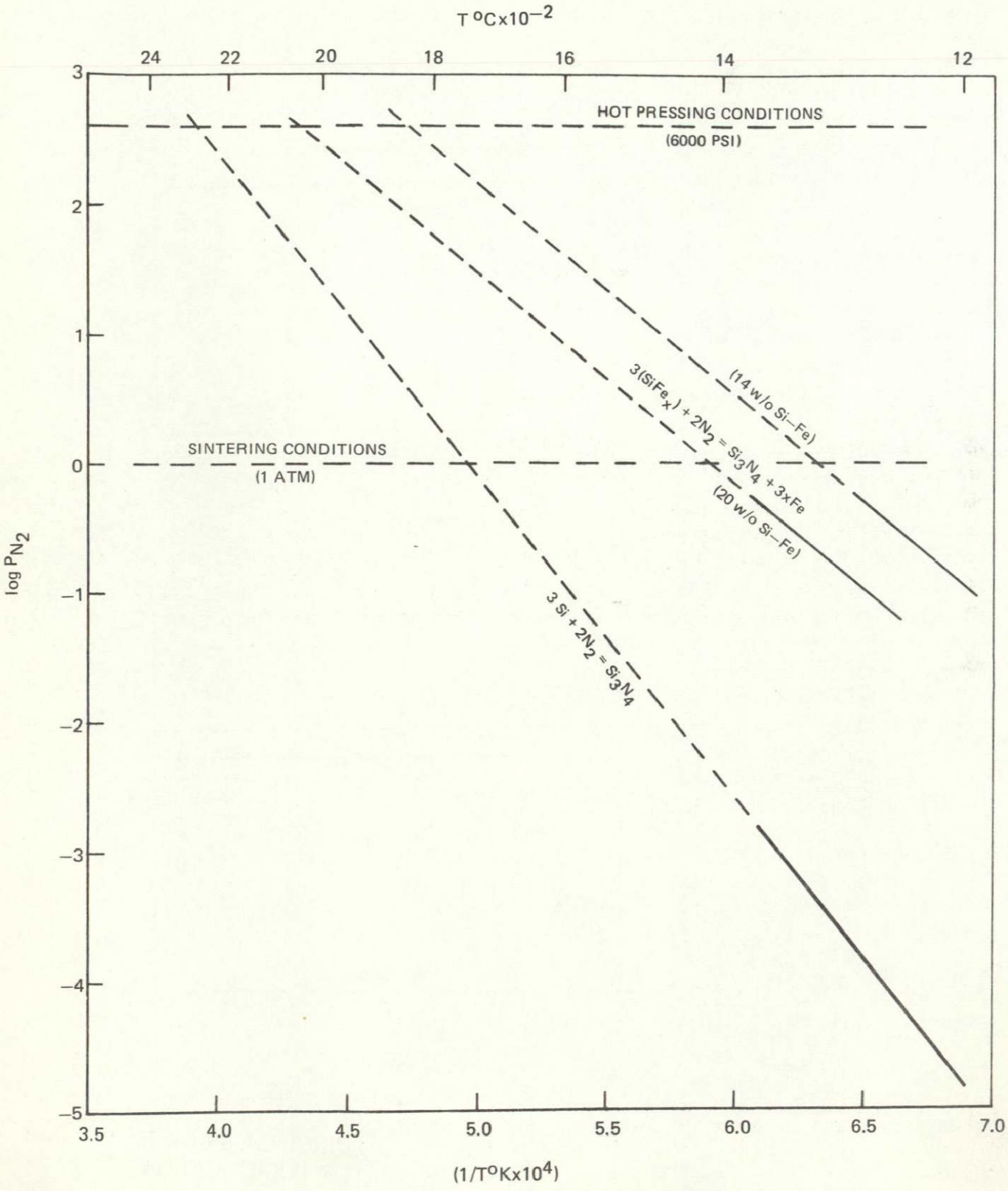

77–08–86–2

sufficiently precise to predict accurately the exact conditions under which transformation will occur, but despite these limitations, the thermochemical data contribute to an understanding of transformations which occur in the Si-N-O system. The present writer also feels that these data contribute to a qualitative understanding of the genisis of high concentrations of metallic inclusion which limit the strength of pressureless sintered β' samples. The starting Si_3N_4 powders used in the batching of various β' compositions contained on the order of 0.5 w/o Fe. The form in which the iron is present is not known, but if present as oxides, these would be reduced to metallic iron under the very low oxygen partial pressure imposed by the carbon susceptor. If any free silicon were present in the starting powders, reaction to form liquid Si-Fe alloy could begin at local sites at temperatures as low as 1220°C. Since at these temperatures no appreciable sintering has occurred the sample has an open porosity on the order of 35-40 percent, so that all the internal surface is available for reaction with the ambient atmosphere. It can be seen from Fig. 42 that when the temperature reaches about 1350°C, Si_3N_4 is unstable in local regions around iron impurities or liquid inclusions that have already formed. There is then a driving force for Si_3N_4 to decompose and alloy inclusions to grow.

In contrast to conditions during pressureless sintering, during hot pressing under typical conditions (6,000 psi or 408 atm) assuming the dies established a closed system, Si_3N_4 would be stable to over 1800°C in the presence of the Fe-Si alloy. By way of contrast, Fig. 43 shows micrographs of (pressureless sintered) sample 676, and a hot pressed sample of similar composition supplied by Dr. John Brennan. Although the latter is not particularly homogeneous in terms of ceramic phases, the virtual absence of metallic inclusions is striking.

It is assumed that analogous reactions occur when ZrO_2 additive is mixed with the β' constituents during pressureless sintering, i.e., reduction of ZrO_2 and alloy formation with silicon thus raising the equilibrium pressure of N_2 and leading to local decomposition of Si_3N_4 (or β' solid solution).

5. Possible Sources of Compositional Variations

Nonreproducibility in sintering behavior between nominally identical batches has been mentioned in regards to β' + CeO_2 and β' + Y_2O_3 samples. In β'2 samples containing 10 w/o CeO_2 where minor phases could be detected by x-rays, these were seen to vary implying either that equilibrium was not necessarily attained during firings or that unaccounted compositional deviations from the nominal composition occurred during preparation. Examples of how minor differences in oxygen content can effect the properties of hot pressed Si_3N_4-Y_2O_3 bodies have been discussed by Lange et al. (Ref. 26) and by Rae et al. (Ref. 25). Figure 44 shows the phase diagram Si_3N_4 - SiO_2 - Y_2O_3 proposed by Lange et al. It can be seen by examining the Si_3N_4 corner of the diagram, that at a constant Y_2O_3 concentration, small difference in SiO_2 content (always present as a surface oxide on Si_3N_4) moves the

COMPARISON OF PRESSURELESS SINTERED AND HOT PRESSED β' MICROSTRUCTURES

A. SINTERED(SAMPLE 676)

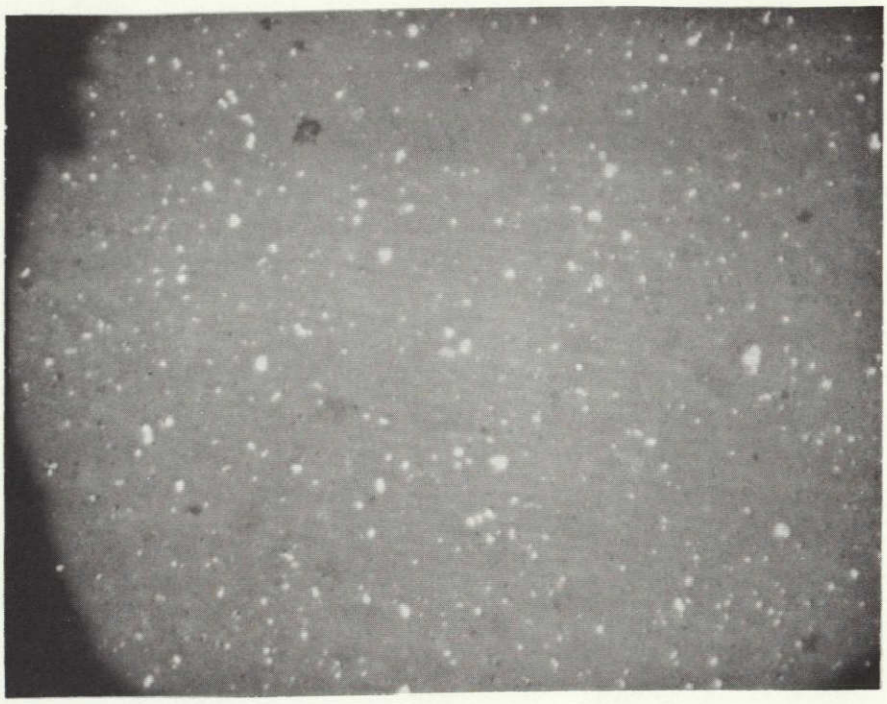

10μ

B. HOT PRESSED

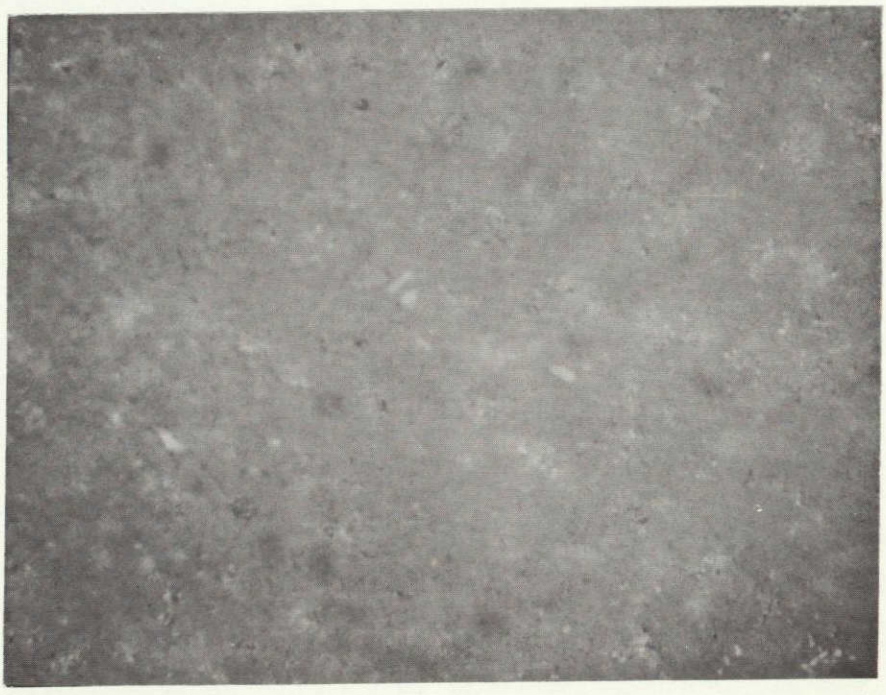

10μ

77–08–86–1

FIG. 44

THE Y_2O_3–Si_3N_4 PHASE DIAGRAM; AFTER LANGE ET AL

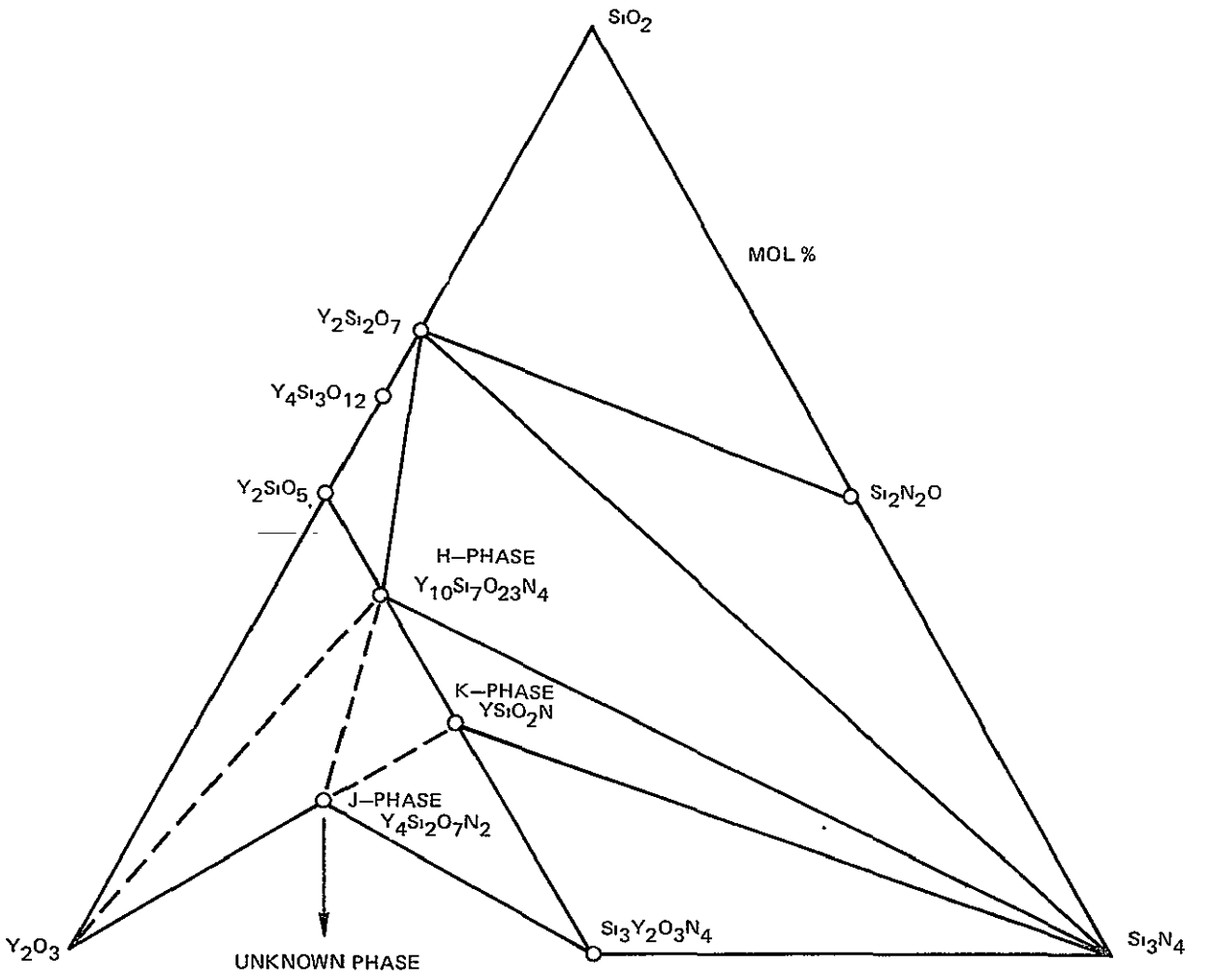

77–08–106–1

overall composition into different compatibility triangles. The details of phase equilibria in the Y-Si-Al-O-N system are not known, but preliminary works at Newcastle (Ref. 25) indicates that no new nitrogen containing crystalline phases occur other than these observed in the Si-Al-O-N and Y-Si-O-N systems. Solid solutions are found between yttrium aluminate phases and ternary Y-Si-O-N phases as shown in Fig. 45, and a region of β' plus liquid (which can be cooled to a glass) is found to extend from Si_3N_4 toward the low melting eutectic in the system Al_2O_3-Y_2O_3. The compositions in the Y-Si-Al-O-N system that were investigated in the present work lay outside the regions of the system for which Rae presents data, and other phases, principally the AlN polytypes discussed by Jack (Ref. 16) become involved in the compatibility relationships. The point to be made is that, whereas in the ternary system Y-Si-O-N slight differences in composition (SiO_2 content) can move the overall composition between four different compatibility triangles, in the quinternary system the overall composition can shift between larger numbers of compatibility pyramids that are as yet undelineated. An attempt was made to pinpoint processing variables that could effect slight alterations of chemistry, and these are discussed below.

a. Media Pick-Up

Batches were formulated assuming that a given weight of material (calculated as SiO_2 and Al_2O_3) would be worn from the media and consequently introduced into the batch. In some instances the prediction was accurate, but in general the actual media loss was somewhat more or less than predicted. In Appendix II we have gone back over the fabrication data and have calculated the deviation of the batch from the calculated composition that was due to variable media wear. The number entered in the column labeled "Deviation (%)" has the following meaning. A positive value means that an excess of aluminocilicate in the amount equal to the indicated percentage of the total β' constituent weight of the batch was introduced. Thus, a measured media weight loss of 2.9 grams when the 100 g β' batch formulation was based on a predicted loss of 2.7 grams, is expressed as a deviation of +0.20 percent. It is not possible to state how positive and negative deviations would effect the phase assemblages in cases where additives such as Y_2O_3 and ZrO_2 are present in the batch because details of phase equilibria for the relevent quinternary systems are not available. It is possible to state how positive and negative deviations would effect the phase assemblages in the absence of such additions. Consider composition β'2 (35 percent Si, 7.86 percent Al, 7.86 percent O, 49.28 percent N). If this is prepared with a +0.5 percent deviation as defined above, the composition would be 35.02 percent Si, 7.85 percent Al, 7.87 percent O, and 49.29 percent N. This would place the composition just inside the two phase field (β' + X) where X phase has the composition 13.0 percent Si, 26.08 percent Al, 52.17 percent O, and 8.71 percent N. Lever rule calculations show that this composition would consist of about 99.3 percent β' and 0.7 percent X. The X phase would be liquid at the sintering temperature and tend to promote sintering. A deviation of -0.5 percent would place the composition in a two phase field where no liquid would be present. Although, as previously stated, details of the relevent quinternary systems are not available, it is reasonable to expect positive deviations to promote liquid formation and sintering.

SOME COMPATIBILITY DATA FOR THE SYSTEM Y–Si–Al–O–N AFTER RAE ET AL

A. THE 2M 3X PLANE OF THE Y–Si–Al–O–N SYSTEM

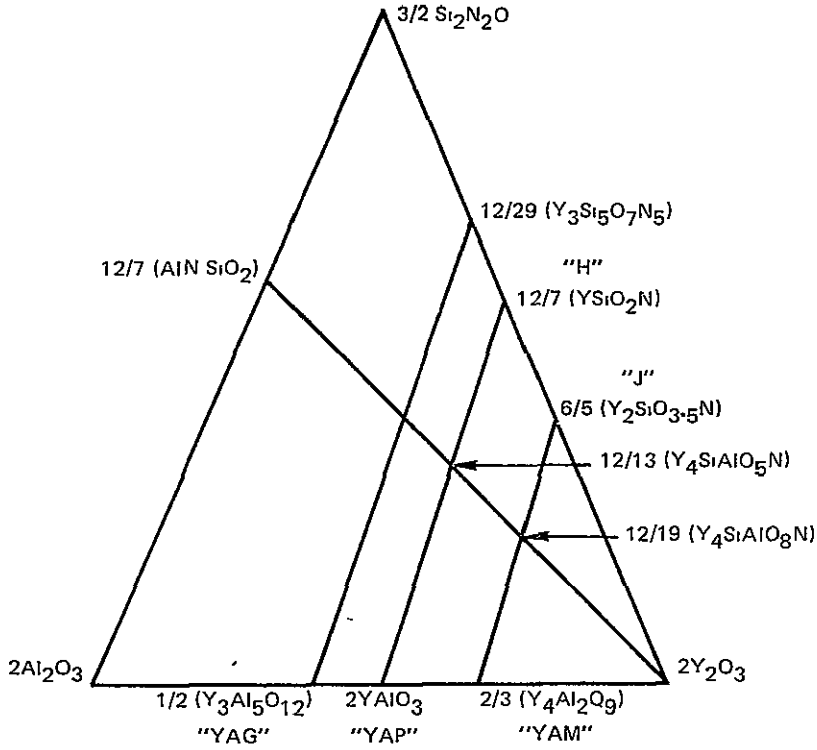

B. THE Y_2O_3–Si_3N_4–Al_2O_3 BEHAVIOR DIAGRAM AT 1700°C

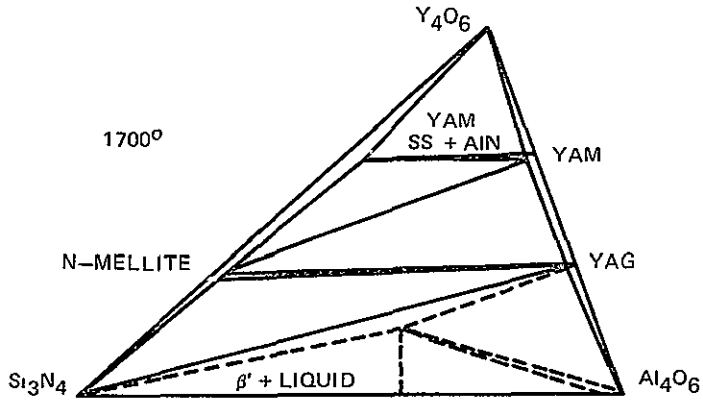

ORIGINAL PAGE IS
OF POOR QUALITY

77–08–106–2

We have gone through Appendix II averaging the density and strength values for all samples showing positive compositional deviation, and also for all samples showing zero or negative deviations. The results are shown in Table 22. There would appear to be a correlation of high strength with positive deviations, but this does not correlate with high density. It is likely that this kind of averaging disregarding specific additives is not particularly instructive, and that such an examination is valid only in the cases of nominally identical compositions. Data are abstracted from Appendix II and grouped according to composition in Table 23. In these tables no clear and consistent trends in properties with compositional deviations due to errors in calculations media attrition are evident.

TABLE 22

AVERAGES OF COMPOSITIONAL DEVIATIONS, BULK DENSITIES, AND FLEXURAL STRENGTHS OF TEST BARS

Average Deviation (%)	Average Bulk Density (g/cc)	Average Strength (kpsi)
+ 0.5	2.98	61
- 0.2	3.02	51

b. Oxidation During Low Temperature Firing

The possibility that significant oxidation of samples could occur during the 600°C air firing of calcined ball milled powders was investigated. The weight changes of samples heated in air for one hour are recorded in Table 24. All samples lost about 0.04 percent after heating to 125°C. Additional heating at 500, 550, and 600°C resulted in increasing weight losses with increasing temperature. At 650°C the sample exhibited a lower weight loss than at 600°C. Oxidation of the samples according to the reaction $Si_3N_4 + 3\ O_2 \rightarrow 3\ SiO_2 + 2\ N_2$ should result in a weight increase of 28 percent at completion.[2] The weight losses observed may be due to the release of sorbed material, or possibly to further loss of organic material not completely removed in the final calcining operation. It can be concluded that measurable oxidation occurs only above 600°C, and that no significant changes in sample stoichiometry resulted from the 1 hour calcining at 600°C.

TABLE 23

COMPOSITIONAL DEVIATION AND AVERAGE DENSITY OF TEST BARS FROM DIFFERENT BATCHES OF THE SAME NOMINAL COMPOSITION

Batch Composition	Batch Number	Deviation (%)	Average Bulk Density (g/cc)
β'1 + 2.5 Y_2O_3	1	+ 0.7	3.08
	2	- 0.2	2.93
β'1 + 5 Y_2O_3	1	- 0.1	2.78
	2	- 0.5	3.20
β'2 + 5 Y_2O_3	1	+ 0.2	3.24
	2	- 0.5	3.26

TABLE 24

WEIGHT CHANGES OF SAMPLES OF β'1 + 2.5 w/o (.75 ZrO_2, .25 Y_2O_3) DURING AIR FIRING TO DIFFERENT TEMPERATURES

	Weight Change After 125°C Heating (%)	Total Weight Change After Additional Firing to Indicated Temperature (%)
Sample 1	-.041	500°C - .095
Sample 2	-.040	550°C - ..097
Sample 3	-.043	600°C - .108
Sample 4	-.044	650°C - .077

c. Other Possible Sources

Variable media pick-up and oxidation during low temperature burn-out do not appear to be sufficient to account for the difference in sintering properties of different batches. Barring errors in weighing out the constituents (which of course is a possibility) it would appear that sources of substantial chemical variability exist that have not yet been identified. Some possible sources may be:

Continued hydrolysis of Si_3N_4 starting powders from atmospheric water during storage so that the oxygen content varies with time.

The presence of variable amounts of water dissolved in the methanol used in ball milling the batches.

Further studies of processing conditions are necessary to insure the maintenance of desired stoichiometry.

6. 1370°C Creep Measurements

Creep measurements were made on sample 737 (composition $\beta'2 + 5\ Y_2O_3$), sample 757 (composition $\beta'2 + 5\ [.925\ ZrO_2\ .075\ Y_2O_3]$), and sample 822 (composition $\beta'2 + 5[.8\ ZrO_2\ .2\ Y_2O_3]$). The creep curves for stress levels of 10,000 psi at 1370°C are shown in Figs. 46, 47 and 48, respectively. Strain was calculated from the formula

$$\varepsilon = \frac{2\ h\ (n+2)}{L^2}\ y_L$$

where h = specimen thickness
L = span
y_L = cross head displacement
n = the empirical stress exponent of creep rate.

The value of n was taken as 1.75. This is the value determined by Din and Nicholson (Ref. 29) for hot pressed Si_3N_4 (Norton HS-130). The creep rate of sample 737 was still decreasing slightly after 55 hours of testing. The rate at this time was 6×10^{-5} hr^{-1}. This may be compared with the steady state creep rate interpolated from data of Din and Nicholson for HS-130 at 10,000 psi stress and 1370°C of 10×10^{-5} hr^{-1}. Sample 757 failed at a strain of 0.030 after only 5 hours, and 822 failed at a strain of 0.047 after 18 hours. Clearly $\beta'2$ composition containing substantial amounts of ZrO_2 are totally inadequate for stressed applications at high temperature.

FIG 46

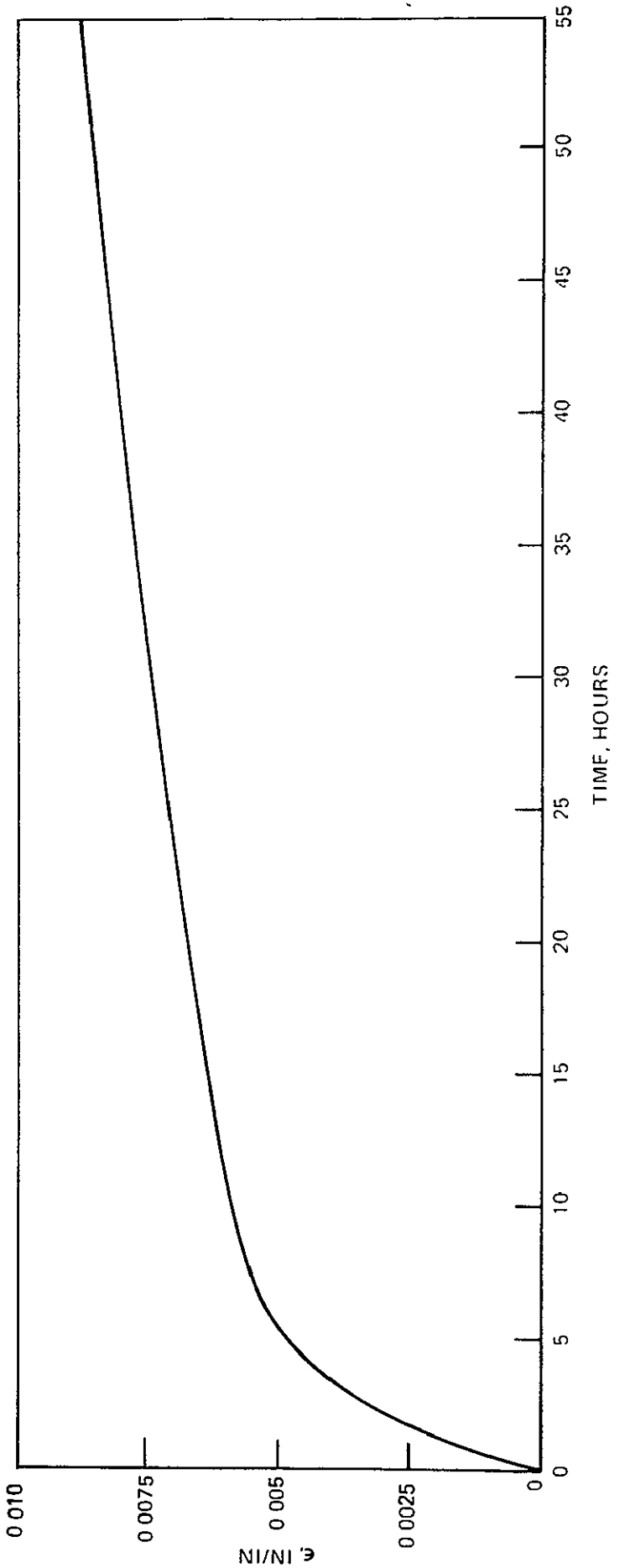

77–03–261–1

FIG 47

CREEP CURVE FOR SAMPLE 757

10KPSI, 1370°C ARGON ATMOSPHERE

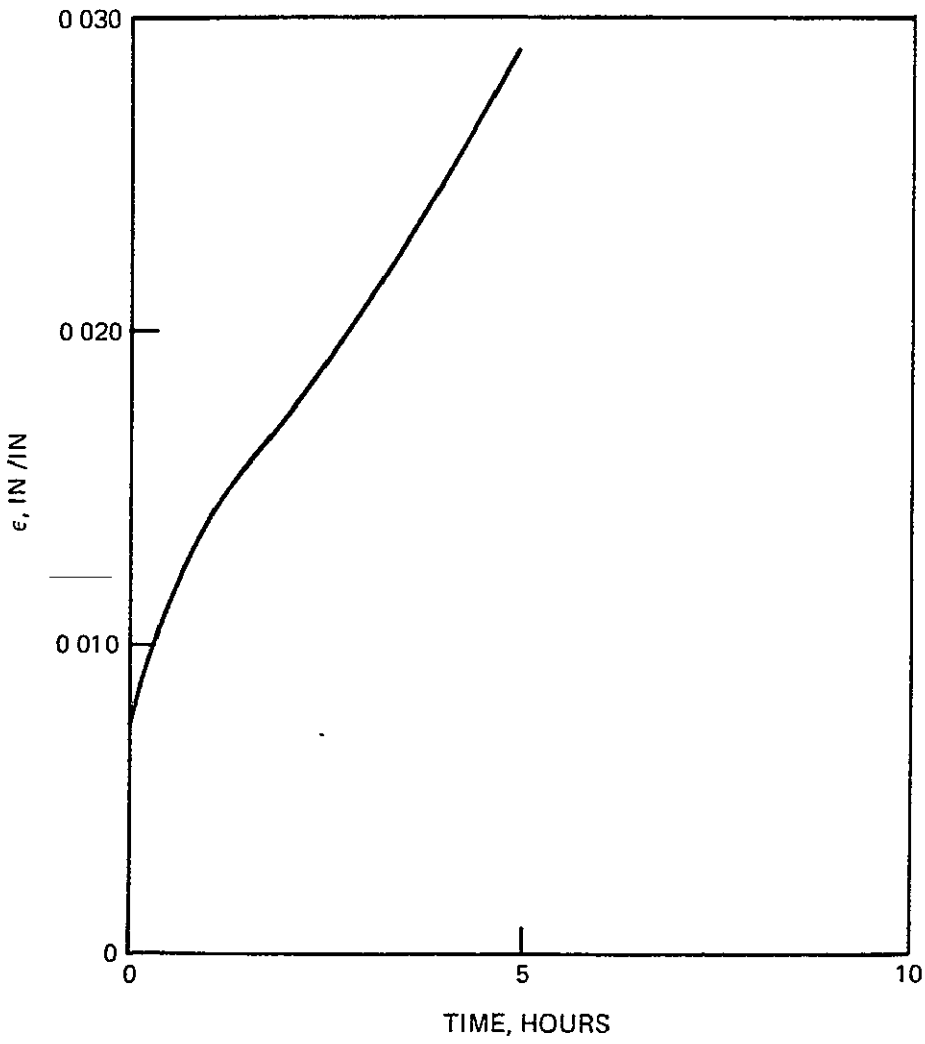

77-04-265-1

CREEP CURVE FOR SAMPLE 822

10KPSI 1370°C AIR ATMOSPHERE

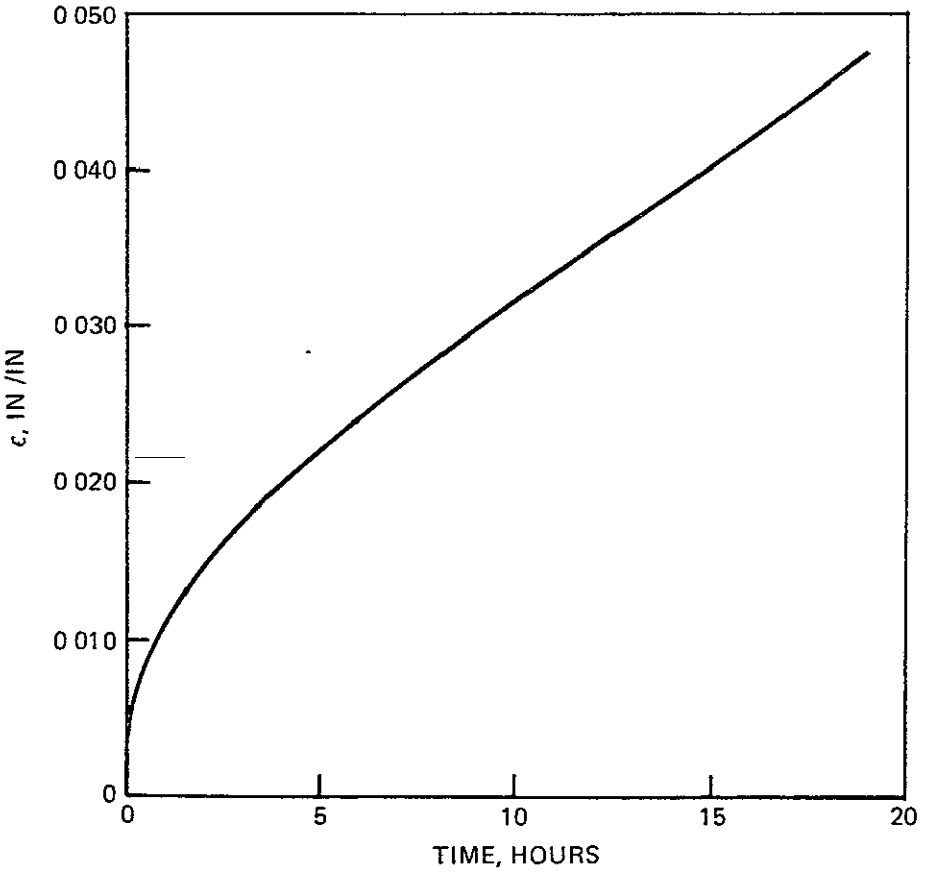

77–04–265–2

7. Oxidation Measurements

a. Initial Measurements

Initial oxidation measurements were performed on fractured flexural test specimens that had been polished on all faces. One half of the specimen was oxidized at 1000°C for periods up to 70 hours, and the other half at 1300°C for periods up to 37 hours. The first compositions investigated were β' compositions containing CeO_2, Y_2O_3, ZrO_2, or $GaPO_4$ and a β'6 composition prepared without additions of foreign oxides by a transient liquid phase technique developed under a different program (Ref. 17). Curves of weight gain vs time for these samples are shown in Figs. 49 and 50. All samples exhibited an initial high rate of weight gain followed by a nearly linear gain after a few hours. The magnitude of the initial weight gain probably depends on factors such as surface finish, open porosity, and the amount and nature of grain boundary phases. As important as the initial gain, is the slope of the subsequent portions of the curves. At 1000°C, except for sample 503 (β'2 + 20 ZrO_2), all samples reached essentially constant weight after 10 hours. These samples exhibited irridescent surface films. Sample 503 however, continued to gain weight and eventually cracked apart. At 1300°C all the samples continued to gain weight at a nearly constant rate up to the point where the measurements were discontinued. The slopes of the linear portions of the curves are shown in Table 25. The β'2 + 10 CeO_2 samples exhibited the highest rate of oxidation. The rate was lower for β' compositions with higher aluminum concentrations (β'4 and β'6). The rates for the β'2 + 20ZrO_2 and β'2 + 10Y_2O_3 were about equal, and 4 times that of the TLP sample. The oxidation product on the CeO_2 bearing samples was a yellowish glass which appeared to have been quite fluid at the oxidation temperature. Samples containing Y_2O_3 and ZrO_2 had thin glazed coatings, whitish in color which gave tridymite like diffraction patterns with additional unidentified peaks.

b. Further Testing New Formulations

i. Rationale

The initial oxidation testing showed that the formulations tested all had rather high oxidation rates relative to that of the TLP sample. These observations guided the selection of new formulations in pursuit of more oxidation resistant bodies. Lower concentrations of the various successful sintering aids were investigated, as were mixtures of ZrO_2 and Y_2O_3 sintering aids which appeared to alleviate the 1000°C crumbling problem encountered using ZrO_2 alone. As these experiments progressed it became apparent that phase equilibria in the systems which contained the oxidation products - particularly the liquidus surface - was a controlling factor in the oxidation behavior of the various formulations. Those formulations whose oxides fell in systems with minimum eutectic temperatures well above the test temperature, (the system SiO_2-Al_2O_3 for the TLP samples and the system SiO_2-Al_2O_3-ZrO_2 for the β'+ ZrO_2 samples) exhibited thin, stable oxide scales whereas formulations whose oxidation

FIG. 49

WEIGHT GAIN OF SiAlON SAMPLES DURING HEATING IN AIR AT 1000°C

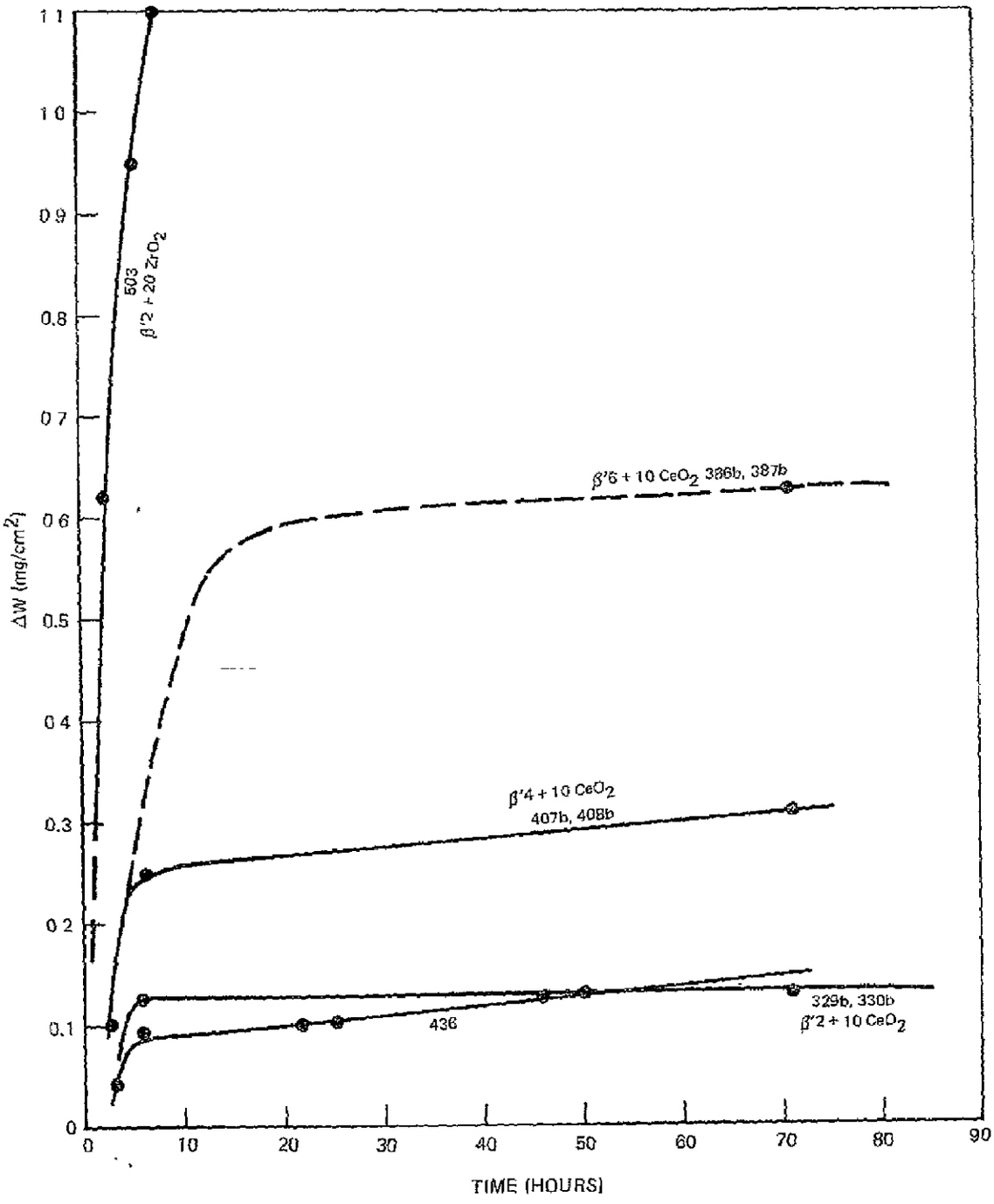

76–09–139–10

WEIGHT GAIN OF SiAlON SAMPLES DURING HEATING IN AIR AT 1300°C

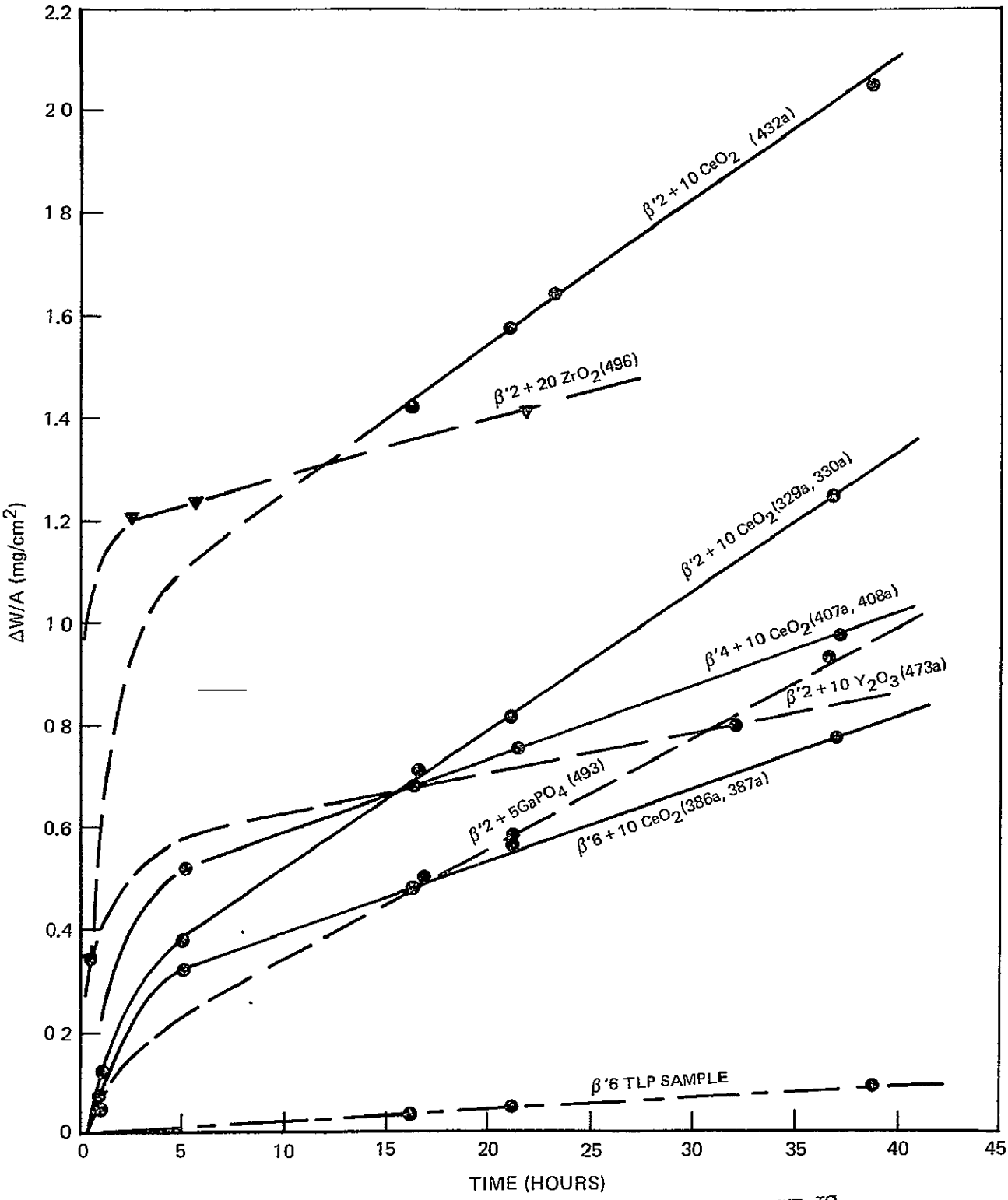

ORIGINAL PAGE IS
OF POOR QUALITY

76–09–139–11

TABLE 25

1300°C OXIDATION RATE DATA FOR VARIOUS SiAlON COMPOSITIONS

Sample Number	Composition	Oxidation Rate ($mg/cm^2 hr$)
432a	β'2 + 10 CeO_2	.027
329a	β'2 + 10 CeO_2	.027
407a	β'4 + 10 CeO_2	.014
386a	β'6 + 10 CeO_2	.014
473	β'2 + 10 Y_2O_3	.008
493	β'2 + 5 $GaPO_4$	.021
496	β'2 + 20 ZrO_2	.010
β'4 TLP	β'4	.002

products fell in the systems with low melting ternary eutectics (e.g., SiO_2-Al_2O_3-Y_2O_3, with a eutectic temperature below 1400°C) formed fluid glasses that afforded little protection. For this reason systems were investigated for which the oxidation products would lie in high melting ternary oxide systems. Hence the choice of Cr_2O_3, TiO_2 and HfO_2 and the investigation of other rare earth oxides as prospective sintering aids. The only SiO_2-Al_2O_3-rare earth system for which the phase diagram was found is the Y_2O_3 system reproduced in Fig. 51. It was assumed that other rare earth systems would be similar, and that the temperature of binary eutectics in the rare earth - SiO_2 systems might be an indicator of the relative temperatures of the lowest ternary eutectics. Fig. 52 is a generalized rare earth - SiO_2 diagram. The eutectic temperatures labeled T_1 and T_2 in those systems for which data was found are listed in Table 26. This shows that the lowest melting eutectic (T_2) in the Y_2O_3 system is in the middle of the range, with La_2O_3 and Nd_2O_3 lower and only Er_2O_3 higher.

FIG. 51

SYSTEM Al_2O_3–Y_2O_3–SiO_2 AFTER BONDAR AND GALAKHOV

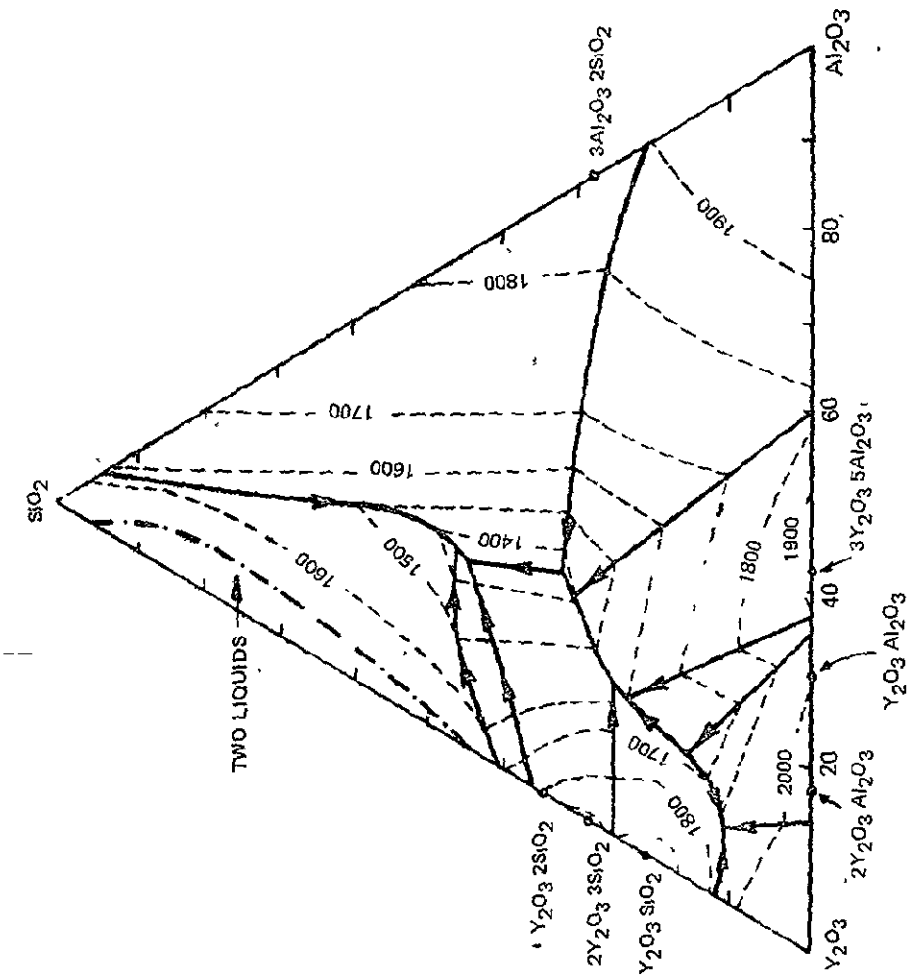

77-06-164-1

FIG. 52

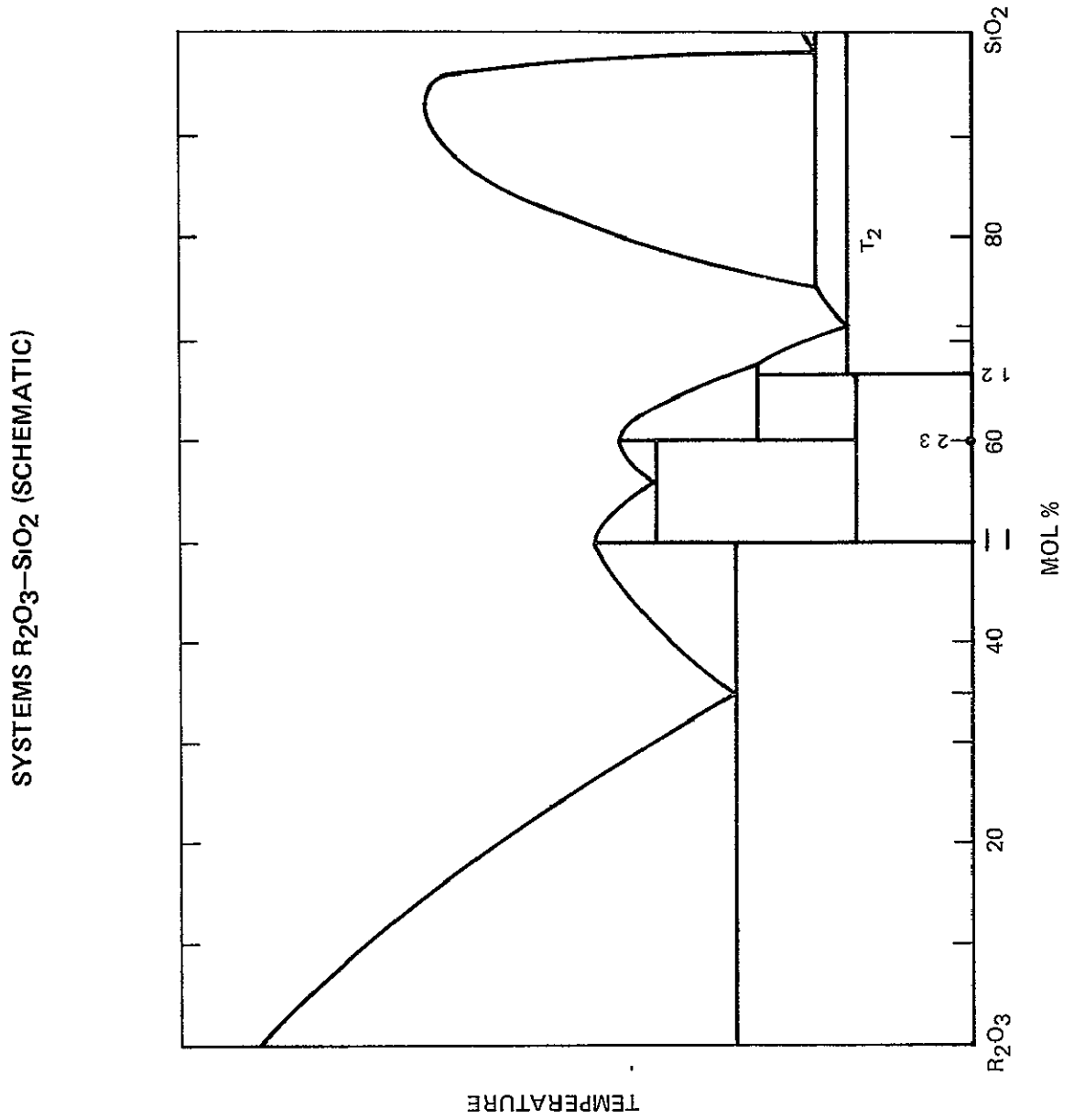

ORIGINAL PAGE IS
OF POOR QUALITY

77–06–164–3

TABLE 26

EUTECTIC TEMPERATURES IN R_2O_3-SiO_2 SYSTEMS

(See Figure 52)

R_2O_3	Ti (°C)	T_2 (°C)
Dy_2O_3	1790	1640
Er_2O_3	1880	1680
Gd_2O_3	1810	1640
La_2O_3	1775	1625
Nd_2O_3	1680	1600
Sc_2O_3	1850	1660
Sm_2O_3	1810	1650
Yb_2O_3	1850	1650
Y_2O_3	1800	1660

ii. Test results

Weight gain with time at 1300°C for β'2 composition containing different concentrations of CeO_2 and Y_2O_3 are shown in Figs. 53 and 54, respectively, and it can be seen that the oxidation rate decreases somewhat with decreasing rare earth concentration. Weight gains at 1400°C for these compositions are compared with TLP samples and β'2 + 5 ZrO_2 in Fig. 55. At this temperature, the films on the Y_2O_3 samples appear to be nonprotective. The thick partially crystallized (cristobalite) glassy films tend to spall during cooling giving erratic weight gain curves. The films on the CeO_2-bearing samples remained all glass and did not spall, but appeared to have been very fluid. The films will be examined in more detail latter in this report. The TLP samples and the β'2 + 5% w/o ZrO_2 samples on the other hand appear to be exceptionally resistant to oxidation, with unmeasurable weight gains after about 20 hours. X-ray diffraction patterns from the surface of sample 594 (β'2 + 5 ZrO_2) showed faint peaks that could be interpreted as zircon ($ZrSiO_4$) in addition to

FIG. 53

WEIGHT GAIN IN AIR AT 1300°C OF COMPOSITION $\beta''2$ PREPARED WITH DIFFERENT PERCENTAGES OF CeO_2

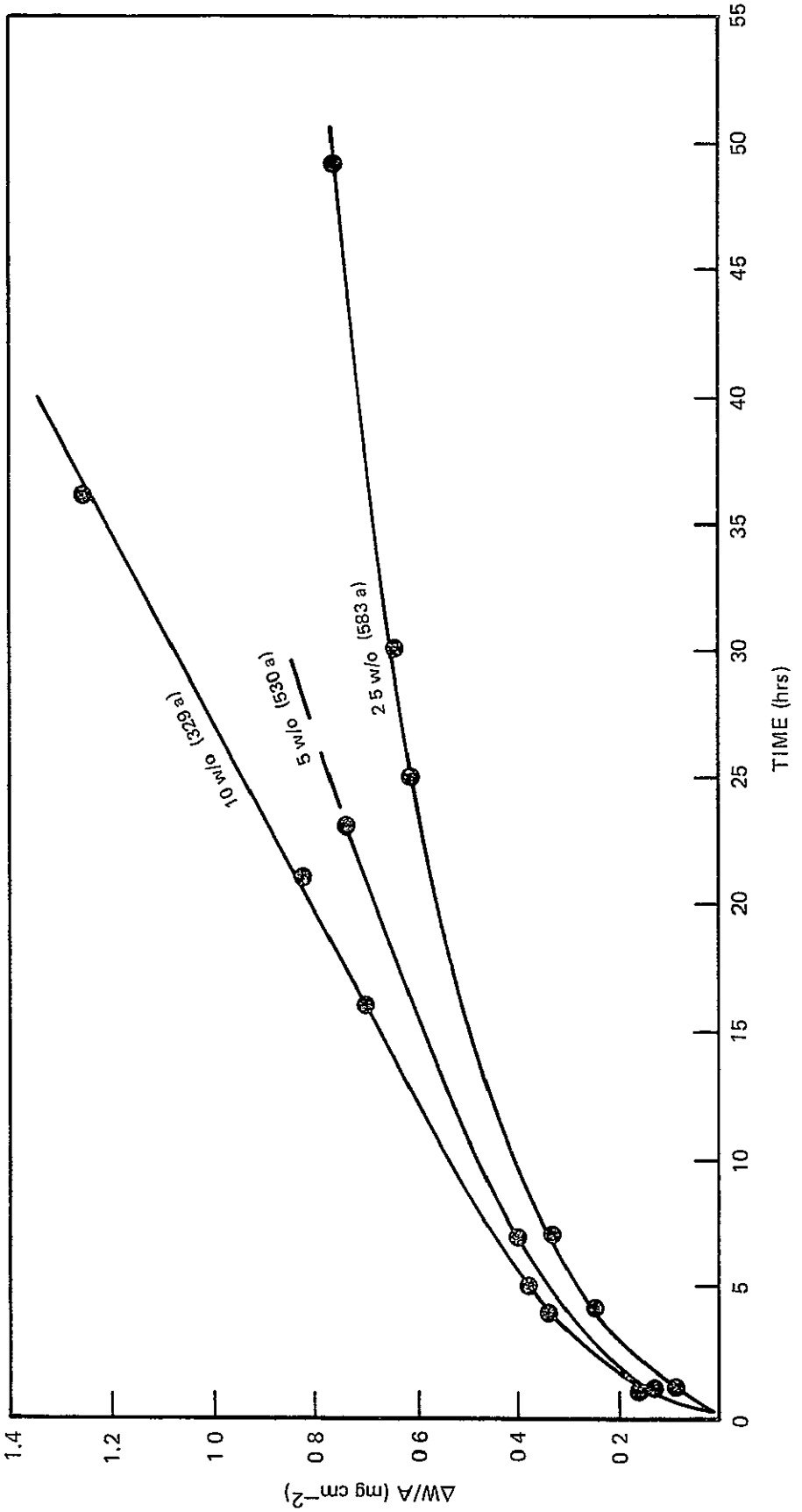

76–10–234–2

FIG. 54

WEIGHT GAIN IN AIR AT 1300°C OF COMPOSITION β''2 PREPARED WITH DIFFERENT PERCENTAGES OF Y_2O_3

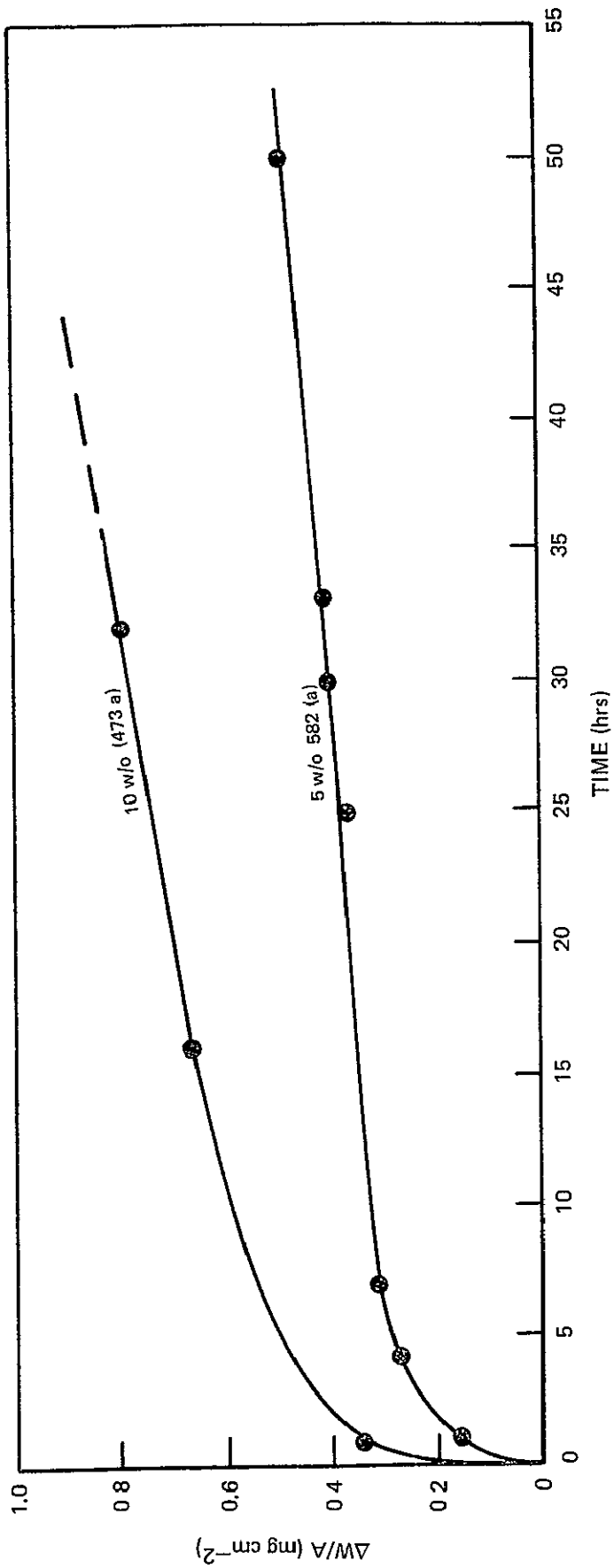

ORIGINAL PAGE IS
OF POOR QUALITY

76–10–234–3

FIG. 55

WEIGHT GAIN IN AIR AT 1400°C OF VARIOUS SiAlON COMPOSITIONS

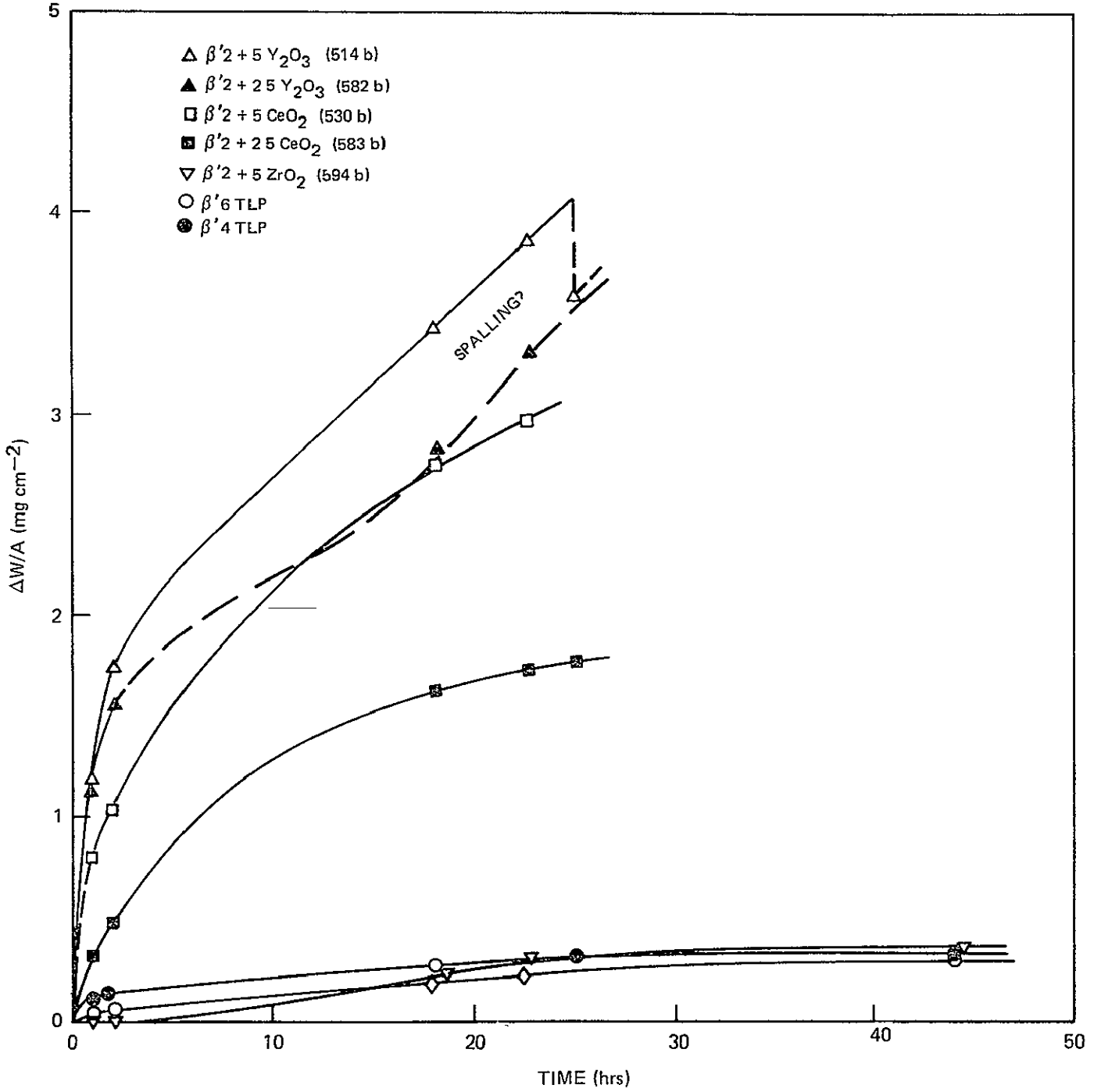

76–10–234–1

strong β' peaks, and the surface had a whitish crystalline appearance as shown in Fig. 56B. However, the β'2 + 5 ZrO_2 bars cracked apart during oxidation at 1000°C as shown in Fig. 56A. Replacement of small amounts of ZrO_2 with Y_2O_3 was made in this formulation in the hope that this would prevent the 1000°C crumbling, and this proved to be the case as shown in Fig. 56C. Replacement of as little as 7.5 w/o of the ZrO_2 (sample 705) was effective in preventing cracking at 1000°C and resulted in formulations that were only slightly inferior to β'2 + 5 ZrO_2 as shown by the weight gain curves, Fig. 57. Samples of compositions β'2 and 3.2 m/o additions of the various rare earth oxides were oxidized at 1400°C and curves for these samples are shown in Fig. 58. As pointed out earlier, these samples exhibited about 10 percent porosity and as a consequence showed a high initial weight gain. Sample 888 for example, showed about twice the initial weight gain as did sample 514 having the same composition. From Fig. 58 it can be seen that the weight gains varied inversely as the binary eutectic temperatures listed in Table 26. This is presumed to be a result of the relative fluidity of the liquid films that formed. This will be illustrated when micrographs of the oxide films are discussed.

β'1 compositions with low concentrations of Y_2O_3 and ZrO_2-Y_2O_3 mixtures were also investigated. These data are superimposed as dashed lines on the data for β'2 compositions in Fig. 59. Some of the data of Fig. 59 are displayed on a parabolic plot $(W/A)^2$ vs t in Fig. 60 for comparison with the data of Trip and Graham (Ref. 30) for the 1400°C oxidation of Norton HS-130 hot pressed Si_3N_4. Only those β'1 and β'2 compositions containing less than about 0.6 w/o Y_2O_3 in mixtures with ZrO_2 appear to offer static oxidation behavior comparable to hot pressed Si_3N_4.

It can be seen from the above figures that in general the oxidation kinetics are complex. We will not attempt to account for the specifics of the oxidation curves. However, examination of the oxide films gives some clues to some of the processes that take place during oxidation. Micrographs of polished sections through oxides layers on samples are shown in Figs. 61 through 66. Figure 61B shows that the oxide film on the β'2 + 5 ZrO_2 sample is too thin to be distinguished clearly because of rounding of the edge during polishing, but at any rate is less than 2μ thick after 43 hours of testing at 1400°C. The same composition with about 20 w/o the ZrO_2 replaced by Y_2O_3 (sample 639) had a partially crystalline scale about 50μ thick after 28 hours (Fig. 61A). The scales became thicker as the Y_2O_3 concentration increased, and for the β'2 + 5Y_2O_3 sample the scale was about 150μ thick after 25 hours (Fig. 62A). These partially crystallized glassy scales appear to be highly stressed and tend to break and pull out during polishing. The scale on the β'2 + 5CeO_2 sample (Fig. 62B) appeared to be all glass with an average thickness of about 60μ. When the β'2 + 5 w/o (3.2 m/o) Y_2O_3 sample was oxidized for periods up to 120 hours, the nature of the oxide layer changed from a partially crystalline film after 25 hours to an all glass (liquid) film shown in Fig. 63. The liquid was apparently quite viscous and had frothed. It would appear the nitrogen diffusion through the liquid is much slower than oxygen diffusion, and nitrogen bubbles form in order to effect the exchange that must occur during oxidation (simplified as $Si_3N_4 + 6O_2 \rightarrow 3SiO_2 + 2N_2$). Most of this froth was broken off prior to mounting and polishing, so that the glass still adhering to the samples in Fig. 63B is ragged and very thin in most

FIG. 56

OXIDIZED SURFACES OF TEST BARS CONTAINING ZrO_2 AND ZrO_2–Y_2O_3 MIXTURES

1000μ

a) 5.0 w/o
ZrO_2
1000°C
48 hrs
(596)

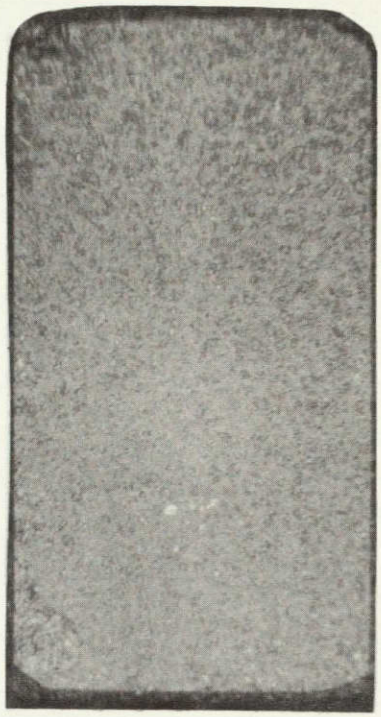

b) 5.0 w/o
ZrO_2
1400°C
45 hrs
(594)

1000μ

c) 5.0 w/o
(·8 ZrO_2 + 0.2 Y_2O_3)
1000°C
48 hrs
(640)

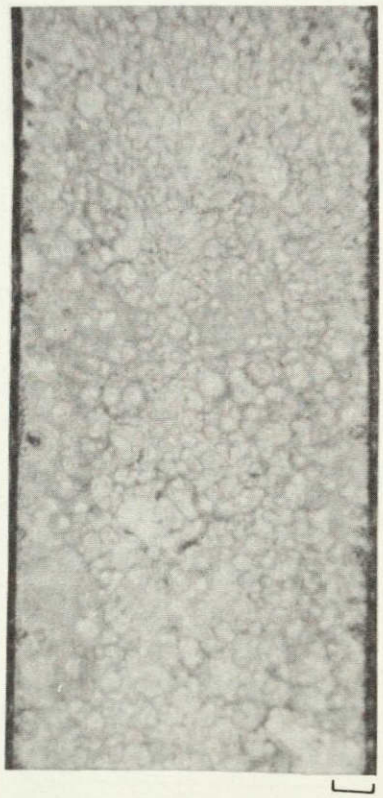

1000μ

d) 5.0 w/o
(·8 ZrO_2 + 0.2 Y_2O_3)
1400°C
28 hrs
(639)

76–12–132–2

WEIGHT GAIN IN AIR AT 1400°C OF COMPOSITION $\beta'2$ PREPARED WITH FIVE WEIGHT PERCENT OF ZrO_2–Y_2O_3 MIXTURES

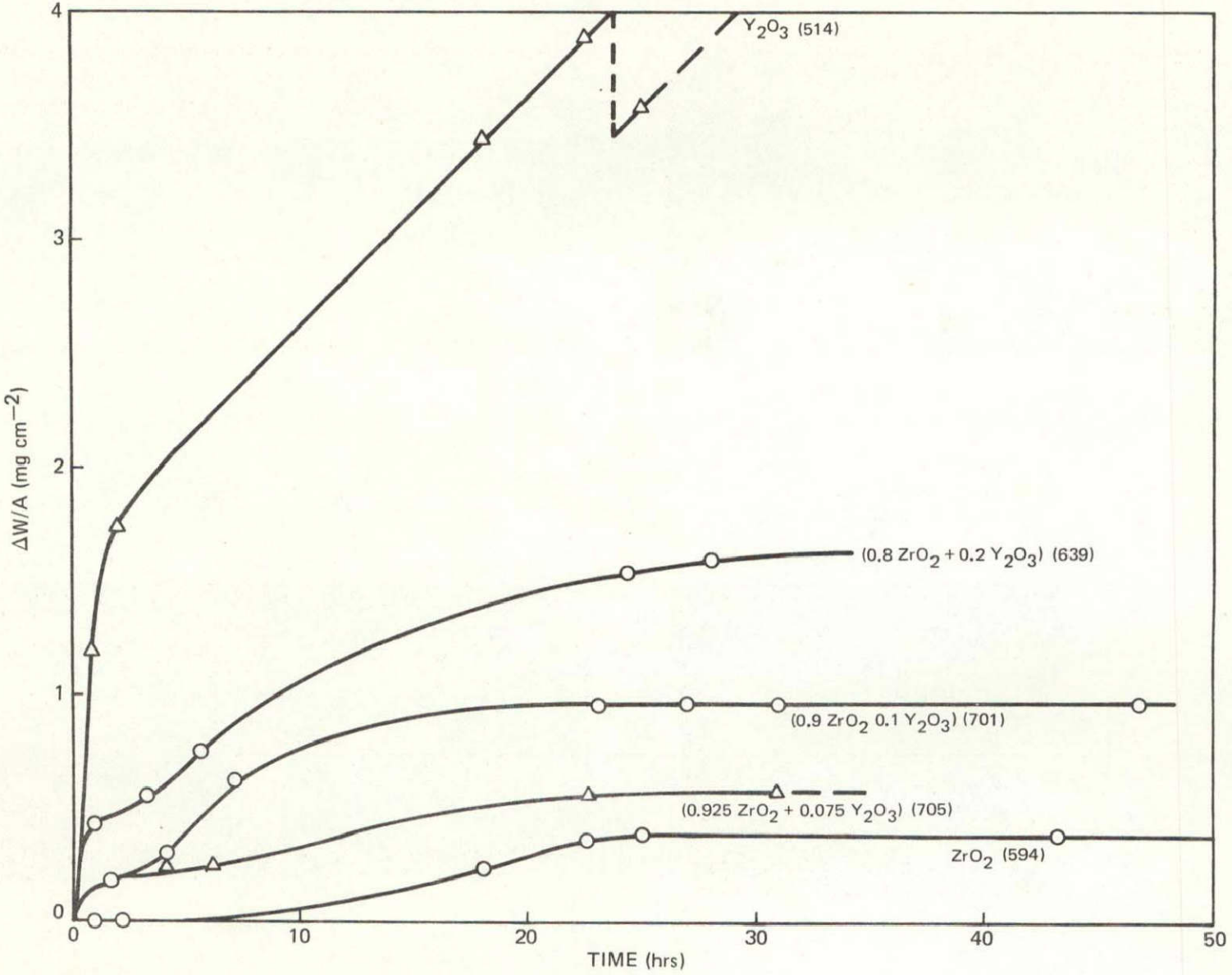

76-12-128-1

FIG. 57

FIG. 56

WEIGHT GAIN IN AIR AT 1400°C OF β'_2 COMPOSITIONS CONTAINING 3.2 m/o OF DIFFERENT RARE EARTH OXIDES

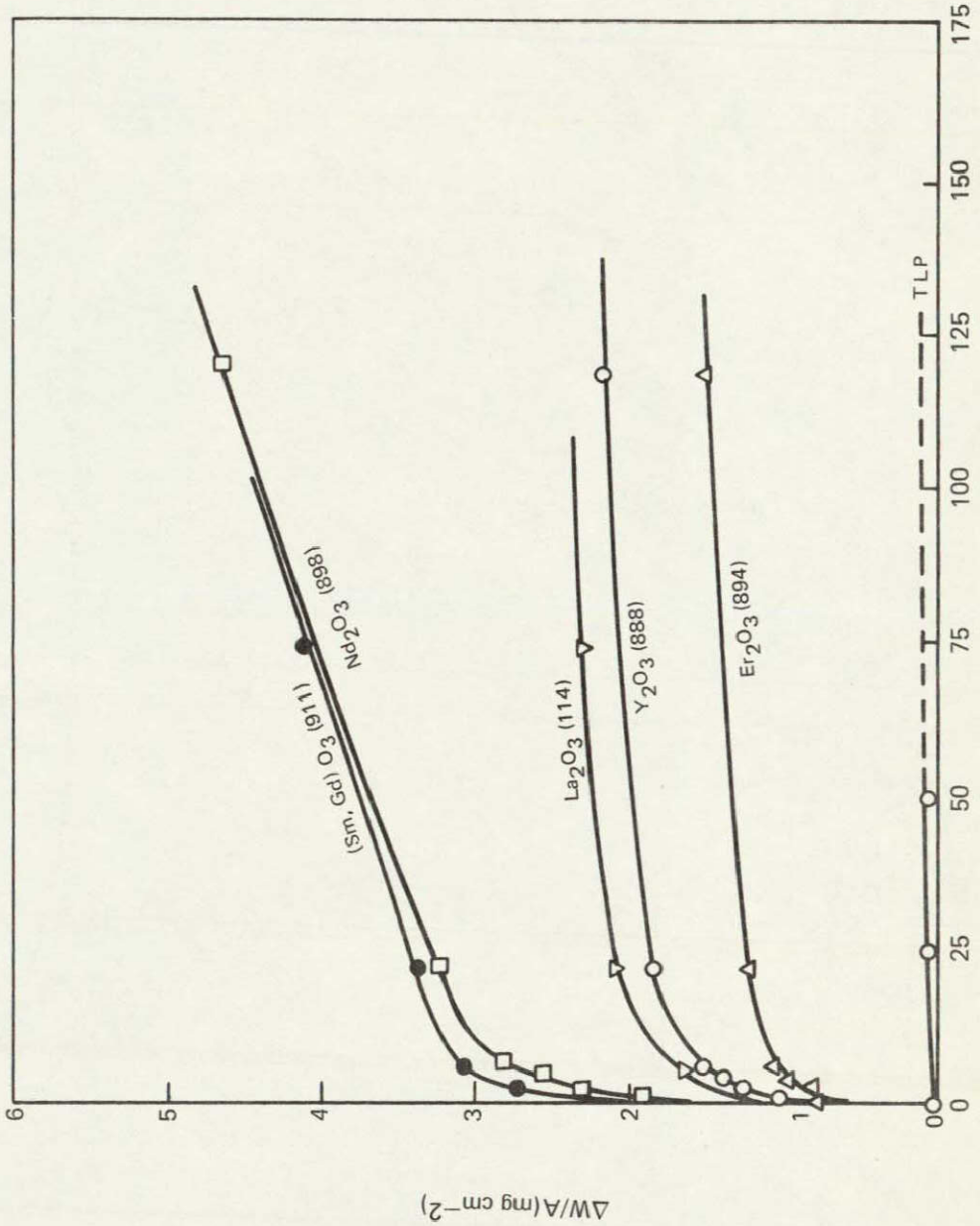

77–06–24–1

FIG. 59

WEIGHT GAIN IN AIR AT 1400°C OF VARIOUS SiAlON COMPOSITIONS (LINEAR PLOT)

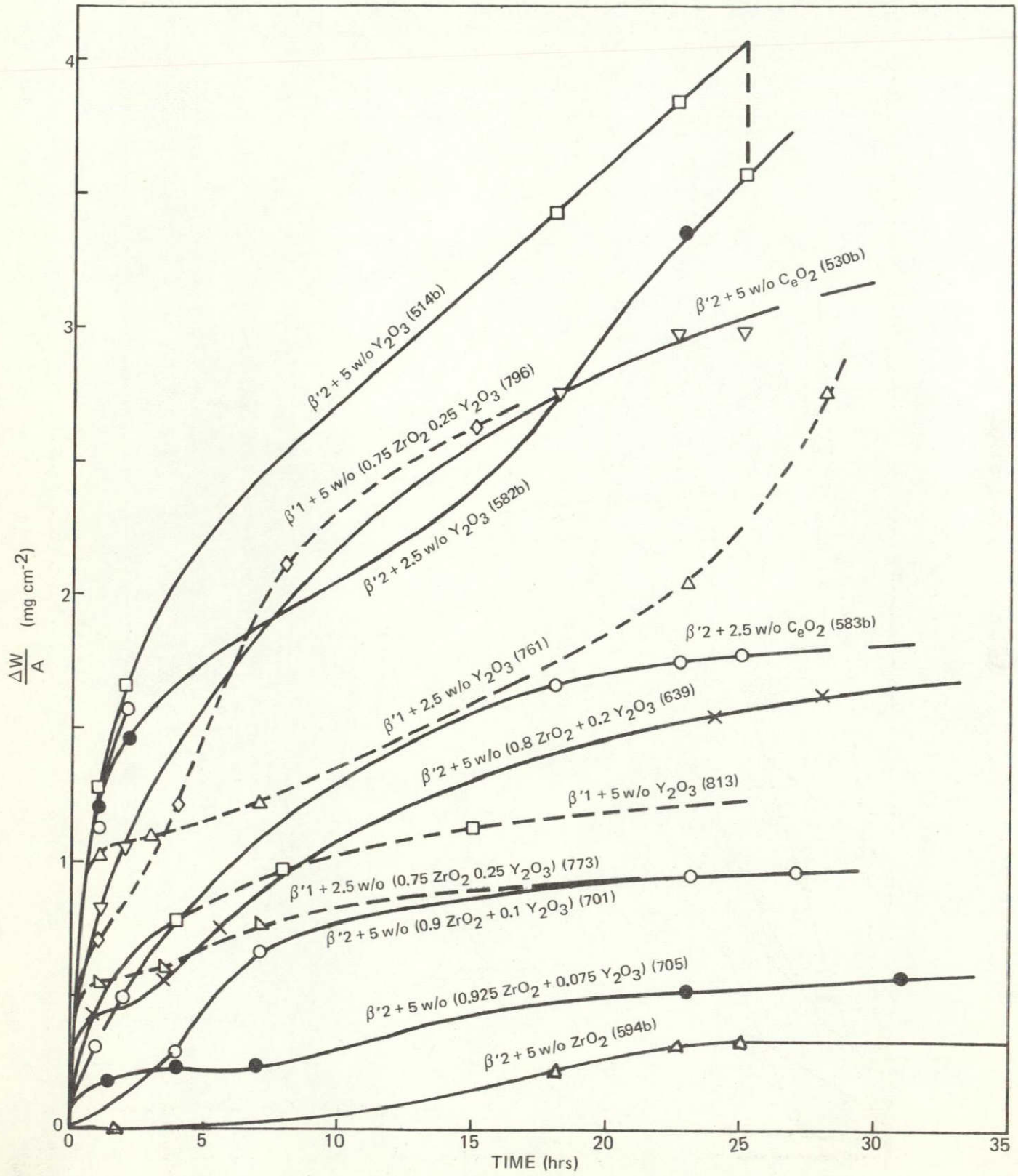

77–03–199–1

FIG. 60

WEIGHT GAIN IN AIR AT 1400°C OF VARIOUS SiAlON COMPOSITIONS (PARABOLIC PLOT)

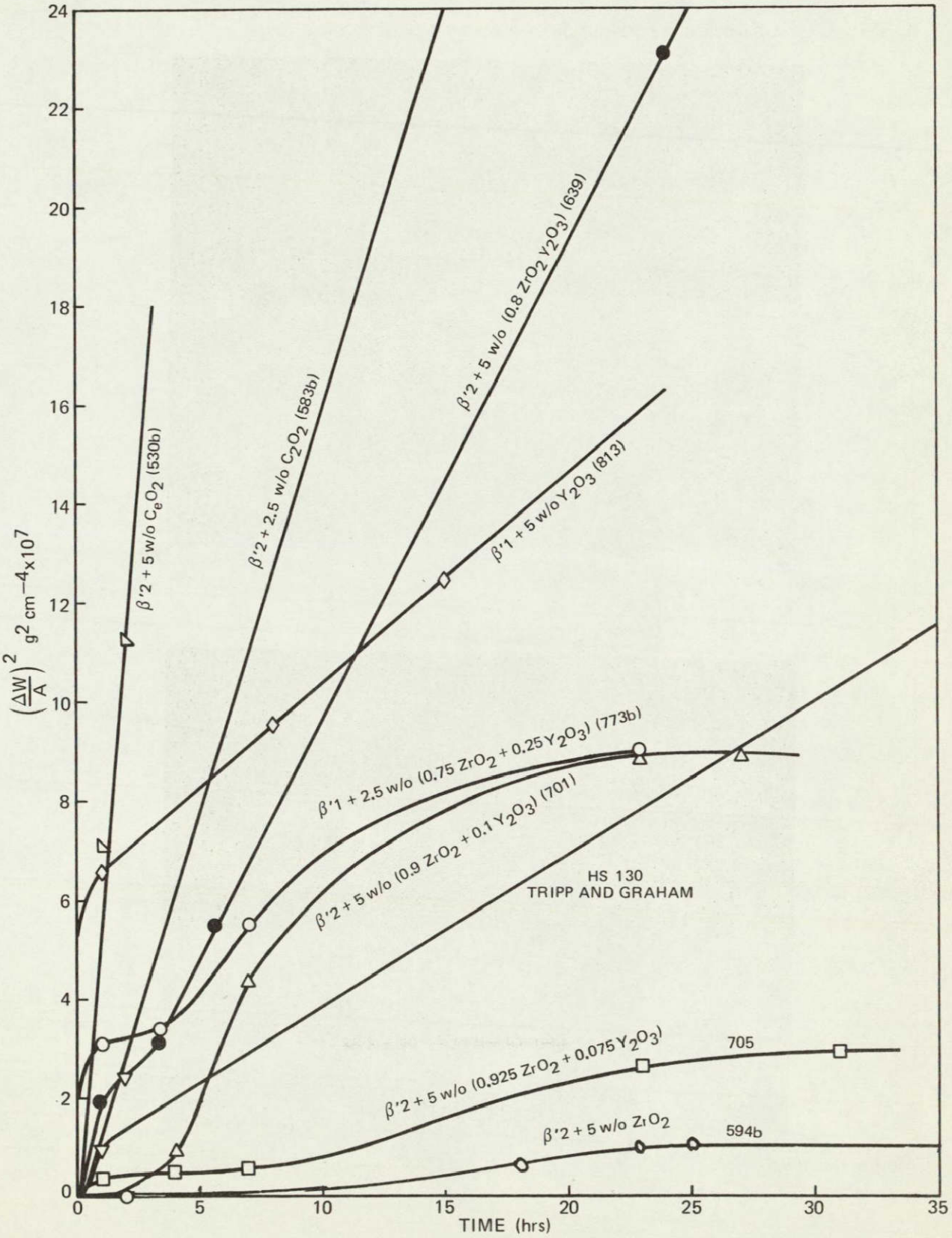

77–03–199–2

SCALES ON OXIDIZED SAMPLES

A. SAMPLE 639, COMPOSTION $\beta'2$ +5W/O(0.8 ZrO_2+0.2 Y_2O_3)

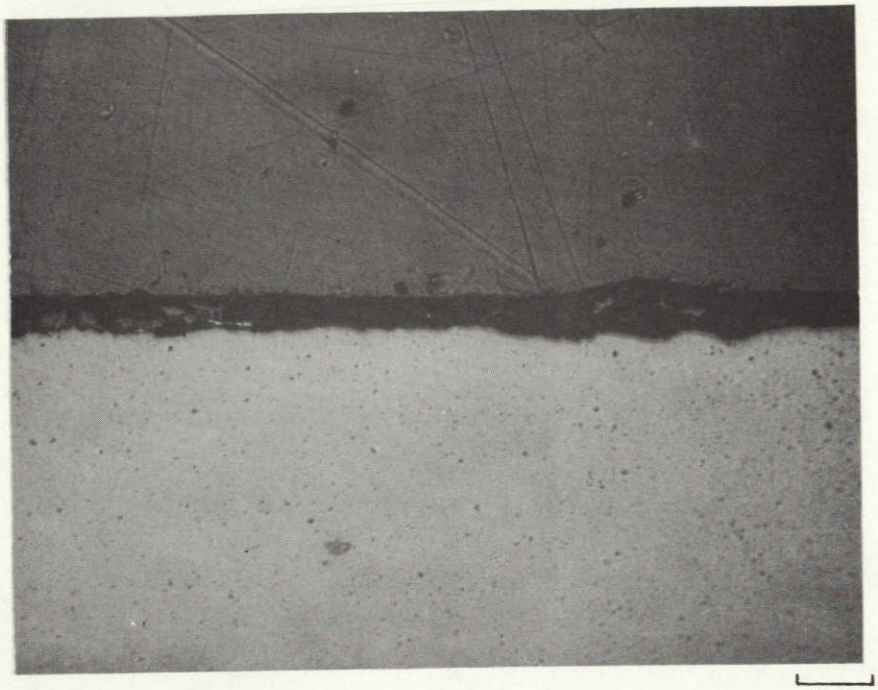

100μ

B. SAMPLE 594b, COMPOSITION $\beta'2$ +5 ZrO_2

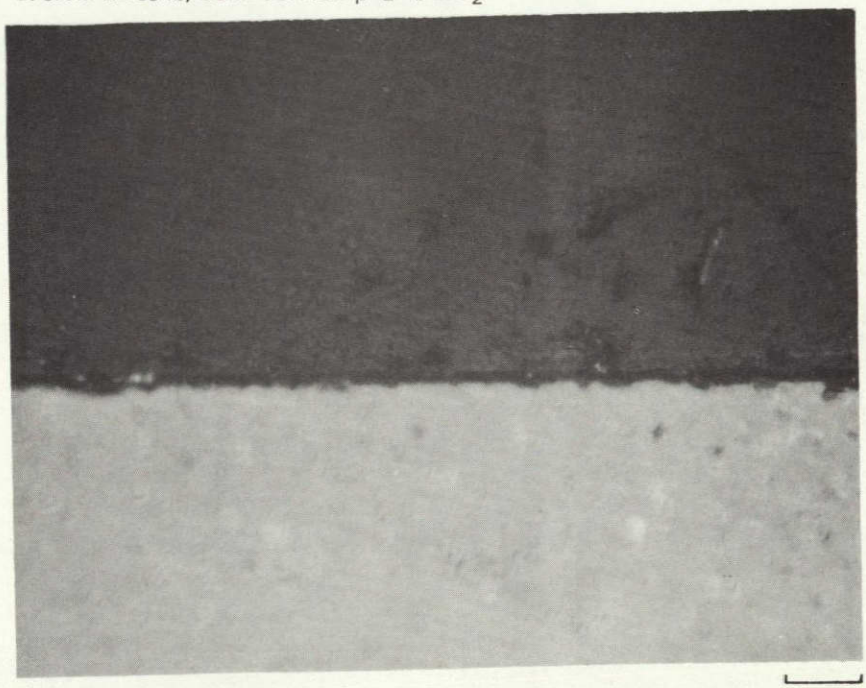

20μ

FIG. 62

SCALES ON OXIDIZED SAMPLES

A. SAMPLE 514b, COMPOSITION $\beta'2$ +5W/O Y_2O_3]

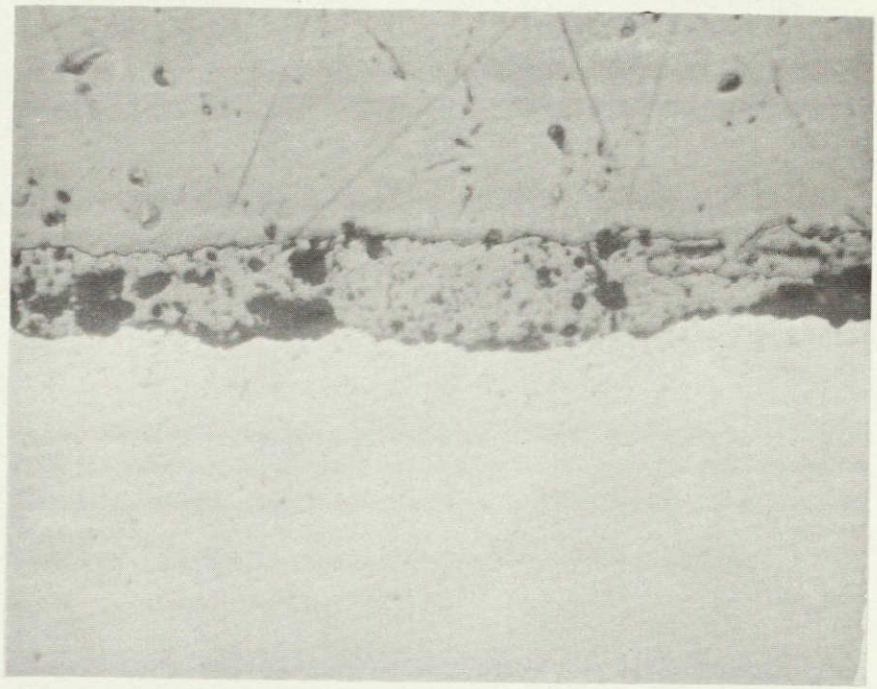

100μ

B. SAMPLE 530 b, COMPOSITION $\beta'2$ +5W/O CeO_2

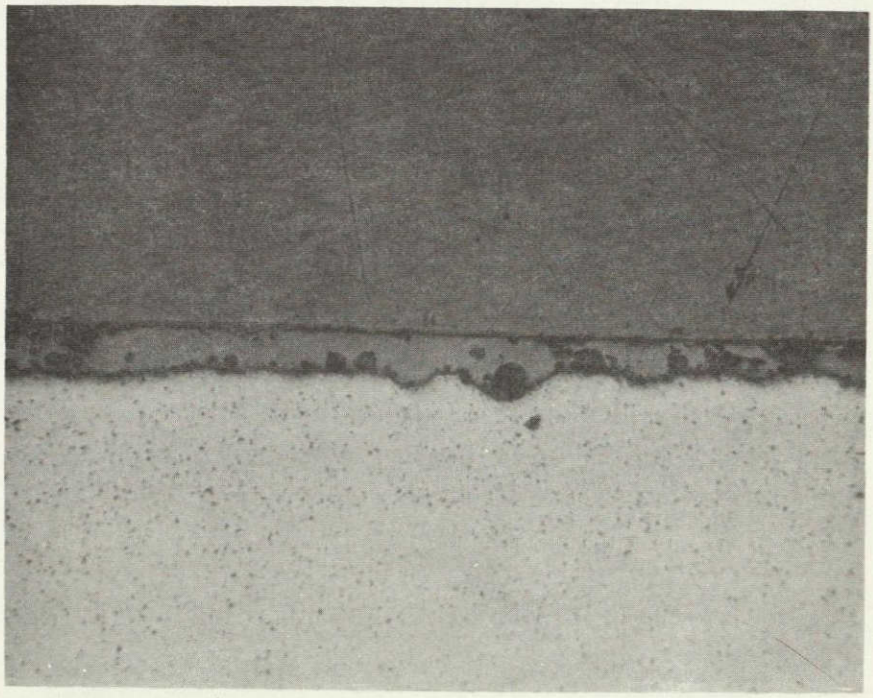

100μ

77–03–218–4

FIG. 63

OXIDE FROTH ON SAMPLE 888

($\beta''2$ + 3.2 m/o Er_2O_3)

A.

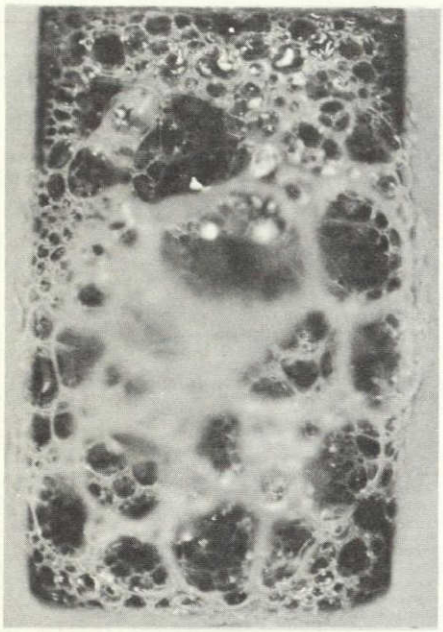

1000 μ

B.

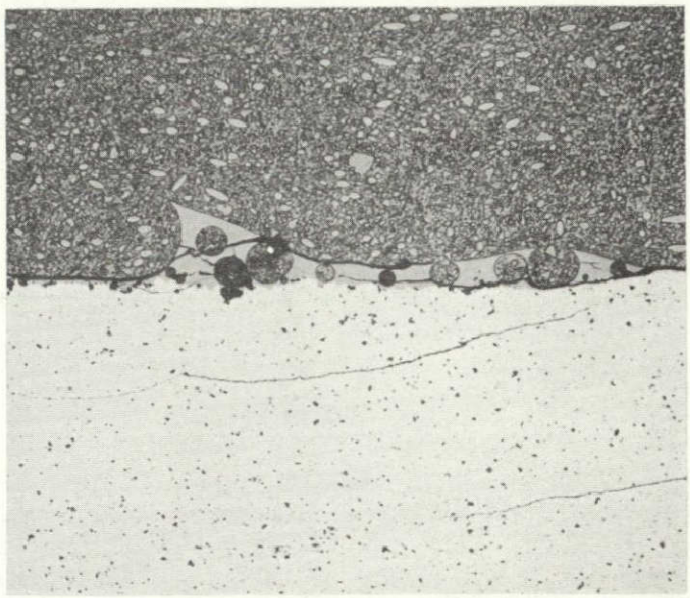

100 μ

C.

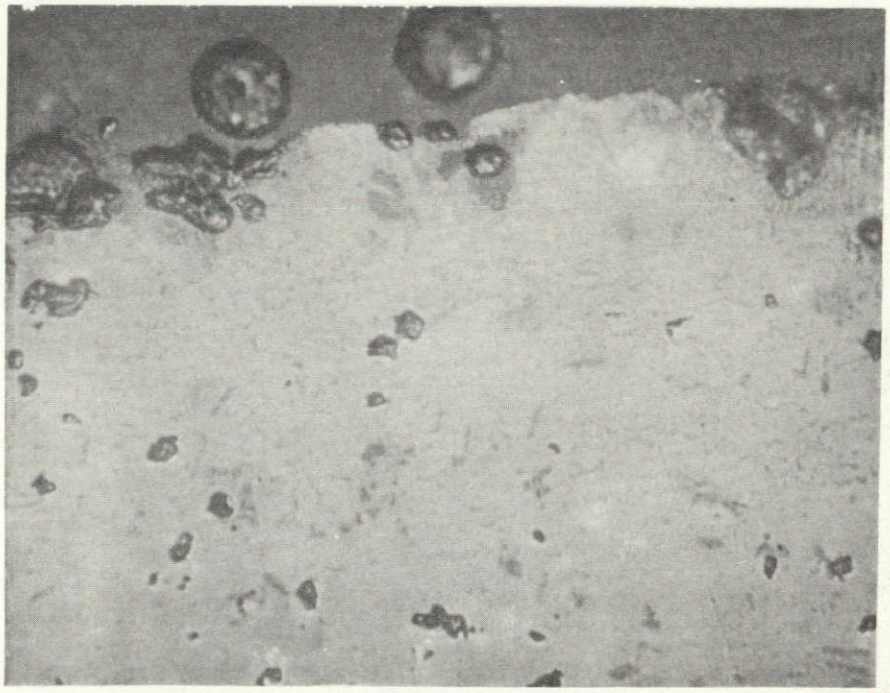

10 μ

77–08–181–2

FIG. 64

OXIDE FROTH ON SAMPLE 894

($\beta''2$ + 3.2 m/o Er_2O_3)

A.

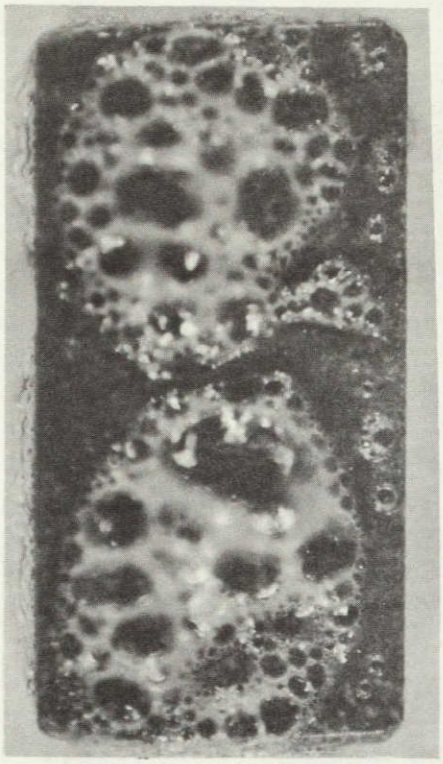

1000 μ

B

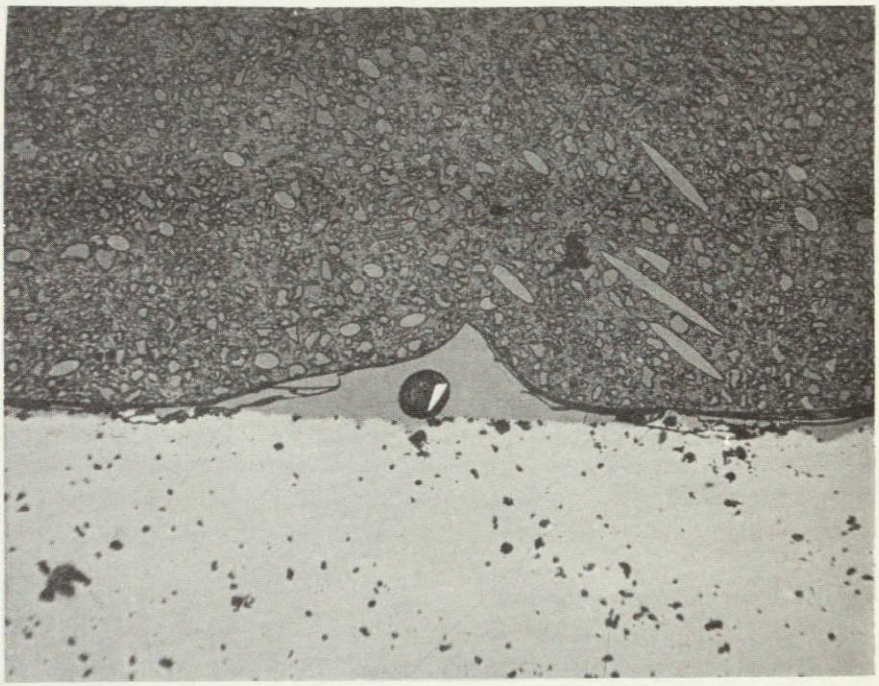

50 μ

C. ELECTRON BACKSCATTER MICROGRAPH

10 μ

77–08–181–1

FIG. 65

OXIDE LAYER ON SAMPLE 898

($\beta''2$ + 3.2 m/o Nd_2O_3)

A.

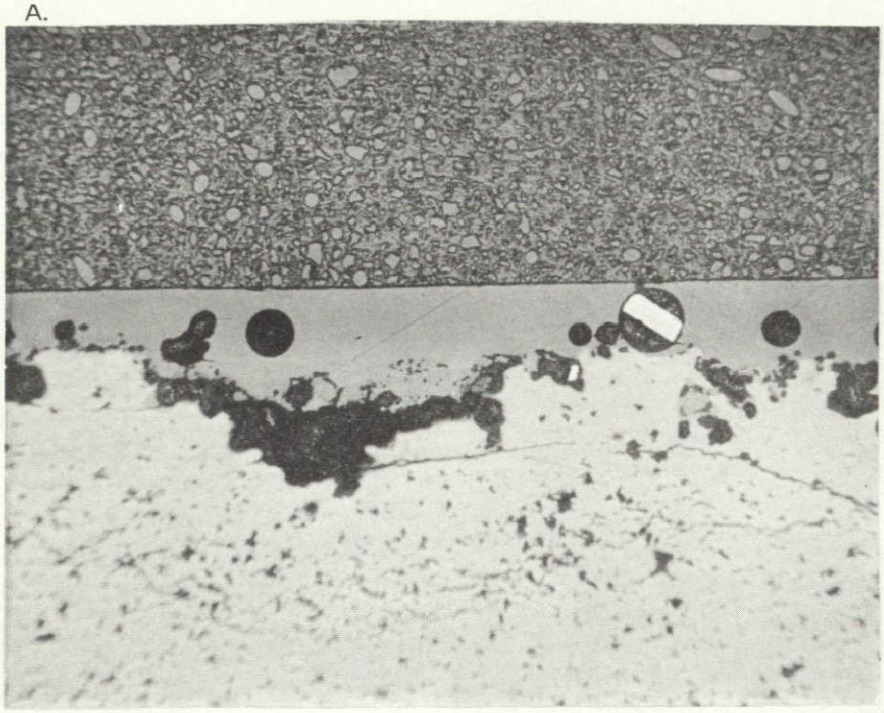

50 μ

B.

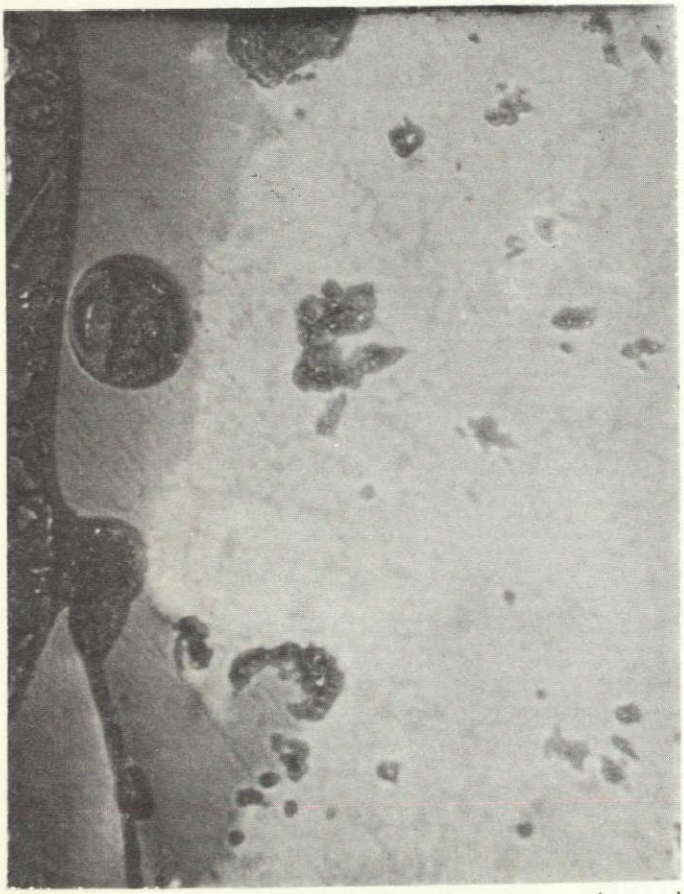

10 μ

C.

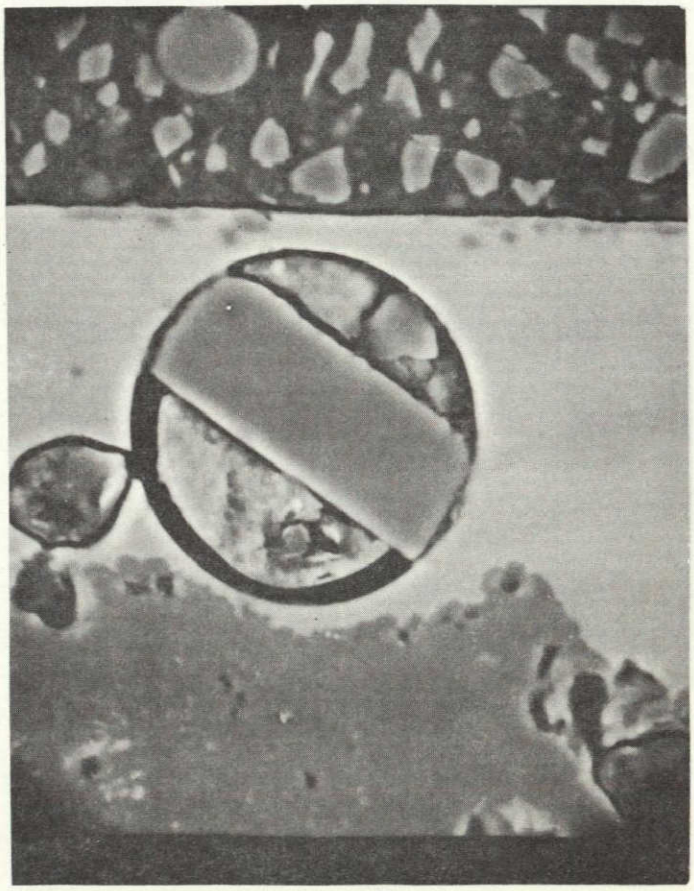

10 μ

77–08–181–3

ORIGINAL PAGE IS
OF POOR QUALITY

FIG. 66

OXIDE LAYER ON SAMPLE 914

($\beta''2$ + 3.2 m/o La_2O_3)

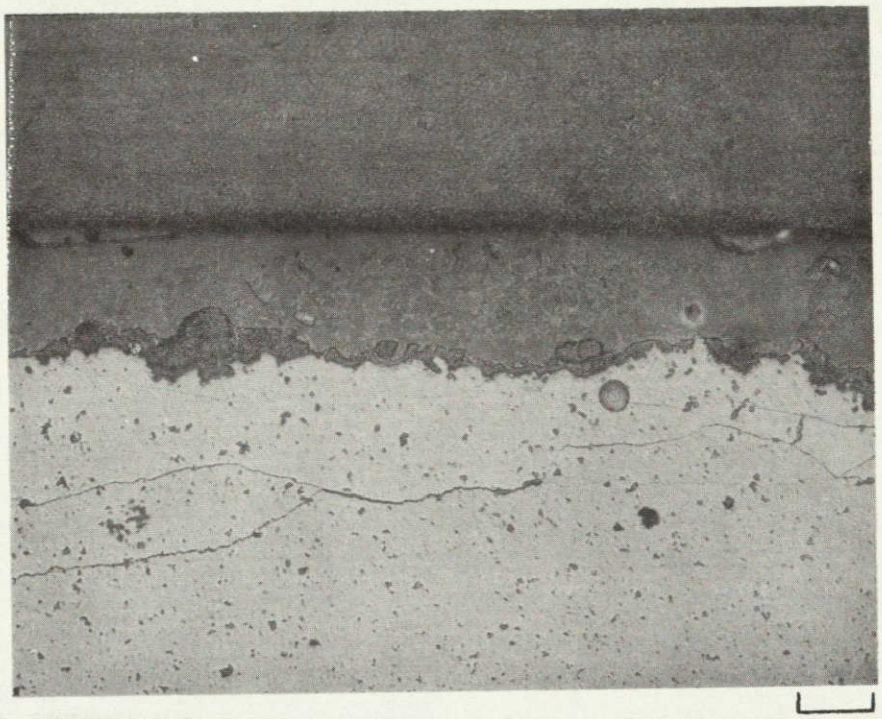

50 μ

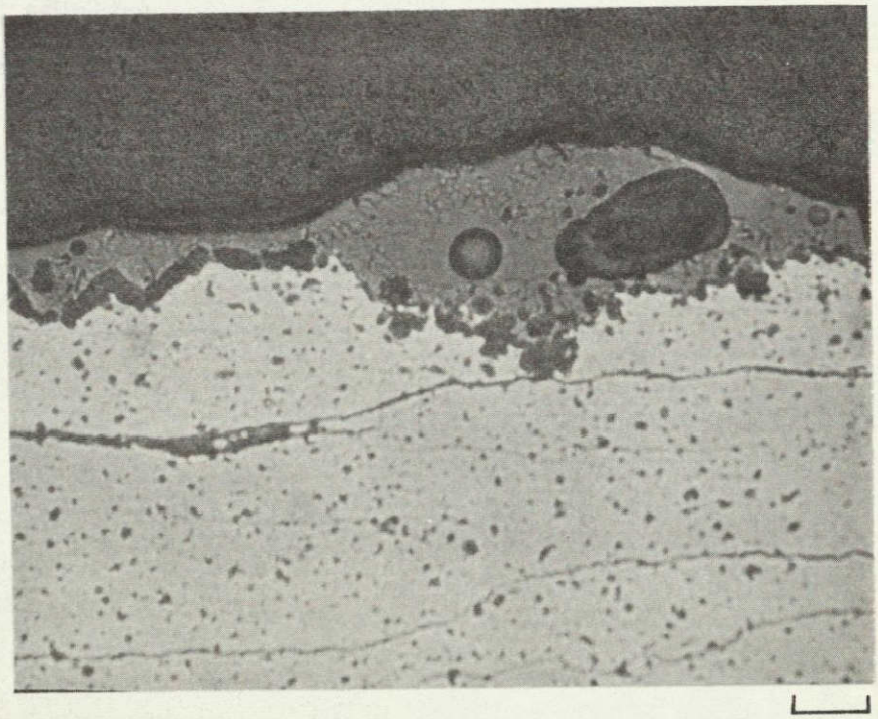

50 μ

77–08–181–6

places. The process by which the partially crystallized (cristobalite) scale which existed for about 24 hours became transformed into a glassy froth after 120 hours can be inferred from the element distribution scans obtained with the electron microprobe and shown in Fig. 67. It can be seen that there is an almost linear gradient of yttrium concentration increasing from a low value at the surface of the bar to a constant value about 0.020 in. below the surface. Yttrium has diffused out of the SiAlON body and become concentrated in the glassy (liquid) phase thus changing it's constitution. (It is assumed that the probe trace intersected the surfaces at regions where the glass had been broken away so that the high concentration in the glass was not detected. That this in fact does happen will be confirmed for the Er_2O_3 and Nd_2O_3 systems shortly.) From Fig. 63C, it can be seen that the grain boundary attack has occurred to a depth of about 75μ below the interface between the liquid on the SiAlON body. It appears from Fig. 63C that gas bubbles may nucleate at points of attack along the interface, but the small voids in this region could be pulled out during polishing.

A similar situation is seen to occur in the β'2 + 3.2 m/o Er_2O_3 sample, and here more details are available. The macrograph and optical micrograph shown in Figs. 64A and B, respectively, are virtually indistinguishable from those of Fig. 63 (except for a highly reflecting inclusion inside the gas bubble shown in Fig. 64B). The greater detail is to be found in Fig. 64C which is an electron back-scatter micrograph of the glassy scale and interface regions. In this type of micrograph, regions of heavy atomic number appear light and regions of low atomic number appear dark. Here it can be seen that there is a "splotchy" distribution of a heavy element (in this case, erbium) in the body of the sample (narrow region at the far right of the micrograph) then a region about 25μ thick in the neighborhood of the interface which appears to be devoid of Er, and finally a heavy concentration in the glassy film. The glassy film contains isolated globular regions and some smaller angular (crystalline?) regions which are low in Er. Liquid immiscibility is reported in the rare earth-SiO_2 systems, and the Y_2O_3-Al_2O_3-SiO_2 system (Figs. 52 and 51, respectively), and it seems likely that the dark globules in Fig. 64C are globules of the silicon rich liquid which can exist in equilibrium with the lighter appearing Er_2O_3 rich liquid. Also faintly visible in the original back-scatter micrograph but probably not in the reproduction (Fig. 64C) is an interface about 5μ "below" (i.e., to the right of) the colloform interface between the Er-rich glass and the Er-denuded region. Thus, it is likely that the surface of the bar which has been denuded of Er as a result of its concentration in the continuous liquid phase is dissolving into a silica rich liquid layer which in turn sheds globules into the continuous liquid phase. Another interpretation of the micrograph is that the continuous liquid phase is itself dissolving the body and undercutting crystalline regions which then float free and become globular as they continue to dissolve in the liquid. The elemental distribution probe trace across sample 894 is shown as Fig. 68, and this confirms the distribution of erbium inferred from Fig. 64C. It also shows a sharp discontinuity in the aluminum concentration in the neighborhood of the solid-liquid interface, with the concentration of aluminum in the erbium-rich liquid being about

FIG 67

ELEMENT DISTRIBUTION PLOTS ACROSS OXIDIZED SAMPLE 888

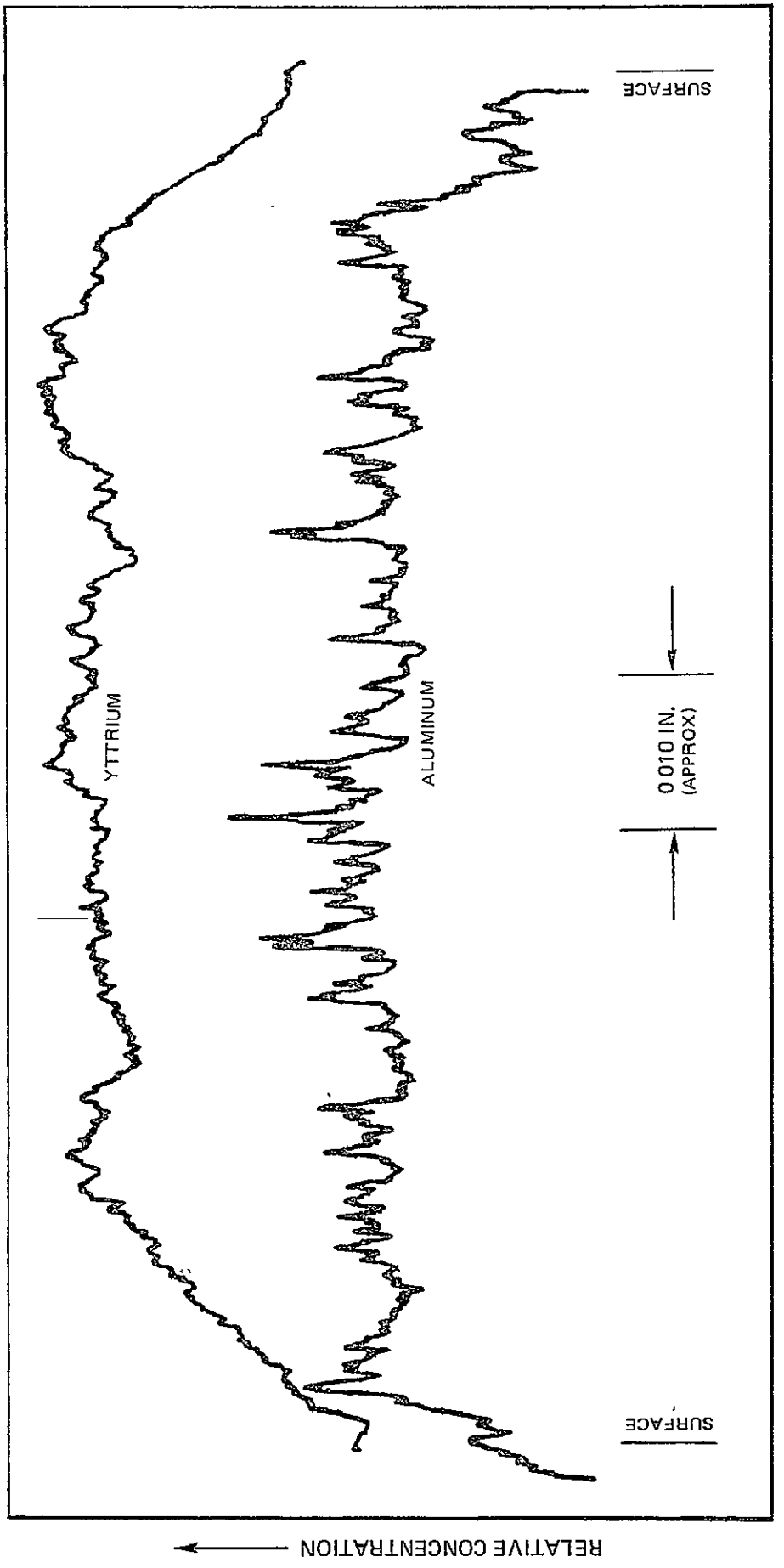

77–08–181–5

FIG 68

ELEMENT DISTRIBUTION PLOTS ACROSS OXIDIZED SAMPLE 894

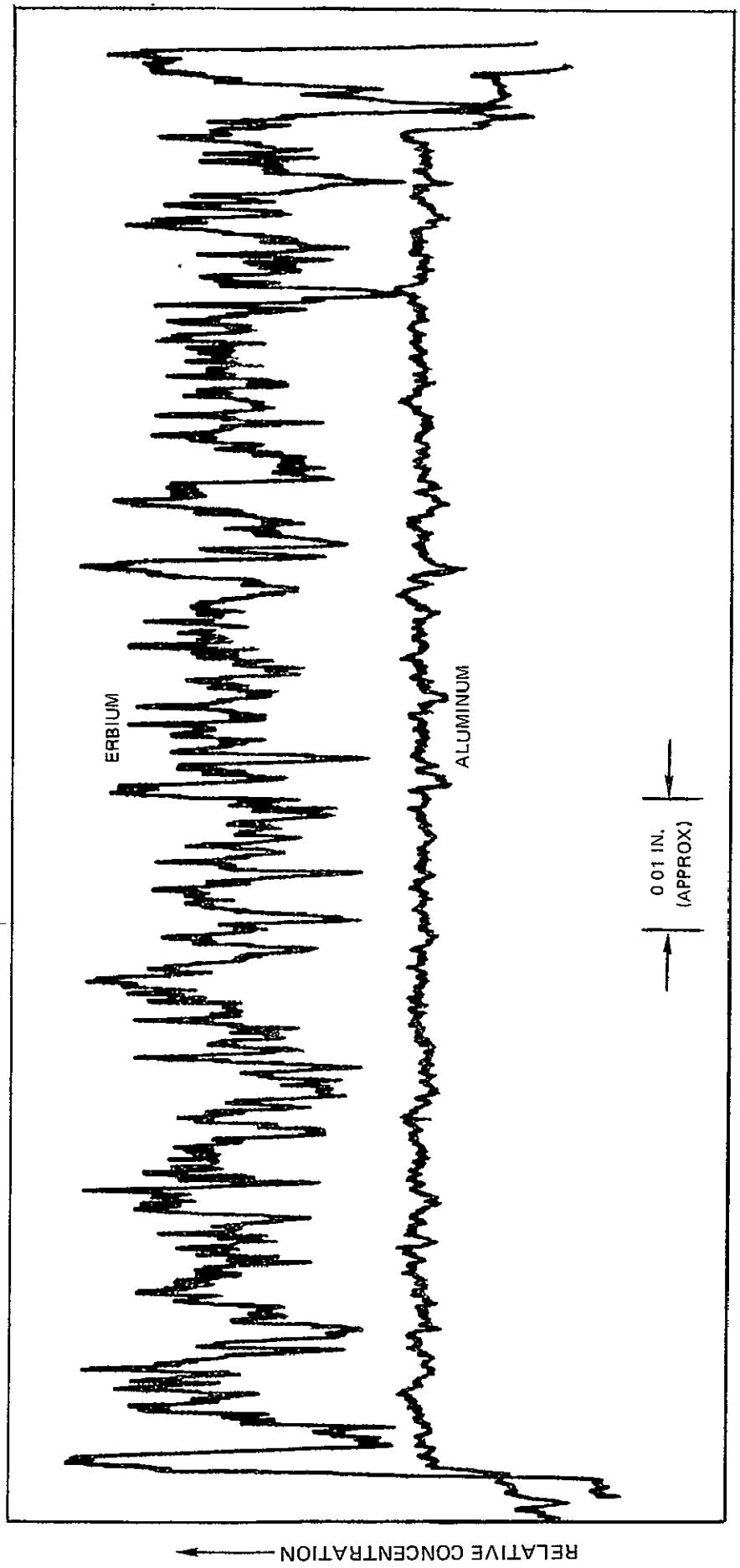

77–08–181–4

half that in the SiAlON body. The low concentration of aluminum in the erbium-rich liquid tends to confirm the two-liquid hypotheses, since if the continuous liquid were of the ternary eutectic composition (assuming the Er_2O_3-Al_2O_3-SiO_2 resembles the Y_2O_3-Al_2O_3-SiO_2 the aluminum concentration should be higher in the continuous liquid than in the SiAlON body.

Figure 65 shows the liquid and interface regions of the β'2 + 3.2 m/o Nd_2O_3 sample. In this case the liquid phase appears to have been more fluid and more corrosive to the SiAlON body than the Y_2O_3- or Er_2O_3-rich liquids. Although bubbles appear in the glass, there was not a great deal of froth formed on the samples probably because bubbles burst and the surface again became smooth as a result of surface tension. The high magnification optical micrograph, 65B, again shows grain boundary attack in the SiAlON body, and the back-scatter micrograph (65C) shows the colloform interface between the Nd_2O_3 rich liquid phase and a Nd-denuded region. In this instance, there is strong evidence that the colloform interface is really a liquid-liquid interface and not a liquid-solid interface. This is the fact that the series of small voids located at about 4 to 5 o'clock outside the large bubble in Fig. 65C are below the colloform interface, whereas these same voids appear at or outside the crystal-liquid interface in Fig. 65B.

Micrographs of the oxide film on the β'2 - 3.2 m/o La_2O_3 sample shown in Fig. 66 shows many of the same features already discussed. In this case the binary eutectic (Table 26), as with the Nd_2O_3 system, was low, and the liquid attack of the surface appeared to be particularly severe. Substructure can be seen in the glass film which again suggests liquid-immicibility.

A particularly interesting phenomenon is the occasional occurrence of silicon crystals inside gas bubbles in the oxide films. Examples of this are seen in Figs. 64 and 65. These crystals appear to have grown from the vapor phase. This suggests that under certain local conditions SiO gas may be involved in the chemical processes involved in the oxidation.

c. Summary of Oxidation Test Results

All β' rare earth oxide compositions studied produced liquid oxidation products which in effect proceeded to dissolve the underlying SiAlON body by a rather complex series of steps. The only compositions investigated that exhibited acceptable resistance to static oxidation were those prepared by a transient liquid technique not involving additional sintering aids, and β' compositions containing ZrO_2 or ZrO_2 combined with small amounts of Y_2O_3.

SECTION V

CONCLUSIONS

Solid solutions having the β Si_3N_4 crystal structure and compositions given by the formula $Si_{3-x}Al_xO_xN_{4-x}$ where $0 < x < 2$ readily form from components in the system Si_3N_4-SiO_2-Al_2O_3-AlN at elevated temperature. However, it has not been found possible to sinter either constituent powders (e.g., Si_3N_4, Al_2O_3 and AlN) or prereacted β' powders to single phase β' bodies having densities greater than about 85 percent of theoretical. It is possible however to sinter to theortical density ceramic bodies in which the major phase (and possibly the only phase detectable by usual x-ray powder diffraction techniques) is β'. This can be accomplished either by choosing compositions in the Si_3N_4-SiO_2-Al_2O_3-AlN system such that liquid is present at the firing temperature, or by introducing "additives" to β' formulations which promote liquid formation and liquid phase sintering at the firing temperature. In either case a grain boundary phase or phases is retained in the sintered body, and the nature of the grain boundary assemblage has a controlling influence on the properties of the body.

Over the course of this program to date a variety of sintering aids were investigated including $AlPO_4$, $GaPO_4$, ZrO_2, ZrC, Cr_2O_3, TiO_2, HfO_2, Y_2O_3, La_2O_3, Er_2O_3, Nd_2O_3 and $GdSmO_3$. Uniformly dense bodies were obtained only with with ZrO_2, Y_2O_3 (and mixtures of these) and rare earth oxide additions. Bodies prepared with these sintering aids exhibited room temperature flexural strengths on the order of 80,000 psi. In the absence of other more deleterious types of flaws, room temperature strength was controlled by the presence of metallic inclusions which result from local decomposition of the Si_3N_4 or β' phases during firing. Decomposition appears to be initiated by the presence of impurities (principally iron, although Zr resulting from decomposition of ZrO_2 and also probably AlP and GaP resulting from decomposition of the orthophasphates have also been involved) which alloy with silicon. Based on thermochemical data presented by Colquhoun et al. (Ref. 28) it is projected that nitrogen pressures on the order of 5000 psi would be required to prevent the formation of metallic inclusion at sintering temperatures of about 1750°C when iron is present in the sample.

While room temperature strength of the sintered ceramic bodies is controlled by flaws (principally inclusions), elevated strength and creep behavior are controlled by the properties of the grain boundary assemblages. Fracture at 1370°C of β' compositions containing ZrO_2 initiated at cracks that develop during loading as a result of flow of the grain boundary phase, and creep tests at 1370°C showed that this flow is rapid at stresses as low of 10,000 psi. β' compositions containing Y_2O_3 exhibited more refractory grain boundary assemblages, and no slow cracks growth

occurred during loading to about 50,000 psi at 1370°C, whereupon brittle fracture occurred. The creep rate of the Y_2O_3 containing β' bodies was about 6×10^{-5} hr^{-1} at 1370°C and a stress level of 10,000 which is comparable to that of commercial hot pressed Si_3N_4 containing MgO.

The oxidation behavior could be correlated with minimum liquidus temperatures in the systems containing the oxidation products. All systems containing Y_2O_3, La_2O_3, or rare earth oxides in time developed oxide films that were liquid at 1400°C and there was evidence that oxygen diffusion through the liquid films was rapid so that the films offered little protection. The mechanism for further oxidation appeared to involve solution of the ceramic body in the liquid film. This dissolution did not occur on smoothly advancing interfaces, but rather advanced preferentially at particular sites so that rough and jagged interfaces developed.

For compositions where the minimum ternary eutectic temperature in the systems containing the oxidation products were above the test temperature, (i.e., in the SiO_2-Al_2O_3, and SiO_2-ZrO_2-Al_2O_3 systems) thin protective crystalline scales developed and the static oxidation rates were low.

No composition has been developed as yet which combines both good oxidation behavior and good high temperature mechanical properties, and this remains the primary goal of this program. However, criteria can be established to guide in the selection of systems to be explored. Consideration should be given to phase equilibrium in the systems that contain the products of oxidation, and all potential compositions can be rejected if the oxidation products lie in a region of the oxide system in which the solidus temperature is below the use temperature of the ceramic. The second criterion is that the solidus temperature in the compatibility region of the parent system falls within certain narrow limits. It should be low enough that liquid will form at reasonable sintering temperatures (say, not higher than 1750°C) and yet be as high above the prospective use temperature (1370°C) as possible so that acceptable high temperature mechanical properties can be assured. A third criterion is that the liquid which forms be fluid at the firing temperature and wets the primary β' phase so that it can diffuse rapidly throughout the structure during sintering.

While these criteria are easy to set down on paper, it is not quite as easy to predict which systems will satisfy them due to a paucity of phase equilibria and property data in potentially relevant systems. One <u>does</u> know from available phase equilibria data, however, a vast number of systems that will <u>not</u> satisfy one or more of the criteria and this is helpful at least in limiting the areas of search.

In addition to the investigation of new systems, a more thorough exploration of the most promising of the current systems is called for. The formulations investigated to date have been restricted to specific regions of the respective systems, that is, to compositions that can be expressed as mixtures of $Si_{3-x}Al_xO_xN_{4-x}$ and various other oxides, e.g., ZrO_2 or Y_2O_3. The bodies that resulted from these formulations can represent only a fraction of the possible minor phase assemblages in the respective systems. One can ask whether formulation in the Zr-Si-Al-O-N system other than β'-ZrO_2 would yield bodies with superior high temperature mechanical properties, or whether other formulations in the Y-Si-Al-O-N system would have better oxidation resistance.

Solid phase compatibility studies in these quinternary system should be undertaken to define the possible assemblages in which β' is the major phase, and bodies of the various types evaluated.

It can be hoped that these complimentary approaches, namely, 1) exploratory investigations in new systems and 2) more thorough investigations of phase compatibility and properties in the most promising systems, will eventually lead to bodies having acceptable properties.

REFERENCES

1. Jack, K. H. and W. I. Wilson: Ceramics Based on the SiAlON and Related Systems, Nature Phys. Sci., 238, 8028 (1972).

2. Oyama, Y. and O. Kamigaito: Solid Solubility of Some Oxides in Si_3N_4. Japan J. Appl. Phys. 10, 1637 (1972).

3. Arrol, W. J.: Properties and Fabrication, paper presented at Second Army Materials Technology Conference, Ceramics for High Performance Applications, Hyannis, Mass., November 13-16, 1973.

4. Oyama, Y.: Solid Solution in the System Si_3N_4 - Ga_2O_3-Al_2O_3. Japanese Journal of Appl. Phys. 12, 500 (1973).

5. Wills, R. R., P. L. Land, and J. M. Wimmer: Reaction Sintered SiAlON Paper, 61-BN-74F, presented at the American Ceramic Society, Williamsburg, Virginia, October 1974.

6. Oyama, Y. and O. Kamigaito: Silicon Nitride-Alumina System Sintered Materials, Yogya-Kyokai-Shi, 80 924 29-38 (327-336) 1972 (Translation, British Library).

7. Hed, A. Z. and W. B. Crandall: Processing of SiAlON-Hot Pressing, paper 14-BC-73F, presented at the American Ceramic Society Meeting, Pittsgurgh, Pennsylvania, September 1973.

8. Wimmer, J. M.: Processing of SiAlON-Background and Sintering, paper 13-BC-73F, presented at the American Ceramic Society Meeting, Pittsburgh, Pennsylvania, September 1973.

9. Lange, F. F.: Fabrication, Microstructure, and Selected Properties of SiAlON Compositions, Final Report, Naval Air System Command, Contract N00019-73-C-0208, February 1974.

10. Drew, P. and M. H. Lewis: The Microstructure of Silicon Nitride/Aluminum Ceramics, J. Mat. Sci, 9, 1833 (1974).

11. Morgan, P. E. D.: Paper 4-52-74, American Ceramic Society Meeting, April 1974. Also, J. Amer. Ceramic Society, 53, 392 (1974).

12. Holmquist, S.: Report, Contract F33615-73-C-4155, April 30, 1975.

13. Land, P. L., et al: Paper 68-B-75, American Ceramic Society Meeting, Washington, D. C., May 6, 1975.

REFERENCES (Cont'd)

14. Gauckler, L. J., et al: Paper 67-B-75, American Ceramic Society Meeting, Washington, D. C., May 6, 1975. Also. J. American Ceramic Society, 58, 346, 1975.

15. Layden, G. K.: Process Development for Pressureless Sintering of SiAlON Ceramic Components, Final Report, Naval Air System Command Contract N00019-75-C-0232, February 1976.

16. Jack, K. H.: SiAlONs and Related Nitrogen Ceramics, J. Mat. Sci. 11, 1135-1158, 1976.

17. Layden, G. K.: Pressureless Sintering of SiAlON Gas Turbine Components, Report Number NADC-75207-30, February 23, 1977.

18. Mazdiyasni, K. S. and C. M. Cooke: American Ceramic Society Bulletin 53, p. 392 (1974), (abstract).

19. Wills, R. R.: Journal of the American Ceramic Society 57, (1974).

20. Lange, F. F.: Final Report, Contract N00019-73-C-0208, February 26, 1974.

21. Rice, R. W. and W. J. McDonough: American Ceramic Society Bulletin 54, p. 406, (1975), (abstract).

22. Terwilliger, G. R. and F. F. Lange: Pressureless Sintering of Si_3N_4, J. Mat. Sci. 10, pp. 1169-1174 (1975).

23. Gazza, G. E: Effect of Y_2O_3 Additions on Hot-Pressed Si_3N_4, Bulletin of the American Ceramic Society 54, pp. 778-781 (1975).

24. Venables, J. D., D. K. McNamara, and R. G. Lye: High Strength Silicon Nitride Prepared with Eutectic Flux Additions, F. L. Riley, Editor, Nitrogen Ceramics, Proceedings of the N.A.T.O. Advanced Study Institute, Canterbury, August 1976.

25. Rae, A.W.J.M., D. P. Thompson, and K. H. Jack: The Role of Additives in the Densification of Nitrogen Ceramics, presented the NATO Advanced Study Institute on Nitrogen Ceramics, Canterbury, England, August 1976.

26. Lange, F. F., S. C. Singhal, and R. C. Kuznicki: Westinghouse Electric Corporation Research and Development Center, Technical Report No. 6, April 1, 1974.

REFERENCES (Cont'd)

27. Wild, S., P. Grieveson, and K. H. Jack: The Thermodynamics and Kinetics of Formation and Phases in the Ge-N-O and Si-N-O System, in Special Ceramics No. 5, P. Popper, Editor, The British Ceramic Research Association, 1972.

28. Colquhoun, I., S. Wild, P. Grieveson, and K. H. Jack: Thermodynamics of the Silicon-Nitrogen-Oxygen System, Proc. Brit. Cer. Society, No. 22, pp. 207-227 (1973).

29. Din, S. U. and P. S. Nicholson: Creep of Hot-Pressed Silicon Nitride, J. Mat. Sci., 10, 1375 (1975).

30. Tripp, W. C. and H. C. Graham: Oxidation of Si_3N_4 in the Range 1300° to 1500°C, J. Amer. Ceram. Society 59, pp. 399-403 (1976).

APPENDIX I

Composition point 3796 (3'2) Sample # 315

atom percent				
	Si = 35	Al b = 7.86	O c = 7.86	N d = 49.28
	28.09 Si 983.15	26.98 Al 212.06	16.00 O 125.76	14.01 N 690.44

28.09 Si + 26.98 Al + 16.00 O + 14.01 N | M = 2011.38

weight of batch | W = 110

milling time* | t = 96 hrs.

constituents (check)	Si_3N_4 W_1 ✓	Al_2O_3 W_2 ✓	Al N W_3 ✓	SiO_2 W_4 = 0

Equations *using High Alumina balls in polyethylene bottles

1 $\frac{28.09\ Si\ W}{M}$ = 53.767 = 0.5958 W_1 + ~~0.4675 W_4~~ + .1344 (0.0014 t)

2 $\frac{26.98\ Al\ W}{M}$ = 11.597 = 0.5292 W_2 + 0.6582 W_3 + 1.478 (0.0154 t)

3 $\frac{16.01\ O\ W}{M}$ = 6.878 = 0.0191 W_1 + 0.4708 W_2 + ~~0.5295 W_4~~ + 1.459 (0.0152 t)

4 $\frac{14.01\ N\ W}{M}$ = 37.758 = 0.3851 W_1 + 0.3418 W_3

work space

① W_1 = 90.018

④ 37.758 − 34.666 = .3418 W_3 W_3 = 9.046

② 11.597 = .5292 W_2 + 5.9540 + 1.478

W_2 = 7.870

③ 6.878 = 1.719 + 3.705 + 1.459

ORIGINAL PAGE IS OF POOR QUALITY

Si_3N_4 W_1 = 90.018	Al_2O_3 W_2 = 7.870	Al N W_3 = 9.046	SiO_2 W_4 = 0

APPENDIX II

FABRICATION AND TEST DATA FOR SiAlON TEST BARS

Sample Number	Composition	Deviation (%)	Firing Condition T (°C)	Firing Condition t (hrs)	Firing Condition Code	Apparent Porosity (%)	Specific Gravity (g/cc)	Bulk Density (g/cc)	Flexural Strength R psi	Test Temp. if Other than Room (°C)	Coefficient of Variation	Mean Strength
428 429 430 431 432	β'2 + 10 w/o CeO_2		1735	2	Ic	0	3.34	3.34	44 37 37 39		7	39.3
436 437 438 439	β'2 + 10 w/o CeO_2		1735	2	Ic	0	3.32	3.32	78 74		7	71.6
440 441 442 443	β'2 + 10 w/o CeO_2		1750	2	Ic	0	3.33	3.33	63 71 72			
471 472 473 474	β'2 + 10 Y_2O_3		1735	1	Ic	0	3.29	3.29	49 85 77		21	70.3
475 476 477 478	β'2 + 10 Y_2O_3		1750	1	Ic	0	3.34	3.34				
479 480 481 482	β'2 + 5 w/o $AlPO_4$		1735	1	Ic	19	3.10	2.51				
483 484 485 486	β'2 + 5 w/o $AlPO_4$		1800	1	Ic							
487 488 489	β'2 + 5 w/o $GaPO_4$		1735	1	Ic							
490 491 492	β'2 + 5 w/o $GaPO_4$		1735	1	Id	18	3.16	2.56				

APPENDIX II

FABRICATION AND TEST DATA FOR SiAlON TEST BARS (Cont'd)

Sample Number	Desired Composition	Deviation (%)	Firing Condition T (°C)	Firing Condition t (hrs)	Firing Condition Code	Weight Loss (%)	Apparent Porosity (%)	Specific Gravity (g/cc)	Bulk Density (g/cc)	Flexural Strength K psi	Test Temp. if Other than Room (°C)
493 494 495	β'2 + 5 w/o $GaPO_4$	0	1780	1	Id		5	2.81	2.66		
496 497 498 499	β'2 + 20 w/o ZnO_2	0	1735	1	Ic	0.90	0	3.46	3.46		
500 501 502 503	β'2 + 20 w/o ZrO_2	0	1700	1	Ic	0 91	0	3.45	3.45	43 59 51	
513 514 515 516	[β'2 + 5 w/o Y_2O_3]·1	+0 2	1735	1	Ic	0.66	0	3.25	3.25	49 60	
517 518 519 520	[β'2 + 5 w/o Y_2O_3]·1	+0.2	1700	1	Ic	0.72	0	3.24	3.24	59 50	
521 522 523 524	[β'2 + 5 w/o Y_2O_3]·1	+0.2	1750	1	Ic	0.91	0	3.24	3.24	72 53 67	
529 530 531 532	β'2 + 5 w/o CeO_2	+0.2	1735	2	Ic	1.04	0	3 25	3.25		
533 534 535 536	β'2 + 5 w/o CeO_2	-0.1	1750	1	Ic	1 00	0	3 24	3.24	52 63 53 63	
537 538 539 540	β'2 + 5 w/o CeO_2	-0.1	1750	2	Ic	1 20	0	3.25	3.25		

II-2

FABRICATION AND TEST DATA FOR SiAlON TEST BARS (Cont'd)

(Page 3 of 7)

Sample Number	Desired Composition	Deviation (%)	Firing Condition T (°C)	Firing Condition t (hrs)	Firing Condition Code	Weight Loss (%)	Apparent Porosity (%)	Specific Gravity (g/cc)	Bulk Density (g/cc)	Flexural Strength K psi	Test Temp. if Other than Room (°C)
560 561 562 563	β'2 + 10 w/o ZrO_2	0	1735	1	Ic	1.3	0	3.34	3.34		
564 565 566 567	β'2 + 10 w/o ZrO_2	0	1650	1	Ic		0	3.16	3.16	35 37 36 38	
568 569 570 571	β'2 + 10 w/o ZrO_2	0	1700	1	Ic	1.00	0	3.20	3.20		
579 580 581 582	[β'2 + 5 w/o Y_2O_3] 2	-0.5	1735	1	Ic	0.58					
583 584 585 586	β'2 + 5 w/o CeO_2		1735	1	Ic	0 70	0	3 12	3 12	41 43 30	
587 588 589 590	[β'2 + 5 w/o Y_2O_3].2	-0.5	1735	1	Ic	0.62				74 69 85	
591 592 593 594	β'2 + 5 w/o ZrO_2	+0.6	1735	1	Ic	1.08	0	3.18	3.18	49 46 52 47	
596 597 598	β'2 + 5 w/o ZrO_2	+0.6	1650	1	Ic		4.5	3.12	2.97		

FABRICATION AND TEST DATA FOR SiAlON TEST BARS (Cont'd)

Sample Number	Desired Composition	Deviation (%)	Firing Condition T (°C)	Firing Condition t (hrs)	Firing Condition Code	Apparent Porosity (%)	Specific Gravity (g/cc)	Bulk Density (g/cc)	Flexural Strength K psi	Test Temp if Other than Room (°C)
621, 622, 623, 624	β'2 + 8 5 w/o HfO_2	-0.4	1735	1	Ic	20.22	3.34	2.66		
625, 626, 627, 628	β'2 + 8.5 w/o HfO_2	-0.4	1700	1	Ic	22.75	3.35	2.59		
629, 630, 631, 632	β'2 + 5 w/o Cr_2O_3	-0.3	1735	1	Ic	20.95	3.10	2.45		
633, 634, 635, 636	β'2 + 8.5 w/o HfO_2	-0.4	1800	1	Ic	21.00	3.12	2.46		
637, 638, 639, 640	β'2 + 5 (0.8 ZrO_2, 0.2 Y_2O_3)	+0.9	1735	1	Ic	0	3.22	3.22		
642, 643, 644, 645	β'2 + 5 w/o Cr_2O_3	-0 3	1775	1	Ic	Severe Reduction				
646, 647, 648, 649	β'2 + 5 w/o Cr_2O_3	-0.3	1690	1	Ic	24.52	3.20	2.57		
650, 651, 652	β'2 + 8.5 w/o HfO_2	-0.4	1775	2	Id	19.72	3.26	2.62		
673, 674, 675, 676	β'2 + 5 (0.8 ZrO_2, 0 2 Y_2O_3)	+0.9	1735	1	Ic				80 74 60 69	

APPENDIX II

FABRICATION AND TEST DATA FOR SiAlON TEST BARS (Cont'd)

Sample Number	Desired Composition	Deviation (%)	Firing Condition T (°C)	t (hrs.)	Code	Apparent Porosity (%)	Specific Gravity (g/cc)	Bulk Density (g/cc)	Flexural Strength K psi	Test Temp. if Other than Room (°C)
700										
701	β'2+ 5 (0.9 ZrO_2,									
702	0.1 Y_2O_3)	-0.3	1735	1	Ic	0	3.20	3.20		
703										
704										
705	β'2+ 5 (0.925 ZrO_2,									
706	0 075 Y_2O_3)	-0.4	1735	1	Ic	.094	3.24	3.24		
707										
734									46	1370
735	[β'2 + 5 w/o Y_2O_3]·2	-0.5	1750	1	Ic	0	3.26	3.26	51	1370
736									50	1370
737									57	
738									57	
739	[β'2 + 5 w/o Y_2O_3] 2	-0.5	1750	1	Ic	0	3.26	3.26	43	
740									37	
741										
742										
743	[β'2 + 5 w/o Y_2O_3]·2	-0.5	1750	1	Ic	0	3.23	3.23		
744										
745										
749										
750	β'2+ 5 w/o (925 ZrO_2,									
751	.075 Y_2O_3)	-0.3	1750	1	Ic	0.7	3.21	3.18		
752										
753										
754	β'2+ 5 w/o (925 ZrO_2,								34	1370
755	.075 Y_2O_3)	-0.3	1735	1	Ic	0.2	3.33	3.33	33	1370
756									33	1370
757										
758	β'2+ 5 w/o (925 ZrO_2,								67	
759	.075 Y_2O_3)	-0.3	1735	1	Ic				47	
760									42	

FABRICATION AND TEST DATA FOR SiAlON TEST BARS (Cont'd)

Sample Number	Desired Composition	Deviation (%)	Firing Condition T (°C)	t (hrs.)	Code	Apparent Porosity (%)	Specific Gravity (g/cc)	Bulk Density (g/cc)	Flexural Strength K psi	Test Temp. if Other than Room (°C)
761										
762	[β'1 + 2.5 w/o Y_2O_3] 1	+0.7	1735	1	Ic	0	3.04	3.04	70	
763									80	
764										
765										
766	[β'1 + 2.5 w/o Y_2O_3]·1	+0.7	1750	1	Ic	0.4	3.11	3.11		
767									56	
768									63	
769										
770	[β'1 + 2.5 w/o Y_2O_3]·1	+0.7	1750	1	Ic				67	
771									42	1370
772									65	1370
773										
774	β'1+ 2.5 w/o (.75 ZrO_2,									
775	.25 Y_2O_3)	+0.6	1735	1	Ic	4.5	2.98	2.84		
776										
778										
779	β'1+ 2 5 w/o (.75 ZrO_2,									
780	.25 Y_2O_3)	+0.6	1760	1	Ic	2.5	2.92	2.85		
781										
785										
786	β'1+ 2 5 w/o ZrO_2	+0.9	1735	1	Ic	25	3.20	2.39		
787										
788										
789										
790	β'1+ 2.5 w/o ZrO_2	+0.9	1775	1	Ic	28	3.19	2.29		
791										
792										
793										
794	β'1+ 5 w/o (.75 ZrO_2,								53	
795	.25 Y_2O_3)	+0.1	1735	1	Ic	0.1	3.02	3.02	49	
796									80	
797										
798	β'1+ 5 w/o (.75 ZrO_2,									
799	25 Y_2O_3)	+0.1	1775	1	Ic	0.1	3.14	3.14		
800										

APPENDIX II

FABRICATION AND TEST DATA FOR SiAlON TEST BARS (Cont'd)

(Page 7 of 7)

Sample Number	Desired Composition	Deviation (%)	Firing Condition T(°C)	t (hrs)	Code	Apparent Porosity (%)	Specific Gravity (g/cc)	Bulk Density (g/cc)	Flexural Strength psi	Test Temp. if Other than Room (°C)
810 811 812 813	[β'1 + 5 w/o Y_2O_3]·1	-0.1	1735	1	Ic	13	3.15	2.72		
814 815 816 817	[β'1 + 5 w/o Y_2O_3]·1	=0.1	1750	1	Ic	11	3.12	2.78		
818 819 820 821	β'1+ 3.5 w/o TiO_2	+1.1	1735	1	Ic	27	3.21	2.36		
822 823 824 825	β'1+ 5 w/o (8 ZrO_2, 2 Y_2O_3)	+0.9	1735	1	Ic	0.5	3.23	3.23		
826 827 828 829	β'1+ 5 w/o (.8 ZrO_2, .2 Y_2O_3)	+0 9	1735	1	Ic	0	3.20	3.21		
830 831 832	[β'1 + 2.5 w/o Y_2O_3] 2	-0 2	1735	1	Ic	1	2.90	2.87		
833 834 835	[β'1 + 2 5 w/o Y_2O_3]·2	-0.2	1750	1	Ic	1	2.93	2.93		
836 837 838	[β'1 + 5 w/o Y_2O_3]·2	-0.5	1750	1	Ic	0	3.20	3.20		
841 842 843	β'1+ 5 v/o ZrO_2	0	1735	1	Ic	18	3.36	2.75		